PHASE 2 INITIAL BOREHOLE DRILLING AND TESTING, IGNACE AREA

WP04c Data Report – Porewater Extraction and Analysis and Petrographic Analysis for IG_BH03

APM-REP-01332-0246 **October 2021**

Golder Associates Ltd. and Hydroisotop

nwmo
NUCLEAR WASTE MANAGEMENT ORGANIZATION
SOCIÉTÉ DE GESTION DES DÉCHETS NUCLÉAIRES

Nuclear Waste Management Organization
22 St. Clair Avenue East, 4th Floor
Toronto, Ontario
M4T 2S3
Canada

Tel: 416-934-9814
Web: www.nwmo.ca

REPORT

PHASE 2 INITIAL BOREHOLE DRILLING AND TESTING, IGNACE AREA

WP4C Data Report – Porewater Extraction and Analysis and Petrographic Analysis for IG_BH03

Submitted to:

Nuclear Waste Management Organization
4th Floor
22 St. Clair Avenue East
Toronto, Ontario, M4T 2S3

Submitted by:

Golder Associates Ltd.
6925 Century Avenue, Suite #100
Mississauga, Ontario
L5N 7K2

NWMO Document: APM-REP-01332-0246 R000

Distribution List

eCopy – Golder

eCopy – NWMO

eCopy – Hydroisotop

WP4C REPORT – POREWATER EXTRACTION AND ANALYSIS AND PETROGRAPHIC ANALYSIS FOR IG_BH03

CLIENT INFORMATION

Project Name:	Phase 2 Initial Borehole Drilling – Ignace Area
Project Number:	1671632
Client PO Number:	2000141
Document Name:	1671632(2401C)_IG_BH03_WP04C_PW_27Sep2021_R7b

Client:	Nuclear Waste Management Organization (NWMO)	
Address:	22 St. Clair Avenue East, 4th Floor	
City:	Toronto	
Province:	Ontario	
Postal Code:	M4T 2S3	
Client Contact:	Laura Kennell-Morrison	Maria Sánchez-Rico Castejón
Telephone:	647-259-3737	647-259-3720
Email:	lkennell@nwmo.ca	msanchez@nwmo.ca

Issue/Revision Index

Issue Code	Revision					Revision Details
	No.	By	Rev'd.	App.	Date	
RI	0	FE/JI	-	-	December 4, 2019	Internal draft for information only
RI	1	FE/JI	-	-	May 19, 2020	Internal draft for information only
RI	2	FE/JI	GWS	-	July 20, 2020	Preliminary draft to NWMO for information only
RR	3	FE/JI	GWS	-	October 27, 2020	Draft report for review and comments
RI	4	FE/JI	GWS	JC	December 18, 2020	Final report released for information
RI	5	FE/JI	GWS	JC	March 15, 2021	Addressed additional NWMO comments received in December and January. Final report released for information
RI	6	FE/JI	GWS	JC	April 21, 2021	Added 1 decimal place to mineral % in Table 6
RI	7	FE/JI	GWS	JC	Sept. 27, 2021	Addressed additional comments by the NWMO

Issue Codes: RR = Released for Review and Comments, RI = Released for Information

SIGNATURES

Prepared by: _____

Dr. Florian Eichinger
Hydroisotop GmbH

Reviewed by: _____

George Schneider, M.Sc., P.Geo.
Project Director - Principal

Approved by: _____

Joe Carvalho, Ph.D., P.Eng.
Senior Geological Engineer - Principal

Table of Contents

TABLES

FIGURES

1.0 INTRODUCTION

The Initial Borehole Drilling and Testing project in the Wabigoon and Ignace Area, Ontario is part of Phase 2 Geoscientific Preliminary Field Investigations of the NWMO's Adaptive Phased Management (APM) Site Selection Phase.

This project involves the drilling and testing of three deep boreholes within the northern portion of the Revell batholith. The second drilled borehole, IG_BH03, is located a direct distance of approximately 21 km southeast of the Wabigoon Lake Ojibway Nation and a direct distance of 43 km northwest of the Town of Ignace. Access to the IG_BH03 drill site is via Highway 17 and primary logging roads, as shown on Figure 1.

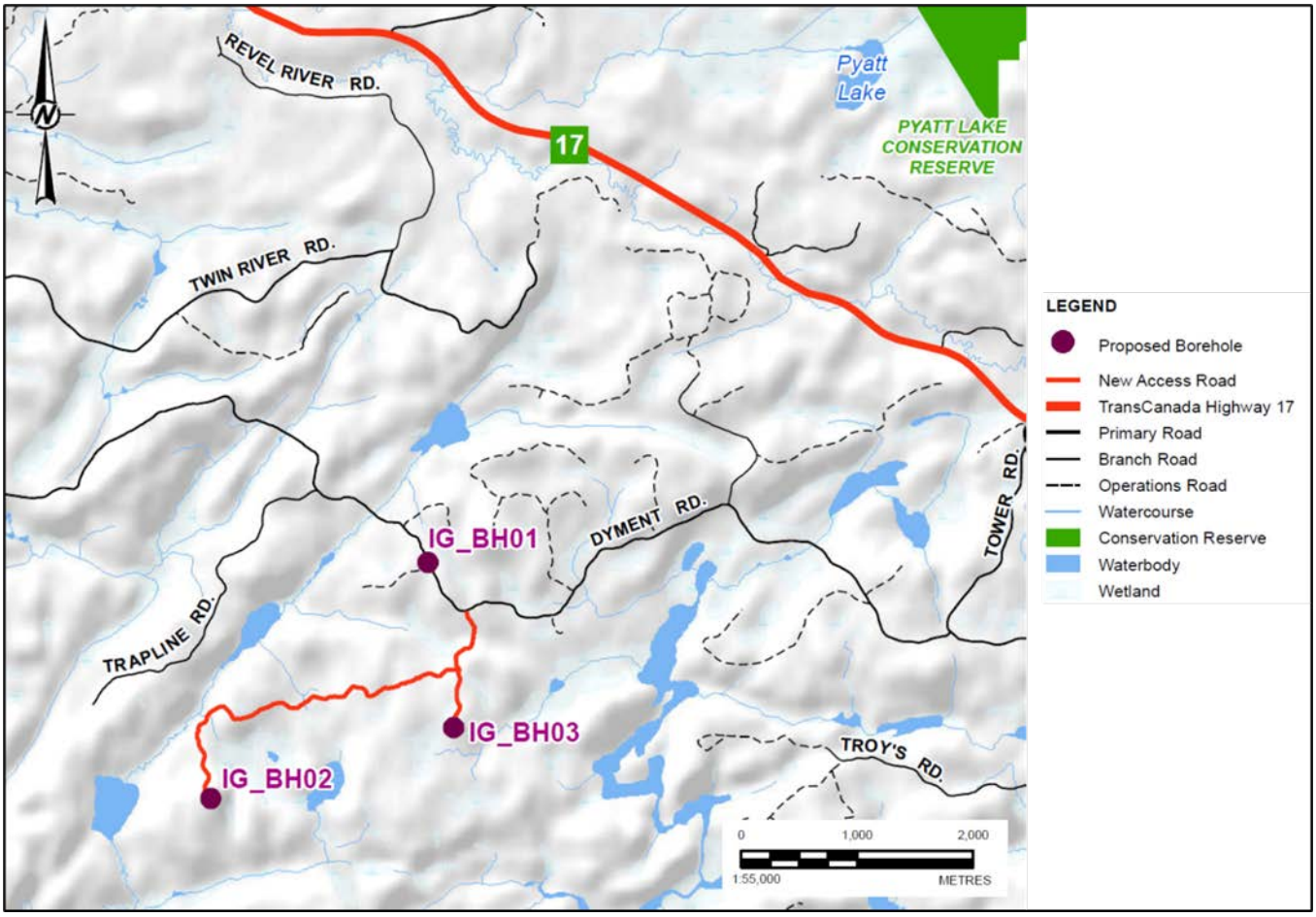

Figure 1: Location of IG_BH03 in relation to the Wabigoon / Ignace Area

The project was carried out by a team at Hydroisotop GmbH, subcontracted by Golder Associates Ltd. (Golder) on behalf of the NWMO. This report describes the testing methodology and results for Work Package 4C (WP4C): Porewater Extraction and Analysis and Petrographic Analysis for IG_BH03. IG_BH03 is an inclined borehole; all depths referred to in the text of this report are in metres below ground surface along the length of the borehole (mbgs (down hole)), or its equivalent metres borehole length (m BHL), rather than true vertical.

1.1 Geological Setting

The approximately 2.7 billion year old Revell batholith is located in the western part of the Wabigoon Subprovince of the Archean Superior Province. The batholith is roughly elliptical in shape trending northwest, is approximately 40 km in length, 15 km in width, and covers an area of approximately 455 km^2. Based on geophysical modelling, the batholith is approximately 2 km to 3 km thick through the center of the northern portion (SGL 2015). The batholith is surrounded by supracrustal rocks of the Raleigh Lake (to the north and east) and Bending Lake (to the southwest) greenstone belts (Figure 2).

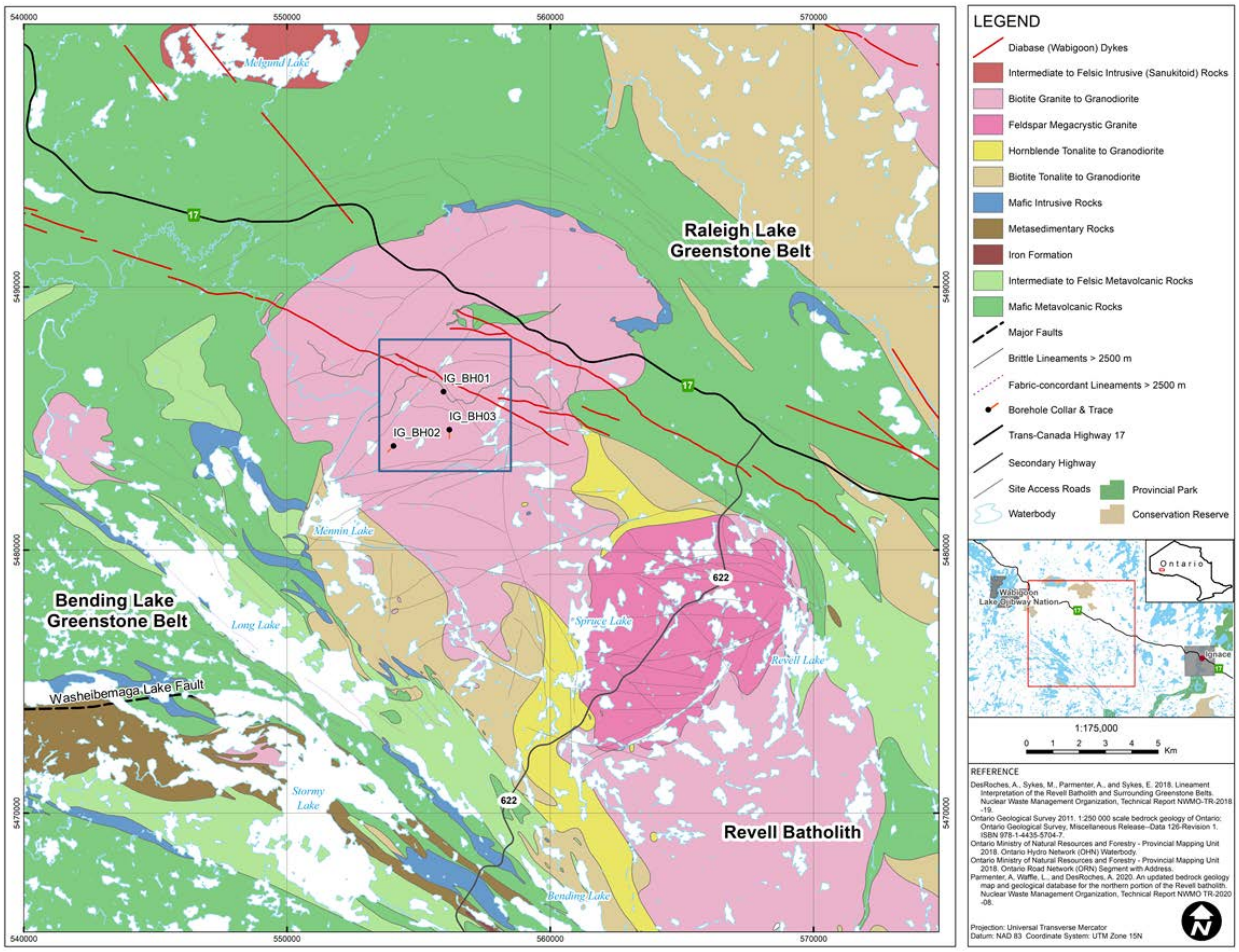

Figure 2: Geological setting and location of boreholes IG_BH01, IG_BH02 and IG_BH03 in the northern portion of the Revell batholith

Borehole IG_BH03 is located within an investigation area of approximately 19 km^2 in size, situated in the northern portion of the Revell batholith. Bedrock exposure in the area is generally very good due to minimal overburden, few water bodies, and relatively recent logging activities. Ground elevations generally range from 400 to 450 m above sea level. The ground surface broadly slopes towards the northwest as indicated by the flow direction of the main rivers in the area. Local water courses tend to flow to the southwest towards Mennin Lake (Figure 1).

Four main rock units are identified in the supracrustal rock group: mafic metavolcanic rocks, intermediate to felsic metavolcanic rocks, metasedimentary rocks, and mafic intrusive rocks (Figure 2). Sedimentation within the supracrustal rock assemblage was largely synvolcanic, although sediment deposition in the Bending Lake area may have continued past the volcanic period (Stone 2009; Stone 2010a; Stone 2010b). All supracrustal rocks are affected, to varying degrees, by penetrative brittle-ductile to ductile deformation under greenschist- to amphibolite-facies metamorphic conditions (Blackburn and Hinz 1996; Stone et al. 1998). In some locations, primary features, such as pillow basalt or bedding in sedimentary rocks are preserved, in other locations, primary relationships are completely masked by penetrative deformation. Uranium-lead (U-Pb) geochronological analysis of the supracrustal rocks produced ages that range between 2734.6 +/-1.1 Ma and 2725 +/-5 Ma (Stone et al. 2010).

Three main suites of plutonic rock are recognized in the Revell batholith, including, from oldest to youngest: a Biotite Tonalite to Granodiorite suite, a Hornblende Tonalite to Granodiorite suite, and a Biotite Granite to Granodiorite suite (Figure 2). Plutonic rocks of the Biotite Tonalite to Granodiorite suite occur along the southwestern and northeastern margins of the Revell batholith. The principal type of rock within this suite is a white to grey, medium-grained, variably massive to foliated or weakly gneissic, biotite tonalite to granodiorite. One sample of foliated and medium-grained biotite tonalite produced a U-Pb age of 2734.2+/-0.8 Ma (Stone et al. 2010). The Hornblende Tonalite to Granodiorite suite occurs in two irregularly-shaped zones surrounding the central core of the Revell batholith. Rocks of the Hornblende Tonalite to Granodiorite suite range compositionally from tonalite through granodiorite to granite and also include significant proportions of quartz diorite and quartz monzodiorite. One sample of coarse-grained grey mesocratic hornblende tonalite produced a U-Pb age of 2732.3+/-0.8 Ma (Stone et al. 2010). Rocks of the Biotite Granite to Granodiorite suite underlie most of the northern, central and southern portions of the Revell batholith. Rocks of this suite are typically coarse-grained, massive to weakly foliated, and white to pink in colour. The Biotite Granite to Granodiorite suite ranges compositionally from granite through granodiorite to tonalite. A distinct potassium (K)-Feldspar Megacrystic Granite phase of the Biotite Granite to Granodiorite suite occurs as an oval-shaped body in the central portion of the Revell batholith (Figure 2). One sample of coarse-grained, pink, massive K-feldspar megacrystic biotite granite produced a U-Pb age of 2694.0+/-0.9 Ma (Stone et al. 2010).

The bedrock surrounding IG_BH02 is composed mainly of massive to weakly foliated felsic intrusive rocks that vary in composition between granodiorite and tonalite, and together form a relatively homogeneous intrusive complex. Bedrock identified as tonalite transitions gradationally into granodiorite and no distinct contact relationships between these two rock types are typically observed (SRK and Golder 2015; Golder and PGW 2017). Massive to weakly foliated granite is identified at the ground surface to the northwest of the feldspar-megacrystic granite. The granite is observed to intrude into the granodiorite-tonalite bedrock, indicating it is distinct from, and younger than, the intrusive complex (Golder and PGW 2017).

West-northwest trending mafic dykes interpreted from aeromagnetic data extend across the northern portion of the Revell batholith and into the surrounding greenstone belts. One mafic dyke occurrence, located to the northwest of IG_BH01, is approximately 15-20 m wide (Figure 2). All of these mafic dykes have a similar character and are interpreted to be part of the Wabigoon dyke swarm. One sample from the same Wabigoon swarm produced a U-Pb age of 1887+/-13 Ma (Stone et al. 2010), indicating that these mafic dykes are Proterozoic in age. It is assumed based on surface measurements that these mafic dykes are sub-vertical (Golder and PGW 2017).

Long, narrow valleys are located along the western and southern limits of the investigation area (Figure 1). These local valleys host creeks and small lakes that drain to the southwest and may represent the surface expression of structural features that extend into the bedrock. A broad valley is located along the eastern limits of the investigation area and hosts a more continuous, un-named water body that flows to the south. The linear and segmented nature of this waterbody's shorelines may also represent the surface expression of structural features that extend into the bedrock.

Regional observations from mapping have indicated that structural features are widely spaced (typical 30 to 500 cm spacing range) and dominantly comprised of sub-vertical joints with two dominant orientations, northeast and northwest trending (Golder and PGW 2017). Interpreted bedrock lineaments generally follow these same dominant orientations in the northern portion of the Revell batholith Figure 2; DesRoches et al. 2018). Minor sub-horizontal joints have been observed with minimal alteration, suggesting they are younger and perhaps related to glacial unloading. One mapped regional-scale fault, the Washeibemaga Lake fault, trends east and is located to the west of the Revell batholith (Figure 2). Ductile lineaments, also shown on Figure 2, follow the trend of foliation mapped in the surrounding greenstone belts. Additional details of the lithological units and structures found at surface within the investigation area are reported in Golder and PGW (2017).

1.2 Technical Objectives

The technical objectives of the porewater testing program are to assess the key chemical and transport properties of the crystalline host rock with depth and within the repository horizon (presently assumed to be between depths of approximately 400 and 600 m). The geochemical results will provide information about the palaeohydrogeological evolution of the bedrock system. Thin section petrographic analyses will be carried out at all sampling depths in order to characterize mineralogy and support the evaluation of the porewater chemistry (obtained by indirect extraction methods, which requires the determination of the in-situ water content and connected porosity). The evaluation of petrophysical parameters requires correlation with the petrographic and mineralogical characteristics of the rock samples.

The associated work tasks include:

- Aqueous extraction experiments to determine initial estimates of pore fluid composition and Total Dissolved Solids (TDS);
- Isotope diffusive exchange experiments, for the determination of stable water isotopes ($\delta^{18}O$ and $\delta^{2}H$);
- Out-diffusion experiments, for determination of porewater stable ion concentrations (Cl and Br), as well as the determination of effective diffusion coefficients, D_e, for Cl;
- Set-up of elemental elution curves during out-diffusion experiments
- $\delta^{37}Cl$ analyses;
- Bulk petrography; and
- Determination of density, water content and porosity for the various subsamples used in the above-listed analytical suites.

The characterization of the porewater composition and the solute transport processes in the rock matrix contribute important information for the long-term safety assessment of deep geological repositories for radioactive waste. Thus, knowledge of the porewater composition will allow better constraints on the processes affecting the near-

field of a repository. In designs where repository construction is restricted to bedrock of low permeability, the first water to interact with the repository barrier materials (e.g., bentonite, Cu-canister) will be the porewater. This interaction could result in changes of the physical and chemical properties of the various barrier materials. Knowledge of the porewater composition and its evolution over recent geological time – particularly during the last thousand to hundreds of thousands of years, in accordance with the expected lifespan of a geologic repository – is considered to be of high importance.

In combination with the knowledge gained about solute transport in the rock matrix, the characterization of porewater also contributes to a better understanding of processes related to the far-field environment around the repository. Thus, it provides valuable information about matrix diffusion as a potential retardation factor for radionuclides, and allows better constraints to be placed on the palaeohydrogeological history of a repository site. Due to the exchange by diffusion between fracture groundwater and matrix porewater, released radionuclides may be temporally immobilized by matrix diffusion, and possible subsequent sorption on mineral surfaces. For radionuclides susceptible to sorption, the accessible surface areas are greatly enhanced by matrix diffusion when compared to the accessible surface area on fracture surfaces alone. Matrix diffusion has the potential to increase solute transport times to the biosphere from the repository.

In contrast to fracture groundwater, porewater cannot be sampled by conventional groundwater sampling techniques. The chemical and isotopic composition of porewater has, therefore, to be derived by indirect extraction techniques based on rock material. In most of these indirect extraction techniques – especially in case of rocks of a porosity below about 2 vol.% – the original porewater concentrations are diluted and need to be back-calculated to in-situ concentrations. This requires a well-defined value for the connected porosity – accessible to different solutes under in-situ conditions. The derivation of such porosity values, as well as solute concentrations, is prone to various perturbations during drilling, core sampling, storage and experiments in the laboratory. The obtained data have to be carefully evaluated for potential perturbations induced by drilling activities, rock stress release and sample treatment in the laboratory in order to derive values that are representative of in-situ conditions. This requires detailed knowledge about the rock composition, the rock texture, and the local stress field, because porewater composition is dependent on these factors as well.

Matrix porewater of ten core samples taken from 238 m to 988 mbgs, (down hole) in IG_BH03, drilled as part of the Phase 2 Initial Borehole Drilling and Testing programme in the Ignace Area for the Nuclear Waste Management Organization (NWMO), was investigated for its chemical and isotopic composition using different methods. Additionally, the crystalline rock core samples were characterised for their petrophysical and mineralogical properties, including water content, water-loss porosity, bulk density, pore diffusion coefficient and mineralogical composition.

2.0 SAMPLING AND SAMPLE PREPARATION

A total of 30 samples from ten depth intervals were taken from borehole IG_BH03 between August 11, 2019 and September 16, 2019 for the characterization of porewater (Table 1). Sampling was conducted by Golder Associates Ltd. (Golder) according to the instructions provided by Hydroisotop GmbH (Hydroisotop), which were applied and approved already during the investigations of core samples from borehole IG_BH01. After recovery from the borehole, the individual core sections (three per depth interval, ten intervals in total) were photographed and immediately packed in a plastic bag, evacuated and sealed airtight. This procedure was repeated for a second plastic bag and a final Al-coated plastic layer. The samples were stored in a refrigerator on site and then sent to Hydroisotop, Germany, in a cooler.

The samples arrived in the lab between August 19 and October 4, 2019. All samples were well packed and arrived in the lab with preserved vacuum in all three layers. At Hydroisotop the samples were stored in the refrigerator at 4°C and prepared between September 19 and October 10, 2019.

The assigned samples were unpacked and immediately wrapped into Parafilm™ and cut by dry-sawing into full-diameter sections. After sawing, the surfaces of the obtained pieces were cleaned with paper towels and again wrapped into Parafilm™. The entire sample preparation was conducted as rapidly as possible (within 10 minutes) after opening the sealed bags, in order to minimize evaporation.

One of the two core sections assigned for porewater investigations (PW0XX) taken from each depth interval was stored and sealed as a retained sample at 4°C in the refrigerator. The analytical program conducted on each sample is summarized in Table 2.

Table 1: Overview of the core samples taken from IG_BH03 for porewater investigations (m BHL is equivalent to mbgs (down hole))

		Depth							
Sample ID	Hydro Lab Nr.	from	to	ave	Length	Date sampled	Time sampled	Date sent	Date arrived
		m BHL	m BHL	m BHL	m		hh:mm		
IG_BH03_AQ001	330760	238.64	238.87	238.8	0.23	11. Aug	01:23	11.08.2019	19.08.2019
IG_BH03_PW001	330761	238.94	239.31	239.1	0.37	11. Aug	01:20	11.08.2019	19.08.2019
IG_BH03_PW002	330762	241.81	242.20	242.0	0.39	11. Aug	03:18	11.08.2019	19.08.2019
IG_BH03_PW003	330938	345.03	345.38	345.2	0.35	14. Aug	21:29	21.08.2019	26.08.2019
IG_BH03_AQ002	330940	345.93	346.06	346.0	0.13	14. Aug	21:32	21.08.2019	26.08.2019
IG_BH03_PW004	330939	347.96	348.34	348.2	0.38	14. Aug	10:48	21.08.2019	26.08.2019
IG_BH03_PW005	330942	459.01	459.44	459.2	0.43	20. Aug	14:07	21.08.2019	26.08.2019
IG_BH03_AQ003	330941	459.99	460.14	460.1	0.15	20. Aug	14:09	21.08.2019	26.08.2019
IG_BH03_PW006	330943	460.86	461.26	461.1	0.40	20. Aug	15:47	21.08.2019	26.08.2019
IG_BH03_PW007	331087	503.72	504.12	503.9	0.40	22. Aug	04:57	27.08.2019	02.09.2019
IG_BH03_AQ004	331085	504.12	504.27	504.2	0.15	22. Aug	04:59	27.08.2019	02.09.2019
IG_BH03_PW008	331088	506.47	506.87	506.7	0.40	22. Aug	15:10	27.08.2019	02.09.2019
IG_BH03_PW009	331089	554.28	554.64	554.5	0.36	25. Aug	16:42	27.08.2019	02.09.2019
IG_BH03_AQ005	331086	554.64	554.77	554.7	0.13	25. Aug	16:44	27.08.2019	02.09.2019
IG_BH03_PW010	331090	558.53	558.94	558.7	0.41	25. Aug	22:18	27.08.2019	02.09.2019
IG_BH03_AQ006	331704	608.52	608.66	608.6	0.14	27. Aug	16:15	02.09.2019	11.09.2019
IG_BH03_PW011	331706	608.66	609.02	608.8	0.36	27. Aug	16:14	02.09.2019	11.09.2019
IG_BH03_PW012	331707	612.60	612.98	612.8	0.38	27. Aug	18:29	02.09.2019	11.09.2019
IG_BH03_AQ007	331705	665.79	665.91	665.9	0.12	29. Aug	17:56	02.09.2019	11.09.2019
IG_BH03_PW013	331708	668.55	668.95	668.8	0.40	29. Aug	22:24	02.09.2019	11.09.2019
IG_BH03_PW014	331709	668.95	669.36	669.2	0.41	29. Aug	22:08	02.09.2019	11.09.2019
IG_BH03_PW015	331711	771.40	771.76	771.6	0.36	02. Sep	12:34	03.09.2019	11.09.2019
IG_BH03_AQ008	331710	771.76	771.92	771.8	0.16	02. Sep	12:36	03.09.2019	11.09.2019
IG_BH03_PW016	331712	777.66	778.08	777.9	0.42	03. Sep	00:20	03.09.2019	11.09.2019
IG_BH03_AQ009	332881	880.02	880.16	880.1	0.14	11. Sep	04:12	16.09.2019	04.10.2019
IG_BH03_PW017	332883	880.16	880.56	880.4	0.40	11. Sep	04:15	16.09.2019	04.10.2019
IG_BH03_PW018	332884	880.96	881.34	881.2	0.38	11. Sep	09:38	16.09.2019	04.10.2019
IG_BH03_PW019	332885	984.52	984.89	984.7	0.37	15. Sep	21:59	16.09.2019	04.10.2019
IG_BH03_AQ010	332882	984.89	985.03	985.0	0.14	15. Sep	22:01	16.09.2019	04.10.2019
IG_BH03_PW020	332886	987.32	987.67	987.5	0.35	16. Sep	00:30	16.09.2019	04.10.2019

Table 2: Overview of the analytical porewater program conducted on core samples from borehole IG_BH03

				Experimental and analytical programme																	
				Aqueous Extraction			Diffusive isotope exchange experiments				Out-diffusion experiments							Grav. WC	Thin section petrography	
Sample ID	Hydro Lab Nr.	Ave. Depth	Date prepared	Exp. Set-Up	Chemical analyses	Grav. WC	Exp. Set-Up	Exp. finished	Isotope Analyses	Grav. WC	Exp. Set-Up	Time Series	Analyses ions	Analyses $\delta^{37}Cl$	Grav. WC	Density	Modelling D_P	Extra Pieces	Preparation	Microscopy
		m BHL																		
IG_BH03_AQ001	330760	238,8	03.09.2019	X	X	X														
IG_BH03_PW001	330761	239,1	03.09.2019																	
IG_BH03_PW002	**330762**	**242,0**	**03.09.2019**				X	X	X	X	X	X	X	X	X	X	X	X	X	X
IG_BH03_PW003	**330938**	**345,2**	**03.09.2019**				X	X	X	X	X	X	X	X	X	X	X	X	X	X
IG_BH03_PW004	330939	348,2	03.09.2019																	
IG_BH03_AQ002	330940	346,0	03.09.2019	X	X	X														
IG_BH03_AQ003	330941	460,1	03.09.2019	X	X	X														
IG_BH03_PW005	**330942**	**459,2**	**03.09.2019**				X	X	X	X	X	X	X	X	X	X	X	X	X	X
IG_BH03_PW006	330943	461,1	03.09.2019																	
IG_BH03_PW007	**331087**	**503,9**	**03.09.2019**				X	X	X	X	X	X	X	X	X	X	X	X	X	X
IG_BH03_AQ004	331085	504,2	03.09.2019	X	X	X														
IG_BH03_PW008	331088	506,7	03.09.2019																	
IG_BH03_PW009	**331089**	**554,5**	**03.09.2019**				X	X	X	X	X	X	X	X	X	X	X	X	X	X
IG_BH03_AQ005	331086	554,7	03.09.2019	X	X	X														
IG_BH03_PW010	331090	558,7	03.09.2019																	
IG_BH03_AQ006	331704	608,6	16.09.2019	X	X	X														
IG_BH03_PW011	**331706**	**608,8**	**16.09.2019**				X	X	X	X	X	X	X	X	X	X	X	X	X	X
IG_BH03_PW012	331707	612,8	16.09.2019																	
IG_BH03_AQ007	331705	665,9	16.09.2019	X	X	X														
IG_BH03_PW013	331708	668,8	16.09.2019																	
IG_BH03_PW014	**331709**	**669,2**	**16.09.2019**				X	X	X	X	X	X	X	X	X	X	X	X	X	X
IG_BH03_PW015	**331711**	**771,6**	**16.09.2019**				X	X	X	X	X	X	X	X	X	X	X	X	X	X
IG_BH03_AQ008	331710	771,8	16.09.2019	X	X	X														
IG_BH03_PW016	331712	777,9	16.09.2019																	
IG_BH03_AQ009	332881	880,1	10.10.2019	X	X	X														
IG_BH03_PW017	**332883**	**880,4**	**10.10.2019**				X	X	X	X	X	X	X	X	X	X	X	X	X	X
IG_BH03_PW018	332884	881,2	10.10.2019																	
IG_BH03_PW019	**332885**	**984,7**	**10.10.2019**				X	X	X	X	X	X	X	X	X	X	X	X	X	X
IG_BH03_AQ010	332882	985,0	10.10.2019	X	X	X														
IG_BH03_PW020	332886	987,5	10.10.2019																	

Note: m BHL is equivalent to mbgs (down hole).

3.0 EXPERIMENTAL SET-UPS AND ANALYTICAL METHODS

Porewater investigations were performed on different types of samples that were subjected to different types of extraction and exchange experiments. This included aqueous extraction and out-diffusion experiments to characterise porewater using chemical tracers, isotope diffusive exchange experiments for the porewater $\delta^{18}O$ and $\delta^{2}H$ composition, and the determination of the water content and water-loss porosity on the respective samples.

Unless otherwise specified, the analytical work has been conducted at Hydroisotop GmbH, Germany.

3.1 Mineralogy and Petrography

Mineralogical and petrographic investigations were performed on rock material from ten PW samples taken along the borehole profile (Table 2). The samples were characterised using thin section microscopy. Modal mineralogy was determined by point counting.

End pieces of the core sections used for out-diffusion experiments (cf. Section 3.3.2) were first weighed and dried to determine the water content of the individual sections. After stable weight was reached (= ± 0.002 g for 14 days), thin sections (with a size of 32 x 20 mm) were produced by standard methods at Geotec Consult, Germany. Petrographic and mineralogical evaluation, description and documentation was performed using transmitted light microscopy.

3.2 Water content and water-loss porosity

The water content was determined on core material used for aqueous extraction experiments and out-diffusion experiments, as well as on the core pieces used for the isotope diffusive exchange technique. Water contents were also determined on extra pieces of core available from those used for the out-diffusion experiments.

The quality of sample preservation upon arrival in the laboratory was assessed by the condition of the sample bags and of the core surface (wet vs. dry).

For water content measurements, drill-core pieces were placed in a crystallization dish, weighed and subsequently dried at 105 °C until stable weight conditions were obtained. Before taking the initial wet weight of the full diameter core sections, the surface was allowed to dry on the balance until stable weight was achieved for ≈10 sec. During the following drying process, weighing was carried out weekly until the sample weight remained constant (± 0.002 g) for at least 14 days.

Water contents were determined on core samples used for aqueous extraction experiments (Table 2). Therefore, one half of the full disc core (191 – 404 g) was broken by a mortar to an edge length of approximately 1 cm, placed in a crystallization dish, weighed and put in the oven at 105 °C for drying. Additionally, the two cut uneven head pieces (for one sample, three pieces) with weights between 83 and 380 g were also weighed and put in the oven to determine the water content. Drying times varied between 14 and 65 days for crushed pieces, and 29 to 65 days for full disc cores.

Water contents also were determined on core pieces used for out-diffusion experiments, with weights between 1453 – 1544 g and on the two cut uneven head pieces with weights between 133 and 236 g. Drying times varied between 84 and 112 days for large sized out-diffusion cores and between 14 and 56 days for the head pieces.

Gravimetric water contents were further determined on crushed core sections used for the single isotope diffusive exchange experiments after equilibration. Their masses varied between 293 and 415 g and drying times ranged between 28 and 77 days.

Finally, the gravimetric water content of the entire core sample (PW and AQ) was determined using the values and weights of the individual pieces. The weighted water content values are scaled based on the masses of the sub-samples relative to the total sample weight. Additionally, the weighted water contents are calculated in Vol.% applying the bulk, wet density determined on out-diffusion cores and aliquots of aqueous extraction cores, assuming a water density of 1.0 g/cm^3.

The calculation of the water-loss porosity (i.e., the connected porosity) from the gravimetric water content requires a measure of the grain density. In rocks of low porosity, the bulk wet density can be used as a proxy for the grain density. A measure for the bulk wet density of the rocks used for out-diffusion and aqueous extraction experiments was obtained from volume and saturated mass of the core samples. The volume was calculated from measurements of height and diameter of the core samples using a Vernier Calliper, with an error of ± 0.01 mm.

Core lengths varied between 3.3 and 5.8 cm for aqueous extraction cores and between 18.7 and 20.0 cm for out-diffusion cores.

From known sample volume and wet mass, the bulk, wet and dry density is obtained by

$$\rho_{bulk,wet} = \frac{m_{rock,wet}}{V_{rock}}, \qquad \rho_{bulk,dry} = \frac{m_{rock,dry}}{V_{rock}} \qquad \text{eq. 1}$$

and the water-loss (connected) porosity, ϕ_{WL}, can be calculated according to

$$\phi_{WL} = WC_{wet} * \frac{\rho_{bulk,wet}}{\rho_{water}} = \phi_{WL} = \frac{m_{pw} \times 100}{r^2 \times h \times \pi \times \rho_{water}}, \qquad \text{eq. 2}$$

where WC_{wet} is the water content based on the wet weight of the rock sample and $\rho_{bulk,wet}$ the bulk wet density of the rock. In a first approximation, the density of water, ρ_{water}, is assumed to be 1 g/cm^3. Due to the low water content of the investigated crystalline rocks, the water content and water-loss porosity determined by the wet weight and bulk, wet density of the sample is essentially equal to those values calculated using the dry weight and bulk, dry density.

As shown by Gaussian error propagation the error of the water content and the water-loss porosity depends predominately on the accuracy of the determination of the mass of porewater measured after unpacking (i.e., on the measured initial wet weight) and the final dry weight of the cores.

3.3 Porewater extraction methods

3.3.1 Aqueous extraction experiments

Aqueous extraction experiments were conducted prior to out-diffusion and isotope exchange experiments to estimate the salinity of the investigated porewaters.

Saturated full disc core sections were crushed by a mortar and sieved by an analytical sieve to a grain size of < 2 mm and 43 to 83 g of rock material were put in a PE bottle, where 67 to 93 ml of deionized water were added. Subsequently the bottle was gently shaken for 24 h. Afterward, the elution was decanted, filtered (0.45 µm) and immediately analysed for their alkalinity, pH and sp. electrical conductivity (using a Metrohm Titrino 785 and WTW LF 325 system). Subsequently, the main anion and cation concentrations were analysed by IC using a Dionex ICS 1500 system. The analytical error of the ion concentration analyses is ± 5 %.

The porewater Cl-concentration was further calculated according to:

$$C_{i,pw} = \frac{C_{i,sol} \times V_{sol} \times 0.001}{m_{pw}}$$ eq. 3

where $C_{i,pw}$ = porewater elemental concentration, $C_{i,sol}$ = analyzed elemental concentration in the aqueous extraction solution, V_{sol} = Volume of aqueous extraction solution and m_{pw} = mass of porewater.

3.3.2 Out-diffusion experiments

Out-diffusion experiments were performed on intact full disc core by immersion into ultrapure water. The volume of test water varied between 124 and 141 ml. During the experiments the two water reservoirs, i.e., porewater and test water, were allowed to exchange until equilibrium. Equilibrium with respect to chloride is considered achieved when the Cl concentration has been constant within the analytical error range (= ±5 %) over a minimum of 14 days.

After placing the core sample in the PE-vessel, the vessel was sealed and put in a vibrating water bath (40 rpm) at a constant temperature of 45 °C to accelerate diffusion. The PE-vessels were covered by a vapour-tight lid, which is equipped with two swagelock™ valves and PEEK™ sampling lines. The core, the experiment container and the test water were weighed before and after the experiment to ensure that no loss of test water occurred during the entire experiment. At specific time intervals of initially a few days, and later a few weeks, 0.5 ml of solution were sampled using a PVC-syringe to determine the chloride concentration as a function of time. The experimental time depended on the equilibration rate in the individual experiments. All out-diffusion experiments were ended between 141 and 169 days.

After equilibrium with respect to chloride was achieved, the vessels were removed from the water bath and cooled to room temperature. Subsequently, the cylinder, the core and the remaining test water was weighed and the supernatant solution was filtered (0.45 µm) and analysed immediately for pH, sp. el. conductivity (EC) and alkalinity (acid capacity 4.3 and base capacity 8.2), and later for major cations and anions and certain trace elements and isotopes.

The major cations (Na, K, Ca, Mg, Sr) and anions (F, Cl, NO_3, Br, SO_4) of the 0.5 ml time series and final test solutions of the out-diffusion experiments were analysed by ion chromatography using a Dionex ICS 1500 system. The relative analytical error of these analyses is ± 5 % based on multiple measurements of external check standard solutions (1σ). The final test solutions with a volume of approximately 100 ml were analysed undiluted and in different dilutions (1:10 and if necessary 1:20). The time series samples were analysed within days after sampling. Due to the low volume the sample could only be measured once in a 1:10 dilution. Consequently, the detection limit is different for each element in the two different solutions.

The alkalinity titration, pH and EC measurements were performed using Metrohm titration systems and a WTW LF325 probe.

TOC and TIC concentrations were analysed on the final solutions using a Shimadzu VCSH analyser with a relative analytical error of ± 5 % based on multiple measurements of external check standard solutions (1σ).

Boron, aluminium, lithium and silica concentrations of out-diffusion test solutions were analysed at Görtler analytical services GmbH, Germany, using a Thermo Fischer ICP-MS system with a detection limit of 0.0001 mg/l and an analytical uncertainty of 5 %.

The $^{37}Cl/^{35}Cl$ isotope ratio, expressed as $d^{37}Cl$ relative to SMOC, was measured by a GC-MS-IRMS system (Thermo Fischer Delta S). Analytical errors were determined by the standard deviation of triplicate analyses of every sample.

Strontium isotope signatures were analysed at Iso Analysis UG, Germany, by a Thermo Fischer MC-ICP-MS system with an analytical uncertainty of 0.0005.

Chloride and bromide concentrations of the experiment solution can be converted to porewater concentrations by applying mass balance calculations if equilibrium between test water and porewater is achieved. With knowledge of the mass of porewater in the rock sample, the chloride and bromide concentration of the porewater can be calculated according to:

$$C_{pw} = \frac{(m_{pw} + m_{TWi} - \sum^{n} m_s) * C_{TW\infty} - (m_{TWi} * C_{TWi}) + \sum^{n} m_s * C_s}{m_{pw}} \qquad \text{eq. 4}$$

where C_{pw} = porewater concentration; m_{pw} = mass of porewater; m_{TWi} = initial mass of test water; C_{TWi} = initial Cl-concentration of test water; m_s = mass of sub sample used for time series; C_s = Cl concentration of sub sample used for time series.

The term $\sum m_s * C_s$ (equation 4) describes the amount of Cl removed from the initial experiment solution for Cl time-series samples. A correction for chloride and bromide in the initial experiment solution ($m_{TWi} * C_{TWi}$) is necessary if this solution is not entirely free of chloride and bromide.

The unit for the porewater concentration is given in mg/kg_{H2O} (and not mg/l) because it is derived on a mass basis rather than a volumetric basis. This is due to the fact that the density of the porewater is not known beforehand, because it depends, in part, on the in-situ salinity of the water, which is unknown.

3.3.3 Isotope diffusive exchange technique

The isotope diffusive exchange technique to determine the water isotope composition, $\delta^{18}O$ and $\delta^{2}H$, of the porewater and the mass of porewater was originally developed by Rogge (1997) and Rübel et al. (2002) for sedimentary rocks and later adapted for crystalline rocks by Waber and Smellie (2005, 2006) and Eichinger et al. (2006). In this method, initially saturated rock material is placed into two vapour-tight containers together with different test waters of known isotope composition. The porewater and test water is then allowed to isotopically equilibrate via the vapour phase without any direct contact between the core material and the test water. The porewater isotope composition and the water content of the rock sample can then be derived by isotope mass balance relationships. It has been shown that the uncertainty of the derived isotope composition largely depends on the ratio of porewater to test water used in the experiments (e.g., Rübel et al. 2002). For crystalline rocks, this ratio was optimised by using larger volumes of rock and smaller volumes of test water in the experiments (e.g., Waber and Smellie 2005, 2006; Eichinger et al. 2006).

For the present samples, 1.8 ml of test water were placed in a Petri dish in the centre of a glass vessel and surrounded by hand crushed core pieces of 4 - 6 cm^3 in size and with a total mass of 293 to 415 g. After an equilibration time of 60 days, the two test waters were removed and analysed by Cavity Ring Down Spectroscopy using a Picarro L 2130-I Analyser. The results for the test waters are reported relative to the VSMOW standard with a precision of ± 0.15 ‰ for $\delta^{18}O$ and ± 1.5 ‰ for $\delta^{2}H$.

Test water and core material were weighed before and after the experiment to assess if test water was lost on the container walls and/or rock material due to evaporation and/or condensation. To minimise condensation, 0.3 mol of NaCl were dissolved in the test water to lower its water vapour pressure. For every sample, two experiments were performed: one using test water with an isotope composition close to that expected in the porewater ("LAB-

sample") and one using test water with an isotope composition far from that expected for the porewater ("ICE-sample").

The test water used for the LAB-sample was normal laboratory tap water ($\delta^{18}O$ = -10.41 ‰ V-SMOW; $\delta^{2}H$ = -73.1 ‰ V-SMOW), while that for the SSI-sample was water from an ice core drilled in Greenland ($\delta^{18}O$ = -29.73 ‰ V-SMOW; $\delta^{2}H$ = -233.4 ‰ V-SMOW). The equilibration time in the three reservoirs – rock porewater, test water and the air inside the container used as a diaphragm – depends on the volume of the container, the size of the rock pieces and the distance of the rock pieces to the test water (see Rogge 1997). Based on the estimations of the minimum time period required for complete isotopic equilibration (cf. Eichinger et al. 2006), an experimental time of 60 days was chosen.

The isotope diffusive exchange technique delivers the $\delta^{18}O$ and $\delta^{2}H$ values and the mass of the porewater present in the connected pore space of the rock sample. These parameters are calculated from the analytical results obtained for the two test water solutions using mass balance relationships according to:

$$m_{pw} * c_{pw}\Big|_{t=0} + m_{tw} * c_{tw}\Big|_{t=0} = (m_{pw} + m_{tw}) * c_{tw}\Big|_{t=\infty} \qquad \text{eq. 5}$$

where *m* = mass, *c* = isotope ratios expressed in the δ notation, *pw* = porewater, *tw* = test water; *t = 0* means the isotope concentrations at the beginning, and *t* = ∞ at the end of the experiment.

The water content of the applied samples is calculated by transformation of equation 5 to

$$WC_{IsoEx} = \left[\frac{m_{TW(Std\,2)} \times m_{Rock(Std1)} \times (C_{TW^{0}(Std\,2)} - C_{TW\infty(Std\,2)}) + m_{TW(Std1)} \times m_{Rock(Std\,2)} \times (C_{TW\infty(Std1)} - C_{TW^{0}(Std1)})}{m_{Rock(Std1)} \times m_{Rock(Std\,2)} \times (C_{TW\infty(Std\,2)} - C_{TW\infty(Std1)})} \right] \times 100 \qquad \text{eq. 6}$$

where m_{Rock} = mass of rock, *Std 1* = test solution 1 and *Std 2* = test solution 2.

Equation 6 can be set up for oxygen and hydrogen isotope ratios of the test water, resulting in two independent values for the mass of porewater.

The $\delta^{18}O$- and $\delta^{2}H$- values of the porewater are calculated by transformation of equation 5 to

$$C_{PW} = \frac{C_{TW\infty(Std1)} \times m_{TW(Std\,2)} \times m_{Rock(Std1)} \times (C_{TW\infty(Std\,2)} - C_{TW^{0}(Std\,2)}) - C_{TW\infty(Std\,2)} \times m_{TW(Std1)} \times m_{Rock(Std\,2)} \times (C_{TW\infty(Std1)} - C_{TW^{0}(Std1)})}{m_{TW(Std\,2)} \times m_{Rock(Std1)} \times (C_{TW\infty(Std\,2)} - C_{TW^{0}(Std\,2)}) - m_{TW(Std1)} \times m_{Rock(Std\,2)} \times (C_{TW\infty(Std1)} - C_{TW^{0}(Std1)})} \qquad \text{eq. 7.}$$

The errors of the calculated $\delta^{18}O$, $\delta^{2}H$ and the mass of porewater are computed for each sample using Gauss' law of error propagation.

4.0 PETROGRAPHY AND MINERALOGY

The interpretation of porewater derived by indirect methods using rock material requires knowledge about the rock composition and the physical properties of the rock. The petrographic and mineralogical investigations provide information about:

- The structure and texture of the rocks, which place constraints on pathways for solute migration.
- The type of pore space where porewater resides (intergranular versus intragranular), and a correlation of the experimentally determined petrophysical properties (porosity, density) with the petrography of the rocks.

Petrographic and mineralogical investigations were conducted on ten core samples taken from borehole IG_BH03 at depths between 238 and 985 mbgs (down hole). Thin sections were produced from the cut-off end pieces of core sections used for porewater out-diffusion experiments. The macroscopic and microscopic petrographic descriptions of the cores, minerals and rock textures were classified according to Bas & Streckeisen (1991) and Le Maitre et al. (2002). The nomenclature and mineral abbreviations, which are compiled in Table 3, were taken from Siivola & Schmid (2007). The mineral sizes are defined according to Schmid et al. (2007). The dimensions of the individual grain sizes are listed in Table 4. Alteration grades of rock forming minerals are defined based on the estimated altered area on individual grains (Table 5).

Table 3: Abbreviations of mineral names recommended by IUGS (Siivola & Schmid 2007)

Mineral Name	Abbreviation
Alkali feldspar	Afs
Apatite	Ap
Biotite	Bt
Clinozoisite	Czo
Epidote	Ep
Muscovite	Ms
Sericite	Ser
Opaque mineral	Op
Plagioclase	Pl
Quartz	Qtz
Titanite	Ttn
Zircon	Zrn

Table 4: Definition of grain sizes recommended by IUGS (Schmid et al. 2007)

Size	Description
>16 mm	Very coarse grained
4-16 mm	Coarse grained
1-4 mm	Medium grained
0.1-1 mm	Fine grained
0.01-0.1 mm	Very fine grained
<0.01 mm	Ultra-fine grained

Table 5: Definition of alteration grades of rock forming minerals

Proportion of crystal area	Degree of alteration
0 %	Unaltered
<40 %	Weakly altered
40-70 %	Moderately altered
>70 %	Highly altered

4.1 General macroscopic and microscopic description of core samples from borehole IG_BH03

The crystalline rock samples of borehole IG_BH03, which were sampled between 238 and 985 mbgs (down hole) and examined in this study, consist of macroscopically homogenous, unaltered granodiorite and tonalite. All samples show an equigranular and phaneritic structure. The core samples are not intersected by open fractures. No foliation is observed in any sample. Quartz, feldspars and biotite are distinguishable macroscopically. The red colour of two core samples (IG_BH03_PW009 and IG_BH03_PW015) is caused by a red-staining of the plagioclase crystals, which is due to iron replacing calcium ions in the plagioclase crystal lattice.

Microscopically, the individual samples consist predominately of quartz, plagioclase, biotite and minor amounts of alkali feldspar in different modal compositions. Muscovite, sericite and epidote/clinozoisite are present as alteration products.

Alteration of alkali feldspar crystals could not be observed, and muscovite is only present in micro fissures of alkali feldspar in some samples. The individual core samples show variable degrees of alteration, mainly in plagioclase and biotite crystals. Plagioclase crystals are moderately to highly sericitized. Only few crystals are unaltered or weakly altered. Very fine to fine grained muscovite, sericite and epidote/clinozoisite are present as alteration products either in the core of sericitized plagioclase or as alteration products over the entire plagioclase crystal. Fine grained muscovite and epidote/clinozoisite crystals are also present at the rim of weakly altered biotite crystals. It also seems that in some thin sections, biotite is partially replaced by epidote/clinozoisite. The colour/pleochroism of biotite varies strongly within each thin section and ranges from dark brown to reddish-brownish and green. The light green(ish) biotite crystals frequently show sutural alteration at the rim, whereas dark brown biotite crystals show less alteration products. In all samples, the intergranular pore space between the individual rock-forming minerals is open and not filled with alteration products. In general, sutural altered biotite grains did not show clear grain boundaries in thin sections.

In samples IG_BH03_PW002, IG_BH03_PW 005, IG_BH03_PW007, IG_BH03_PW011 and IG_BH03_PW015 alteration to chlorite could be observed in some biotite crystals whereas in samples IG_BH03_PW003, IG_BH03_PW009, IG_BH03_PW014, IG_BH03_PW017 and IG_BH03_PW019 biotite crystals were unaltered or weakly altered and showed no chloritization of biotite.

4.2 Modal composition of individual core samples from borehole IG_BH03

The modal composition of the individual samples was determined by point counting, which screened the entire thin section (about 35 x 20 mm).

The core samples consist mainly of quartz, plagioclase, alkali feldspar, biotite and muscovite + epidote/ clinozoisite in different modal compositions (Table 6). Opaque minerals, apatite, zircons and titanite are present as accessories (Table 6). The individual samples have varying proportions of altered plagioclase. The grade of alteration of plagioclase crystals also varies within the individual thin sections (Table 6).

Plagioclase is the most abundant mineral in all investigated rock samples with varying contents between 45 and 58 Vol.% (Table 6). The normalized proportion of altered plagioclase areas varies between 56 and 79 Vol.% of the detected plagioclase grains (Table 7). The proportion of quartz and alkali feldspar varies between 26 and 45 Vol.% for quartz and between 1 and 16 Vol.% for alkali feldspar (Table 6). Alteration of alkali feldspar could not be observed in any sample. The proportion of biotite is between 4 and 13 Vol.% in the investigated samples (Table 6). Minerals showing abnormal ("vibrant") or abnormal blue interference colours are summarized as muscovite and epidote/clinozoisite in Table 6 and are present in the range between 2 and 5 Vol.% in the investigated samples.

According to the modal composition determined by point counting, which is consistent with visual observations of the core in hand specimen, the individual core samples can be classified after Bas & Streckeisen (1991) and Streckeisen (1974) as phaneritic granodiorite to tonalite. The classification/nomenclature is specified by the modal mineral content of quartz (Q), plagioclase (P) and alkali feldspar (A) (Q + A + P = 100 Vol.%). After Streckeisen (1974), core samples containing 20 - 60 Vol.% quartz are defined as granodiorite with a proportion of 65 - 90 Vol% plagioclase of total feldspar (A + P = 100 Vol.%) and tonalite with a proportion of 90 - 100 Vol.% plagioclase of total feldspar (A + P = 100 Vol.%) (Table 7). The more current classification/nomenclature of Bas & Streckeisen (1991) used in this report differs from the classification/nomenclature of Streckeisen (1974). After Bas & Streckeisen (1991) the modal mineral contents of quartz, plagioclase and alkali feldspar of the individual core samples are plotted in a simplified ternary diagram (Figure 3). The percentage of alkali feldspar, determined by point counting in samples IG_BH03_PW002, IG_BH03_PW003, IG_BH03_PW005, IG_BH03_PW007, IG_BH03_PW009, IG_BH03_PW014 and IG_BH03_PW017 is in the range of 10 - 17 Vol.% of the total proportion of quartz, plagioclase and alkali feldspar (Q + A + P = 100 Vol.%, Table 7). These samples lie within the classification field of granodiorite (Figure 3). In the other samples (IG_BH03_PW011, IG_BH03_PW015 and IG_BH03_PW019), the percentage of alkali feldspar varies between 2 and 4 Vol.% of the entire proportion of quartz, plagioclase and alkali feldspar (Table 7). These samples plot within the classification field of tonalite (Figure 3). For the calculation of the proportions of quartz, plagioclase and alkali feldspar in the samples the sericitized portion of plagioclase was added to the unaltered plagioclase (i.e., Pl + altered Pl).

Table 6: Modal composition (Vol.%) of the occurring minerals obtained using point counting; Modal compositions of accessories were not determined (The modal percentage of accessories is <1 Vol.%)

Sample	Depth	Qtz	Pl	Altered Pl	Afs	Bt	Ms + Ep + Czo	Accessories
	mbgs (down hole)	Vol.%	Vol.%	Vol.%	Vol.%	Vol.%	Vol.%	Minerals
IG_BH03_PW002	242.0	41.0	15.9	24.8	8.9	4.4	5.0	Op, Ap, Zrn
IG_BH03_PW003	345.2	40.2	18.2	22.7	10.2	6.1	2.6	Op, Ap, Zrn
IG_BH03_PW005	459.2	34.6	10.6	38.6	10.2	4.1	1.9	Op
IG_BH03_PW007	503.9	26.4	13.4	33.7	8.1	13.0	5.4	Op, Ap, Zrn

Sample	Depth	Qtz	Pl	Altered Pl	Afs	Bt	Ms + Ep + Czo	Accessories
	mbgs (down hole)	Vol.%	Vol.%	Vol.%	Vol.%	Vol.%	Vol.%	Minerals
IG_BH03_PW009	554.5	33.6	11.5	31.9	12.2	5.4	5.4	Op, Ap, Zrn
IG_BH03 _PW011	608.8	43.2	19.5	27.7	2.4	5.5	1.7	Op, Ap, Zrn, Ttn
IG_BH03_PW014	669.2	32.5	20.8	27.1	9.0	7.5	3.1	Op, Ap, Zrn
IG_BH03_PW015	771.6	41.6	16.8	28.6	3.8	5.8	3.4	Op, Ap, Zrn, Ttn
IG_BH03_PW017	880.4	28.5	20.2	27.1	15.9	6.1	2.2	Op, Ap, Zrn
IG_BH03_PW019	984.7	45.2	15.8	28.1	1.4	6.8	2.7	Op, Ap, Zrn, Ttn

Table 7: Normalized modal composition (Vol.%) of quartz, plagioclase and alkali feldspar obtained using point counting and classification of rock types

Sample	Depth	Qtz	Pl + altered Pl	Afs	Rock type[1)]	Proportion Afs of total feldspar	Rock type[2)]
	mbgs (down hole)	Vol.%	Vol.%	Vol.%		Vol.%	
IG_BH03_PW002	242.0	45	45	10	Granodiorite	18	Granodiorite
IG_BH03_PW003	345.2	44	45	11	Granodiorite	20	Granodiorite
IG_BH03_PW005	459.2	37	52	11	Granodiorite	17	Granodiorite
IG_BH03_PW007	503.9	32	58	10	Granodiorite	15	Granodiorite
IG_BH03_PW009	554.5	38	49	14	Granodiorite	22	Granodiorite
IG_BH03 _PW011	608.8	46	51	3	Tonalite	5	Tonalite
IG_BH03_PW014	669.2	36	54	10	Granodiorite	16	Granodiorite
IG_BH03_PW015	771.6	46	50	4	Tonalite	8	Tonalite
IG_BH03_PW017	880.4	31	52	17	Granodiorite	25	Granodiorite
IG_BH03_PW019	984.7	50	49	2	Tonalite	3	Tonalite

according to [1)]Bas & Streckeisen (1991) and [2)]Streckeisen (1974)

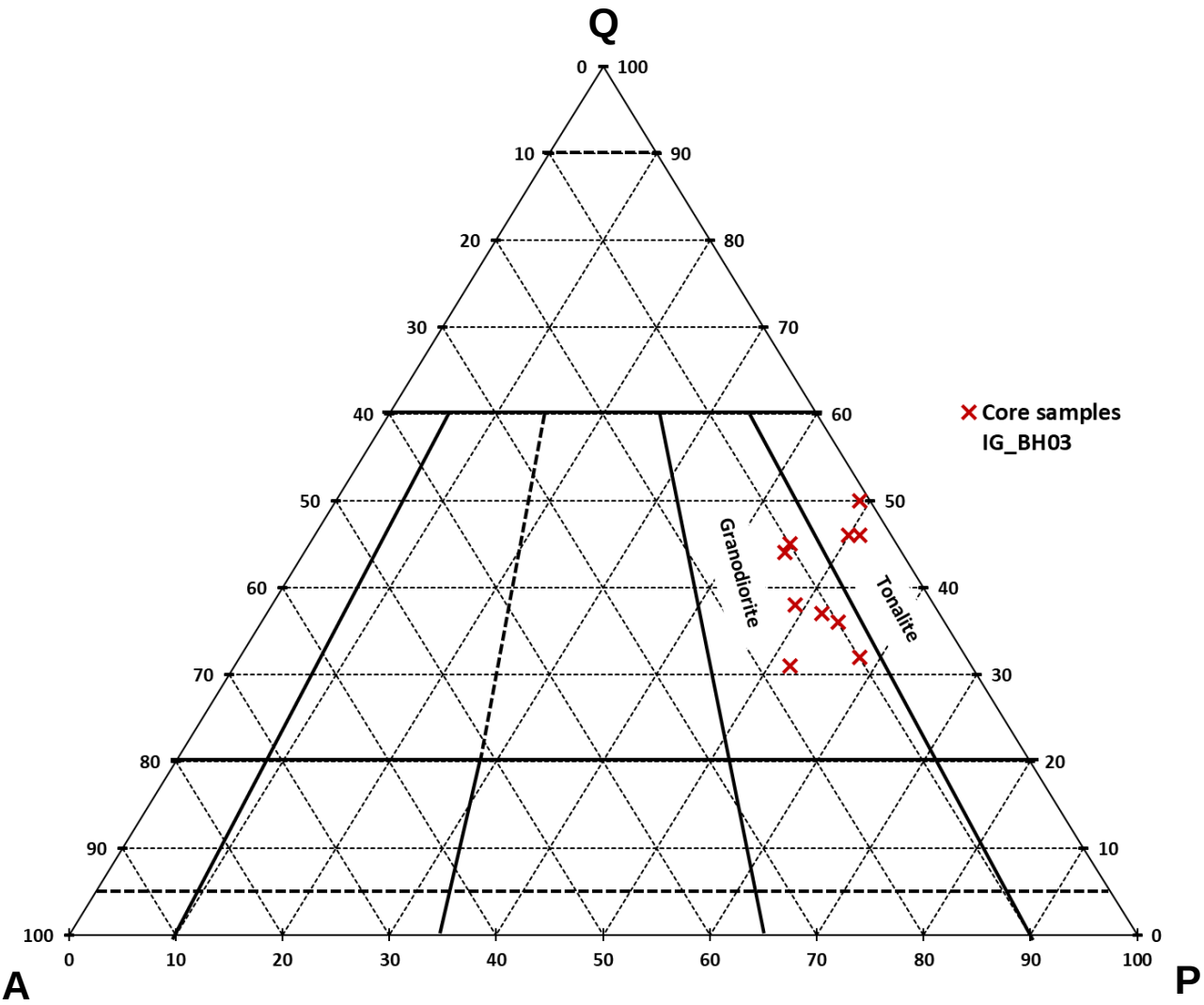

Figure 3: Classification/nomenclature according to the modal mineral content (Q + A + P = 100 Vol.%) of the individual core samples plotted in a simplified ternary Streckeisen diagram after Bas & Streckeisen (1991).

4.3 Microscopic petrographic description of individual core samples from borehole IG_BH03

Sample IG_BH03_PW002 (242.0 mbgs (down hole))

Sample IG_BH03_PW002 is a homogenous, equigranular, phaneritic granodiorite. Macroscopically, medium to coarse grained feldspars, and fine to medium grained quartz and biotite can be distinguished (Figure 4a, b). Fine grained sericite, muscovite and epidote/clinozoisite are observed microscopically as alteration products in plagioclase and around undefined grain boundaries of plagioclase and biotite (Figure 4c-k). Quartz and alkali feldspar are free from alteration products (Figure 4g, k). Very fine grained apatite, zircon, and opaque minerals are present as accessories.

Plagioclase (41 Vol.%) occurs as xenomorphic-hypidiomorphic fine to medium grained crystals, which are mainly moderately to highly altered. Few crystals are weakly altered. Plagioclase crystals contain fine grained sericite, bladed muscovite crystals and/or epidote/clinozoisite, mainly in the core of the crystal (Figure 4f, g, i), whereas the rim is free of alteration products. In some plagioclase crystals the core is only replaced by clinozoisite (Figure 4f). Lamellar twinning can be observed in few crystals, which are weakly altered.

Quartz (41 Vol.%) is present as fine to medium grained crystals and mainly occurs as clusters. Fine grained quartz is mainly present at grain boundaries to plagioclase and biotite, whereas medium grained crystals occur mostly within clusters. Medium grained quartz is frequently surrounded by fine grained quartz (Figure 4c, e, k).

The main group of biotite (12 Vol.%) is present as xenomorphic, fine to medium grained bladed crystals showing mainly brown and greenish colours/pleochroism (Figure 4c-e, h). Microfissures are frequently filled with needle-like muscovite. In association with plagioclase clinozoisite/epidote can frequently be observed as alteration product at biotite grain boundaries. It seems that some biotite crystals are partially replaced by epidote/clinozoisite (Figure 4h). Few biotite crystals show alteration to chlorite (Figure 4e). Very fine grained opaque apatite and zircon minerals can be observed as inclusions in the minor group of weakly altered biotite crystals.

About 9 Vol.% is alkali feldspar occurring as xenomorphic coarse grained crystals showing microcline twinning (grating-type structure) (Figure 4g, k). Alteration of alkali feldspar is not observed. Only in association with biotite, fine grained muscovite is present in microfissures of some alkali feldspar crystals.

Muscovite and epidote/clinozoisite make up to 5 Vol.%. Muscovite is mainly present as very fine to fine grained needle-like inclusions (sericite) or fine grained bladed crystals in moderately to highly sericitized plagioclase (Figure 4e-k). At few biotite grain boundaries muscovite also replaces biotite in the shape of fine grained bladed crystals. Epidote/clinozoisite showing abnormal yellow/blue interference colours occurs mainly as fine grained, rarely as medium grained granular crystals in the core of sericitized plagioclase and next to altered biotite (Figure 4e-k). Epidote/clinozoisite also partially replaces some biotite crystals (Figure 4h).

The intergranular pore space between quartz and feldspar minerals is open and not filled with alteration products (Figure 4c, g, k), which appears to reflect natural conditions. Along sutural weakly altered biotite grains, a clear grain boundary is generally not observed. In the vicinity of altered minerals, the intergranular pore space is also open.

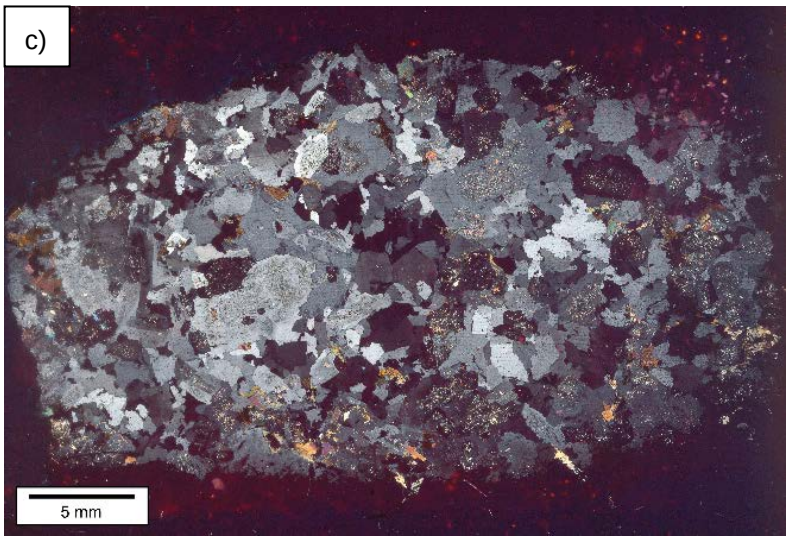

Figure 4: Sample IG_BH03_PW002 (242.0 mbgs (down hole)): a) Macroscopic appearance of the core, b) Macroscopic appearance of the core section PW002 used for thin section production c) Overview of the mineral assemblage under transmitted, cross-polarized light, d) Overview of the mineral assemblage under transmitted plane-polarized light, e) Chloritized biotite in association with weakly altered plagioclase containing bladed muscovite and granular epidote/clinozoisite under transmitted, cross-polarized light, f) Plagioclase with core containing epidote/clinozoisite under transmitted, cross-polarized light, g) Sericitized plagioclase imbedded in unaltered alkali feldspar under transmitted, cross-polarized light, h) Biotite partially replaced by epidote/clinozoisite and sericitized plagioclase under transmitted, cross-polarized light, i) Zoned plagioclase sericitized in the core and free of alteration products at the rim under transmitted, cross-polarized light, k) Altered plagioclase and unaltered quartz and alkali feldspar under transmitted, cross-polarized light.

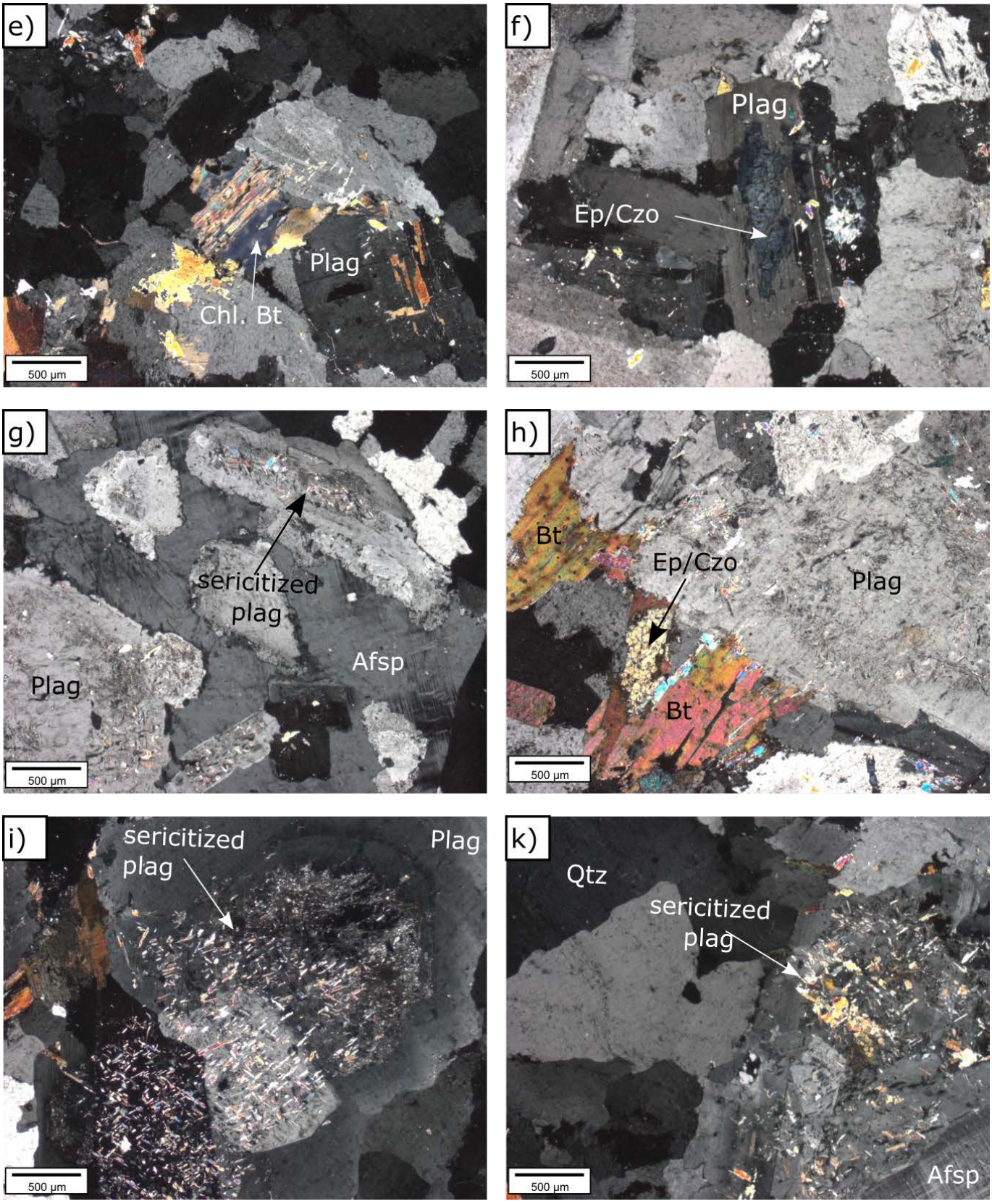

Sample IG_BH03_PW003 (345.2 mbgs (down hole))

Sample IG_BH03_PW003 is a homogenous, equigranular and phaneritic granodiorite. Macroscopically, medium to coarse grained feldspar and fine to medium grained quartz and biotite form the bulk of the rock (Figure 5a, b). Microscopically, muscovite, sericite and epidote/clinozoisite are observed as alteration products (Figure 5c-k). Opaque minerals and hypidiomorphic-idiomorphic very fine to fine grained zircon crystals with pleochroitic haloes and apatite appear as accessories.

Plagioclase (41 Vol.%) is present as xenomorphic-hypidiomorphic mainly medium grained crystals. Few crystals are coarse grained. The main group of plagioclase is moderately to highly altered and contains fine grained sericite, fine grained stalky and bladed muscovite and/or fine grained granular epidote/clinozoisite (Figure 5e-k). In moderately altered plagioclase crystals microfissures in the core are frequently filled with fine grained needle like sericite, whereas the rim is free of alteration products. In few weakly altered placioclase crystals lamellar twinning is observed (Figure 5h).

Quartz makes up to 41 Vol.% of the rock. Xenomorphic, fine to medium grained crystals frequently appear as clusters (Figure 5c, k). Few fine grained opaque minerals are present as accessories between quartz grains.

Biotite (6 Vol.%) is mainly present as unaltered to weakly altered, xenomorphic, fine to medium grained bladed crystals with varying colours/pleochroism (Figure 5c-f, h, i). In association with unaltered alkali feldspar fine grained needle like, but also stalky or bladed muscovite is present as a margin and at sutural grain boundaries of weakly altered biotite. In association with medium to highly altered plagioclase epidote/clinozoisite is present at biotite grain boundaries or biotite is replaced partially by epidote/clinozoisite (Figure 5h, i). Very fine to fine grained opaque minerals, apatite and zircons with pleochroitic haloes can be observed as inclusions in some weakly altered biotite.

Alkali feldspar (10 Vol.%) occurs as xenomorphic medium to coarse grained crystals showing microcline twinning or a microperthite texture (Figure 5f). The crystals are unaltered, but few fissures are filled with fine grained muscovite and epidote/clinozoisite.

The content of muscovite and epidote/clinozoisite in this sample is about 3 Vol.%. Muscovite occurs as fine grained needle-like inclusions (sericite) or as stalky and bladed crystals in moderately to highly sericitized plagioclase (Figure 5b, c, e, g). In association with weakly altered biotite, muscovite is present at sutural grain boundaries of biotite (Figure 5f, i). Epidote/clinozoisite showing abnormal blue/yellow or colourful interferences are associated with weakly altered biotite and moderately to highly altered plagioclase. (Figure 5c-k).

The pore space between quartz and feldspar crystals is open and not filled with alteration products (Figure 5e-g). Along sutural altered biotite grains, a clear grain boundary is generally not observed. In the vicinity of altered minerals, the intergranular pore space is also open.

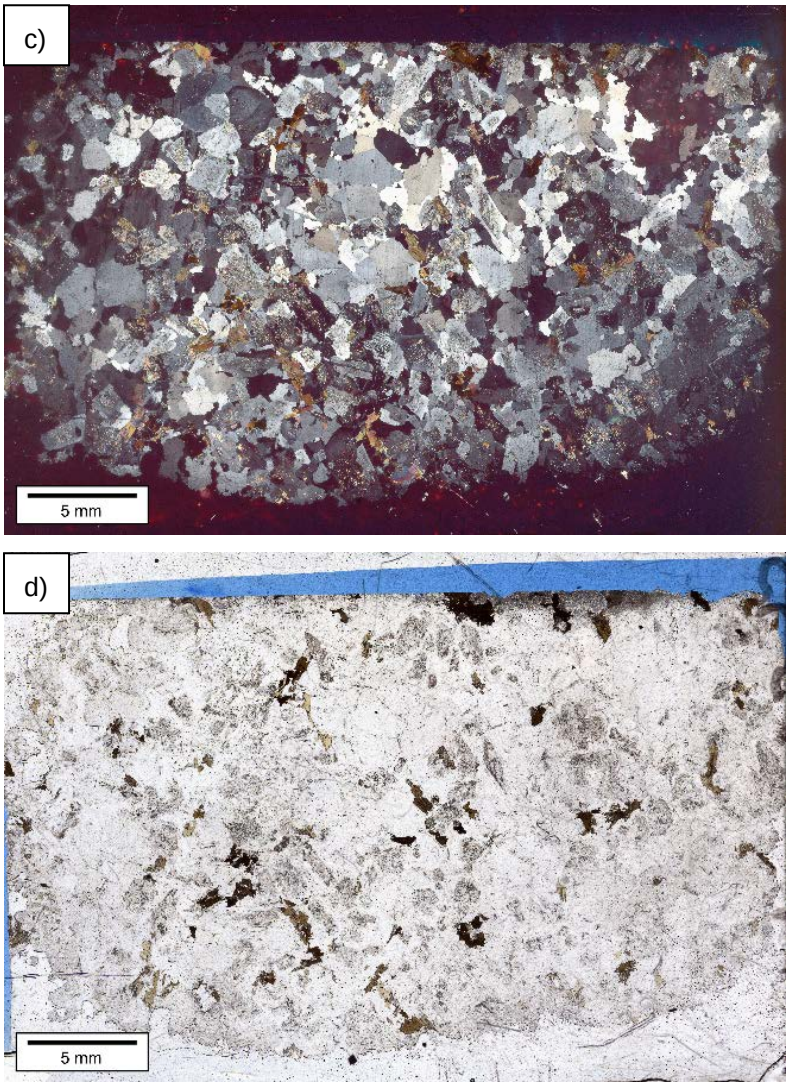

Figure 5: Sample IG_BH03_PW003 (345.2 mbgs (down hole)): a) Macroscopic appearance of the core, b) Macroscopic appearance of the core section PW003 used for thin section production c) Overview of the mineral assemblage under transmitted, cross-polarized light, d) Overview of the mineral assemblage under transmitted plane-polarized light, e) Sericitized plagioclase, weakly altered biotite and unaltered quartz under transmitted, cross-polarized light, f) Highly altered plagioclase imbedded in unaltered alkali feldspar under transmitted, cross-polarized light, g) Quartz cluster without alteration products and sericitization of sericitized core of plagioclase crystal under transmitted, cross-polarized light, h) Weakly chloritized biotite partially replaced by epidote/clinozoisite, sericitized plagioclase and unaltered quartz under transmitted, cross-polarized light, i) Altered biotite partially replaced by epidote/clinozoisite under transmitted, cross-polarized light, k) Needle like fine grained sericite and granular fine grained epidote/clinozoisite in microfissures of plagioclase under transmitted, cross-polarized light.

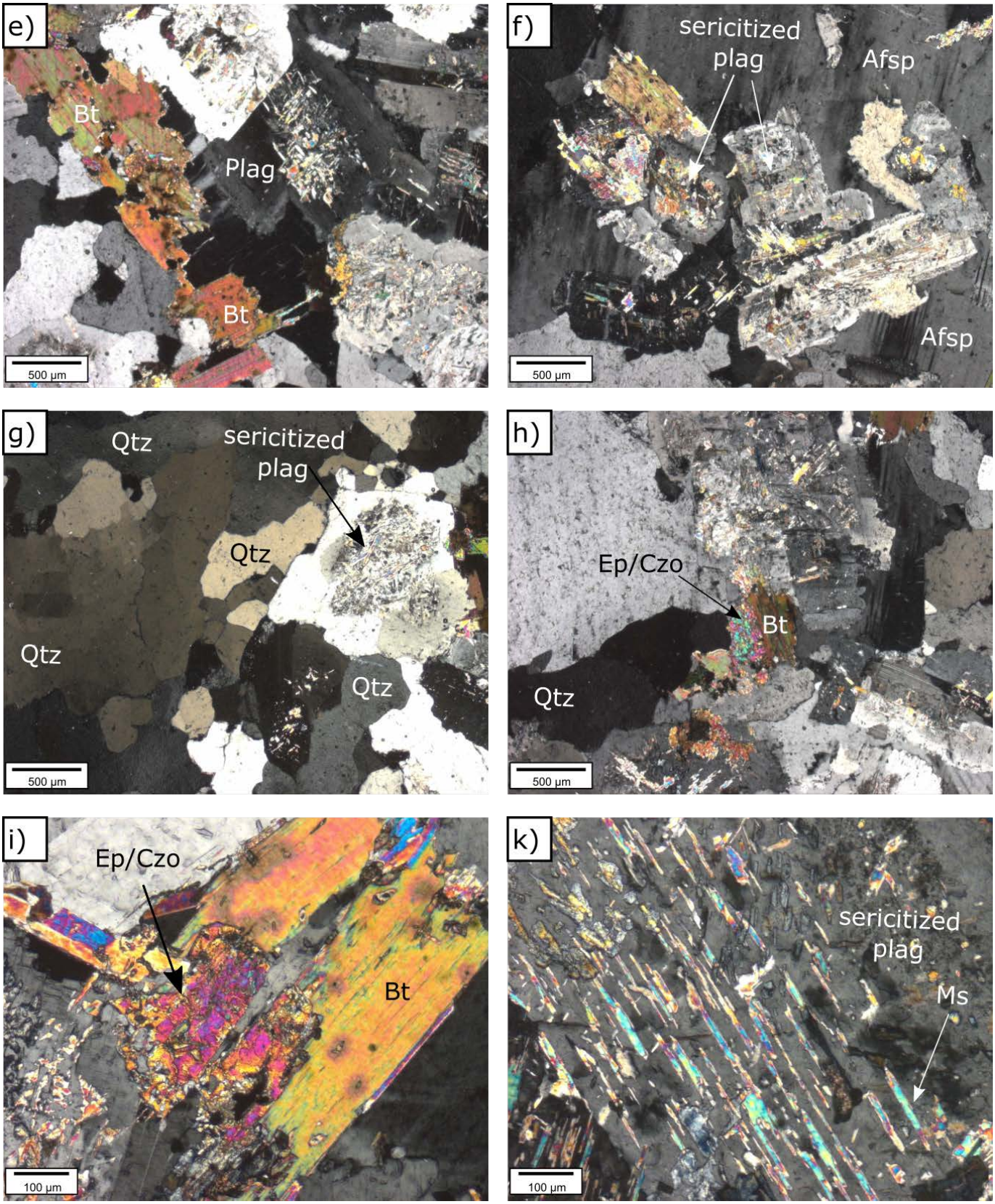

Sample IG_BH03_PW005 (459.2 mbgs (down hole))

The texture of the granodiorite sample IG_BH03_PW005 is homogenous, equigranular and phaneritic. Macroscopically, medium to coarse grained feldspar, quartz and biotite form the bulk of the rock (Figure 6a, b). Minor amounts of muscovite, sericite and epidote/clinozoisite are observed microscopically as alteration products (Figure 6c-e, g-k). Opaque minerals appear as accessories.

Plagioclase (50 Vol.%) occurs as xenomorphic-hypidiomorphic fine to medium grained crystals, which are moderately to highly altered. Moderately altered crystals contain very fine grained needle-like sericite and stalky or bladed muscovite mainly in the core of the crystal (Figure 6g). Also, stalky and bladed very fine and fine grained muscovite and epidote/clinozoisite appear as inclusions in highly altered plagioclase crystals (Figure 6e, i, k). Few weakly altered crystals show lamellar twinning.

Quartz (35 Vol.%) is present as xenomorphic, fine to medium grained crystals. Quartz crystals are frequently arranged in the shape of medium grained clusters surrounded by fine grained crystals (Figure 6f).

Biotite (4 Vol.%) is present as xenomorphic-hypidiomorphic fine to medium grained bladed crystals with varying colours/pleochroism (Figure 6c). The main group of biotite crystals shows abnormal interference colours due to a strong alteration to chlorite (Figure 6e, h). It seems that some weakly altered but also chloritized biotite crystals are partially replaced by epidote/clinozoisite (Figure 6e, h). Very fine grained opaque minerals apatite and zircon can be observed as inclusions in the minor group of weakly altered crystals.

Alkali feldspar (10 Vol.%) occurs as xenomorphic-hypidiomorphic medium grained unaltered crystals. Microcline twinning and lamellae of albite are observed in some alkali feldspar crystals (Figure 6e,g).

Bladed to stalky muscovite and granular epidote/clinozoisite (2 Vol.%) occur together with sericite as very fine to fine grained inclusions in moderately to highly sericitized plagioclase (Figure 6e,g, i, k). Few epidote/clinozoisite crystals occurring in altered plagioclase crystals show a hypidiomorphic shape (Figure 6i). Epidote/clinozoisite shows abnormal blue/yellow or colorful interferences. Stalky muscovite is also present at grain boundaries of few weakly altered and chloritized biotite crystals.

The grain boundaries between quartz and feldspar crystals are open and no alteration product is present in the pore space (Figure 6f, g). Along weakly chloritized biotite, a clear grain boundary is frequently not observed (Figure 6e,h). In the vicinity of altered minerals, the intergranular pore space is also open.

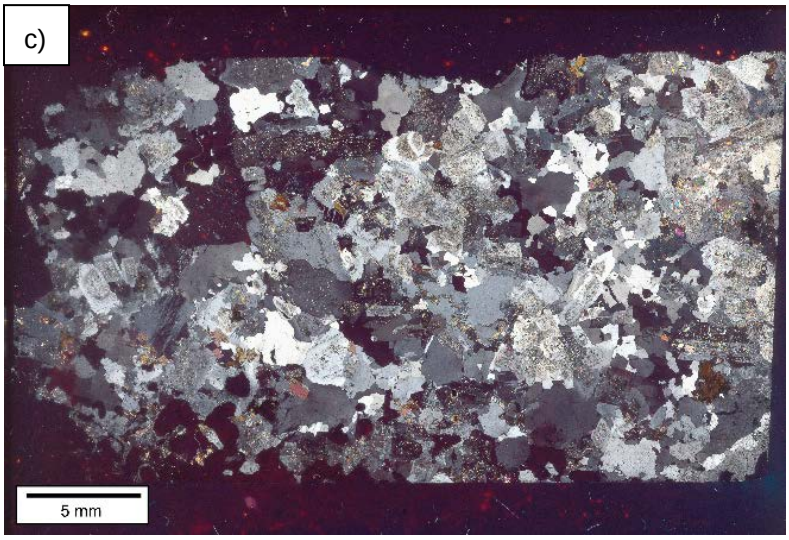

Figure 6: Sample IG_BH03_PW005 (459.2 mbgs (down hole)): a) Macroscopic appearance of the core, b) Macroscopic appearance of the core section PW005 used for thin section production c) Overview of the mineral assemblage under transmitted, cross-polarized light, d) Overview of the mineral assemblage under transmitted plane-polarized light, e) Sericitized plagioclase, chloritized biotite and unaltered alkali feldspar under transmitted, cross-polarized light, f) Quartz cluster with open grain boundaries under transmitted, cross-polarized light, g) Moderately altered plagioclase with alteration prodcucts mainly in the core and unaltered alkali feldspar under transmitted, cross-polarized light, h) Chloritized biotite with margin of fine grained epidote/clinozoisite on unaltered alkali feldspar under transmitted, cross-polarized light, i) Altered plagioclase with fine grained epidote/clinozoisite inclusions under transmitted, cross-polarized light, k) Needle like fine grained sericite and bladed muscovite inclusions in altered plagioclase under transmitted, cross-polarized light.

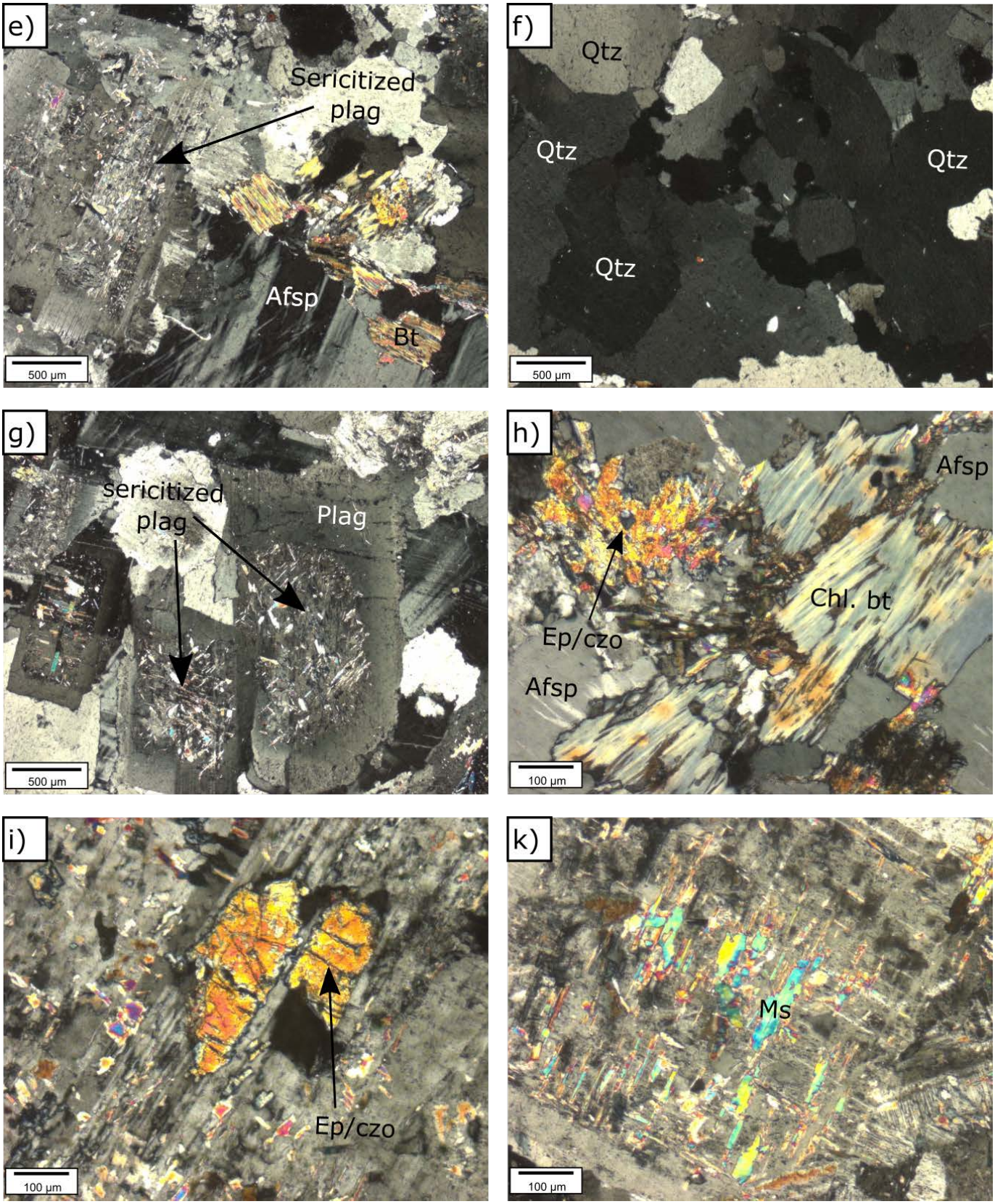

Sample IG_BH03_PW007 (503.9 mbgs (down hole))

Macroscopically, sample IG_BH03-PW007 is a homogenous, equigranular and phaneritic granodiorite containing mainly fine to medium grained feldspar, quartz and biotite (Figure 7a, b). Microscopically, muscovite, sericite and epidote/clinozoisite are observed as alteration products (Figure 7c-f). Very fine grained zircon with pleocroitic haloes, apatite crystals and opaque minerals are present as accessories. The biotite content (13 Vol.%) is high compared to the other samples, whereas the quartz content (26 Vol.%) is significantly lower.

Plagioclase (47 Vol.%) is mainly present as xenomorphic-hypidiomorphic fine to medium (few coarse) grained crystals showing a moderate to high degree of alteration. Moderately altered plagioclase crystals often contain very fine to fine grained needle like sericite, bladed or stalky musocite and granular epidote/clinozoisite, whereas the rim is free of alteration products (Figure 7f). Highly altered plagioclase contains alteration products in the whole crystal. Few weakly altered plagioclase grains only contain epidote/clinozoisite in the core (Figure 7k).

Quartz (26 Vol.%) is present as xenomorphic, fine to medium grained unaltered crystals. Quartz frequently forms clusters with few medium grained and mainly fine grained crystals (Figure 7h).

Biotite (13 Vol.%) is mainly present as xenomorphic, fine to medium grained crystals showing colours/pleochroism in the range of dark brown(ish) to light green(ish) (Figure 7d). Frequently very fine to fine grained granular epidote/clinozoisite and stalky muscovite is observed at grain boundaries to sericitized plagioclase, but in the vicinity of unaltered quartz and alkali feldspar and weakly altered plagioclase biotite shows no alteration products. Only few crystals show alteration to chlorite (Figure 7i). Very fine grained zircons with pleochroitic haloes and apatite crystals are observed as inclusions in weakly altered biotite.

Minor amounts of alkali feldspar (8 Vol.%) are present as xenomorphic fine to medium grained crystals. Alkali feldspar is unaltered and frequently shows microcline twining or lamellae of albite.

Bladed or stalky muscovite and epidote/clinozoisite (5 Vol.%) are present as very fine to fine grained inclusions in sericitized plagioclase and in association with weakly altered or chloritized biotite (Figure 7e, f, g, i, k). Fine grained xenomorphic-hypidiomorphic epidote/clinozoisite with abnormal blue/yellow and colourful interferences also partially replaces some weakly or chloritized biotite crystals (Figure 7i).

The pore space between quartz and feldspar grains is open and no alteration products are observed (Figure 7e, h). In the presence of alteration products at the grain boundaries of altered or chloritized biotite grains, a clear grain boundary generally is not observed (Figure 7e, g, i).

Figure 7: Sample IG_BH03_PW007 (503.9 mbgs (down hole)): a) Macroscopic appearance of the core, b) Macroscopic appearance of the core section PW007 used for thin section production c) Overview of the mineral assemblage under transmitted, cross-polarized light, d) Overview of the mineral assemblage under transmitted plane-polarized light, e) Sericitized plagioclase, weakly altered biotite with margin of fine grained muscovite and unaltered alkali feldspar under transmitted, cross-polarized light, f) Sericitized plagioclase and biotite under transmitted, cross-polarized light, g) Sericitized plagioclase in association with weakly altered biotite and epidote/clinozoisite under transmitted, cross-polarized light, h) Quartz cluster with open grain boundaries under transmitted, cross-polarized light, i) Chloritized biotite partially replaced by epidote/clinozoisite under transmitted, cross-polarized light, k) Plagioclase containing fine grained epidote/clinozoisite under transmitted, cross-polarized light

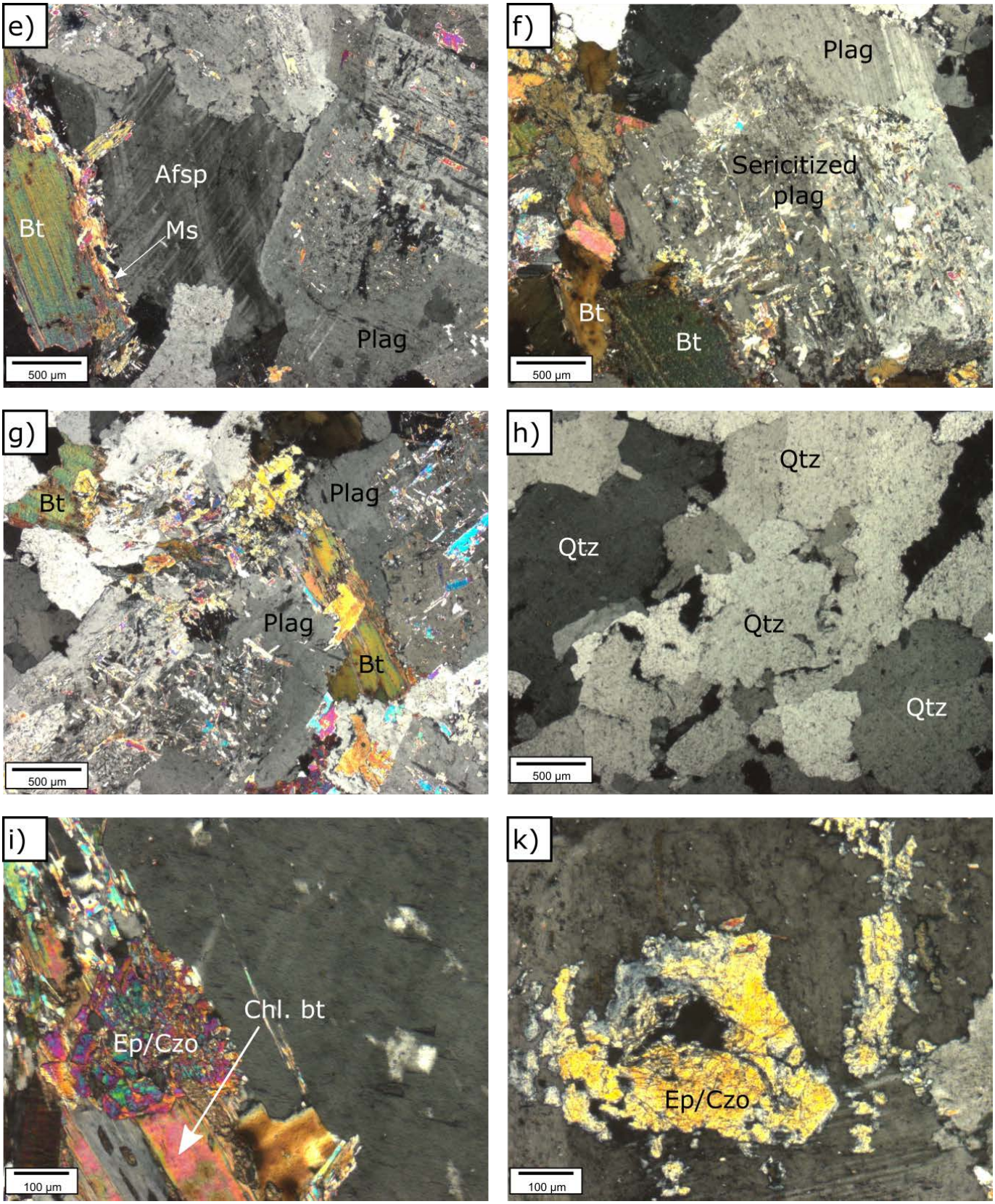

Sample IG_BH03_PW009 (554.5 mbgs (down hole))

Sample IG_BH03-PW009 is a homogenous, equigranular, phaneritic granodiorite (Figure 8a, b). Macroscopically, fine to medium grained feldspar, quartz and biotite can be distinguished (Figure 8b). The red colour of some plagioclase in this rock sample might be due to iron replacing some calcium ions in the plagioclase crystal lattice (staining of plagioclase crystals). Minor amounts of muscovite, sericite and epidote/clinozoisite are observed microscopically as alteration products (Figure 8c-k). Apatite, zircon and opaque minerals are present as accessories.

Plagioclase (44 Vol.%) occurs as xenomorphic-hypidiomorphic fine to medium grained crystals which are moderately to highly altered. The main group of plagioclase contains bladed or stalky fine grained muscovite, granular epidote/clinzoisite and microfissures filled with very fine grained sericite (Figure 8f, g, h). In few moderately altered plagioclase crystals lamellar twinning can be observed (Figure 8h).

Quartz (34 Vol.%) mainly occurs as xenomorphic-hypidiomorphic fine to medium grained crystals. Few quartz grains are coarse grained. Quartz is frequently arranged in the shape of clusters and no alteration products can be observed between quartz grains (Figure 8c).

Biotite (5 Vol.%) occurs in minor amounts in the sample. Biotite is present as xenomorphic-hypidiomorphic fine to medium grained crystals showing no or a low degree of alteration (Figure 8i, k). Weakly altered crystals are associated with granular epidote/clinozoisite and fine grained needle-like muscovite which is present as a margin around weakly altered biotite and at sutural grain boundaries (Figure 8e, i, k). Few weakly altered biotite grains are associated with hypidiomorphic to idiomorphic epidote/clinozoisite (Figure 8i, k). Very fine grained zircons with pleochroitic haloes and apatite crystals are observed as inclusions in weakly altered biotite.

Alkali feldspar (12 Vol.%) occurs as xenomorphic fine to coarse grained crystals. They are mainly free from alteration products, but in association with biotite, few crystals show muscovite and epidote/clinozoisite in microfissures (Figure 8e). Few crystals show microcline twinning or lamellae of albite (Figure 8e, f).

Very fine grained sericite, and very fine to fine grained muscovite and epidote/clinozoisite (5 Vol.%) occur as alteration products in moderately to highly sericitized plagioclase and in association with weakly altered biotite (Figure 8e-k). In association with weakly altered biotite, muscovite is present at sutural grain boundaries of biotite (Figure 8i, k). Few fine grained epidote/clinozoisite crystals show a hypidiomorphic shape (Figure 8k).

The pore space between quartz grains is open and not filled with alteration products (Figure 8c, g). In association with weakly altered biotite, the grain boundaries are not defined due to a margin of fine grained needle-like muscovite (Figure 8k).

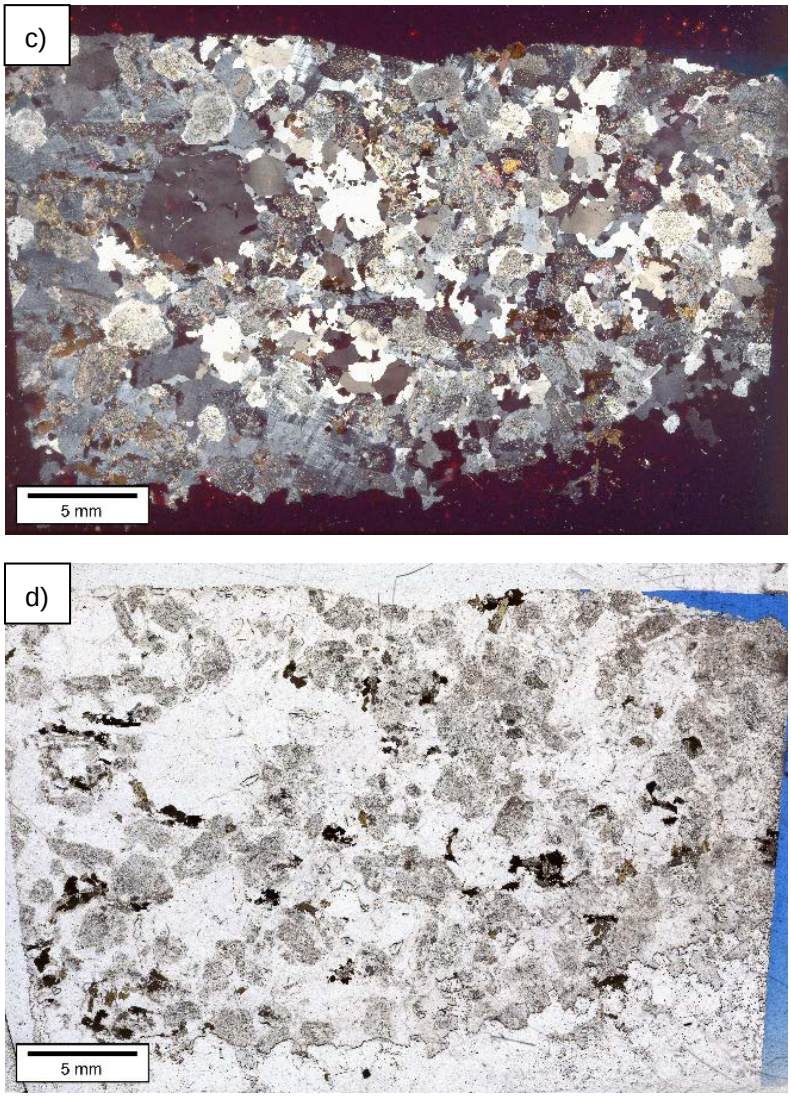

Figure 8: Sample IG_BH03_PW009 (554.5 mbgs (down hole)): a) Macroscopic appearance of the core, b) Macroscopic appearance of the core section PW009 used for thin section production c) Overview of the mineral assemblage under transmitted, cross-polarized light, d) Overview of the mineral assemblage under transmitted plane-polarized light, e) Weakly altered biotite partially replaced by epidote/clinozoisite and margin of fine grained muscovite embedded in unaltered alkali feldspar under transmitted, cross-polarized light, f) Sericitized plagioclase, weakly altered biotite partially replaced by epidote/clinozoisite on unaltered alkali feldspar showing microcline twinning under transmitted, cross-polarized light, g) Highly sericitized plagioclase associated with epidote/clinozoisite and fine grained quartz at quartz/plagioclase grain boundary under transmitted, cross-polarized light, h) Highly altered plagioclase containing sericite, bladed muscovite and granular epidote/clinozoisite under transmitted, cross-polarized light, i) Weakly altered biotite partially replaced by epidote/clinozoisite and unaltered quartz under transmitted, cross-polarized light, k) Weakly altered biotite with margin of muscovite and embedded epidote/clinozoisite under transmitted, cross-polarized light.

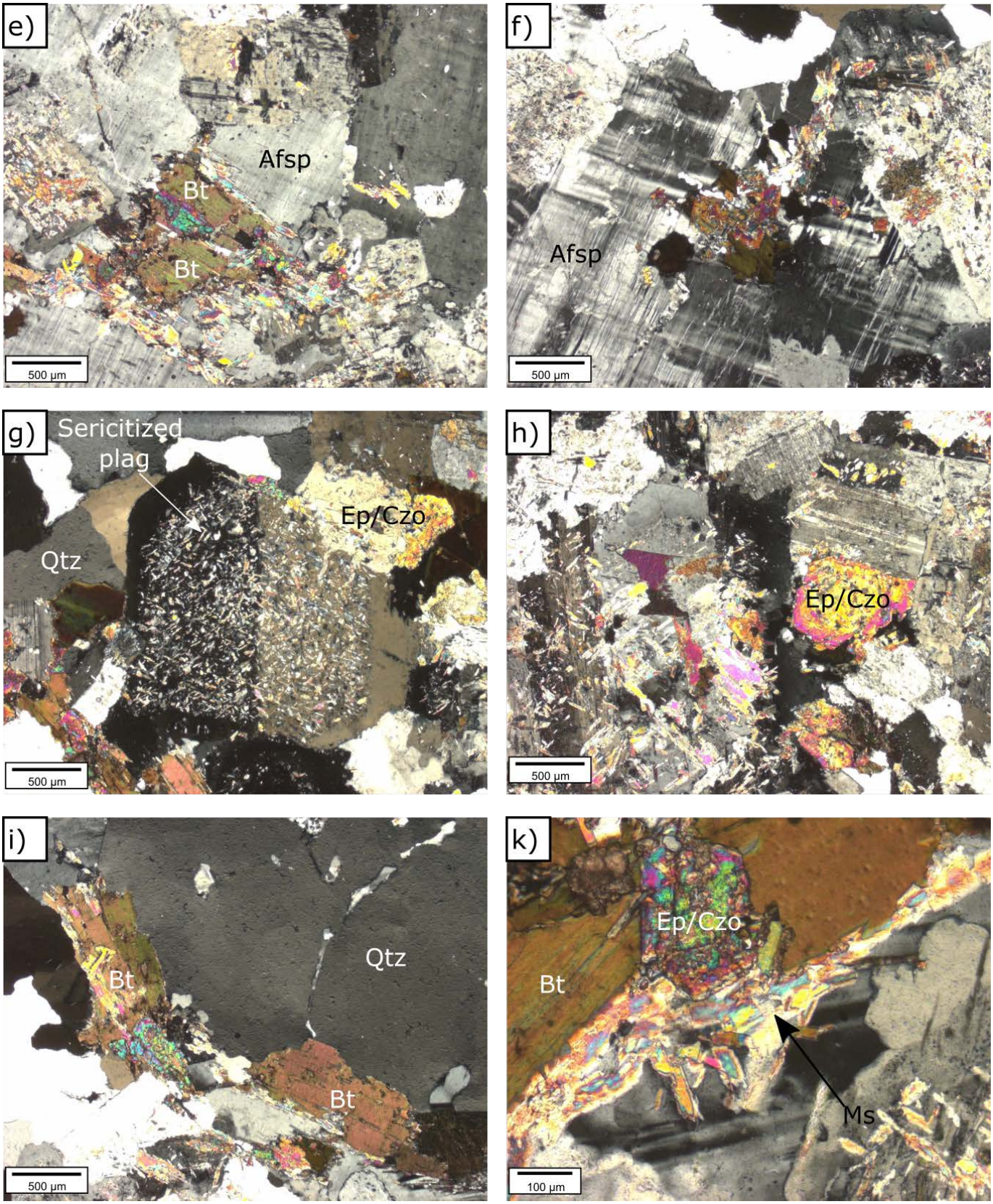

Sample IG_BH03_PW011 (608.8 mbgs (down hole))

Sample IG_BH03_PW011 consists of a homogenous, equigranular, phaneritic tonalite (Figure 9a, b). Macroscopically, no alteration is observed and fine to medium grained feldspar, quartz and biotite can be distinguished. Minor amounts of muscovite, epidote/clinozoisite and sericite are observed microscopically as alteration products (Figure 9c-k). Apatite, zircon, titanite and opaque minerals are present as accessories.

Plagioclase (48 Vol.%) occurs as xenomorphic-hypidiomorphic fine to medium grained crystals, which show variable degrees of alteration. In some weakly to moderately altered plagioclase crystals a strong zonation with alteration products only occurring in the core of the grain can be observed (Figure 9f, h, i). Few unaltered and some weakly to moderately altered crystals show lamellar twinning. In moderately to highly altered plagioclase very fine grained sericite, bladed and stalky muscovite and/or granular epidote/clinozoisite are present (Figure 9g, h, i). In some crystals only granular epidote/clinozoisite is present as alteration product (Figure 9g).

Quartz (43 Vol.%) is present as xenomorphic, fine to medium grained crystals, which are frequently arranged in the shape of clusters (Figure 9c, e, g). No alteration products are observed between quartz grains.

Biotite (5 Vol.%) appears as xenomorphic-hypidiomorphic fine to medium grained bladed crystals which are unaltered or weakly altered and show varying colours/pleochroism (Figure 9c, d, e, k). Few crystals show alteration from biotite to chlorite (Figure 9i). In association with quartz, alkali feldspar and unaltered to weakly altered plagioclase biotite grains show sutural grain boundaries with a margin of very fine grained needle like muscovite (Figure 9k). In the vicinity to altered plagioclase also fine grained granular epidote/clinozoisite is present (Figure 9i). Few fine grained titanite crystals and very fine grained zircons with pleochroitic haloes and apatite crystals are observed as inclusions in unaltered and weakly altered biotite.

The alkali feldspar content (2 Vol.%) is very low compared to the other samples. Alkali feldspar occurs as unaltered xenomorphic-hypidiomorphic fine to medium grained crystals, which show microcline twinning.

Minor amounts of sericite, muscovite and epidote/clinozoisite (2 Vol.%) occur as very fine to fine grained inclusions in weakly to highly sericitized plagioclase (Figure 9f-i). In association with weakly altered biotite, muscovite frequently forms a sutural texture at the grain boundaries (Figure 9k). Compared to some other samples the amount of alteration products is relatively low in this rock sample. This might be due to the low amount of biotite and a lower overall alteration degree in rock sample PW011.

The pore space between grain boundaries of quartz and feldspar is open and not filled with alteration products (Figure 9e-g). Along sutural altered biotite grains, no clear grain boundary can be observed (Figure 9k). The pore space also is open if no alteration minerals are present.

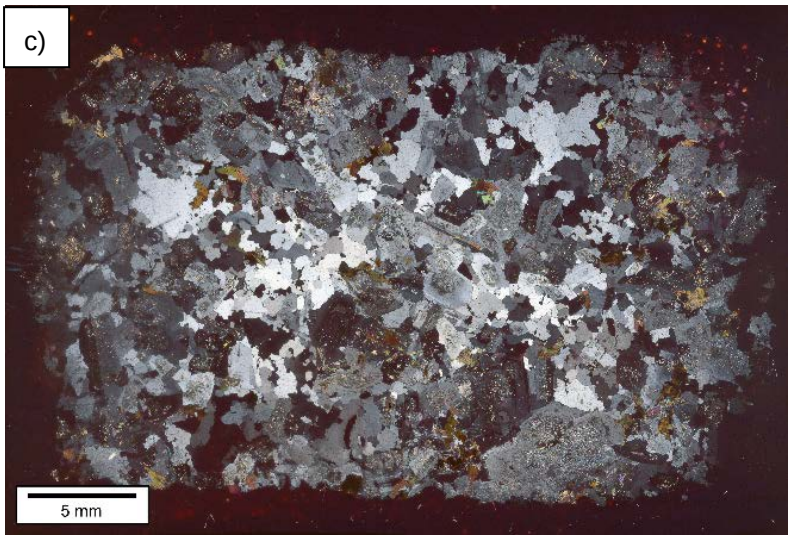

Figure 9: Sample IG_BH03_PW011 (608.8 mbgs (down hole)): a) Macroscopic appearance of the core, b) Macroscopic appearance of the core section PW011 used for thin section production c) Overview of the mineral assemblage under transmitted, cross-polarized light, d) Overview of the mineral assemblage under transmitted plane-polarized light, e) Quartz cluster with open grain boundaries and unaltered biotite under transmitted, cross-polarized light, f) Weakly altered plagioclase and unaltered quartz under transmitted, cross-polarized light, g) Unaltered quartz and moderately altered plagioclase containing granular epidote/clinozoisite under transmitted, cross-polarized light, h) Moderately altered plagioclase in association with weakly altered biotite and epidote/clinozoisite under transmitted, cross-polarized light, i) Weakly altered plagioclase, weakly chloritized biotite and epidote/clinozoisite under transmitted, cross-polarized light, k) Weakly altered biotite and margin of muscovite at sutural grain boundaries under transmitted, cross-polarized light.

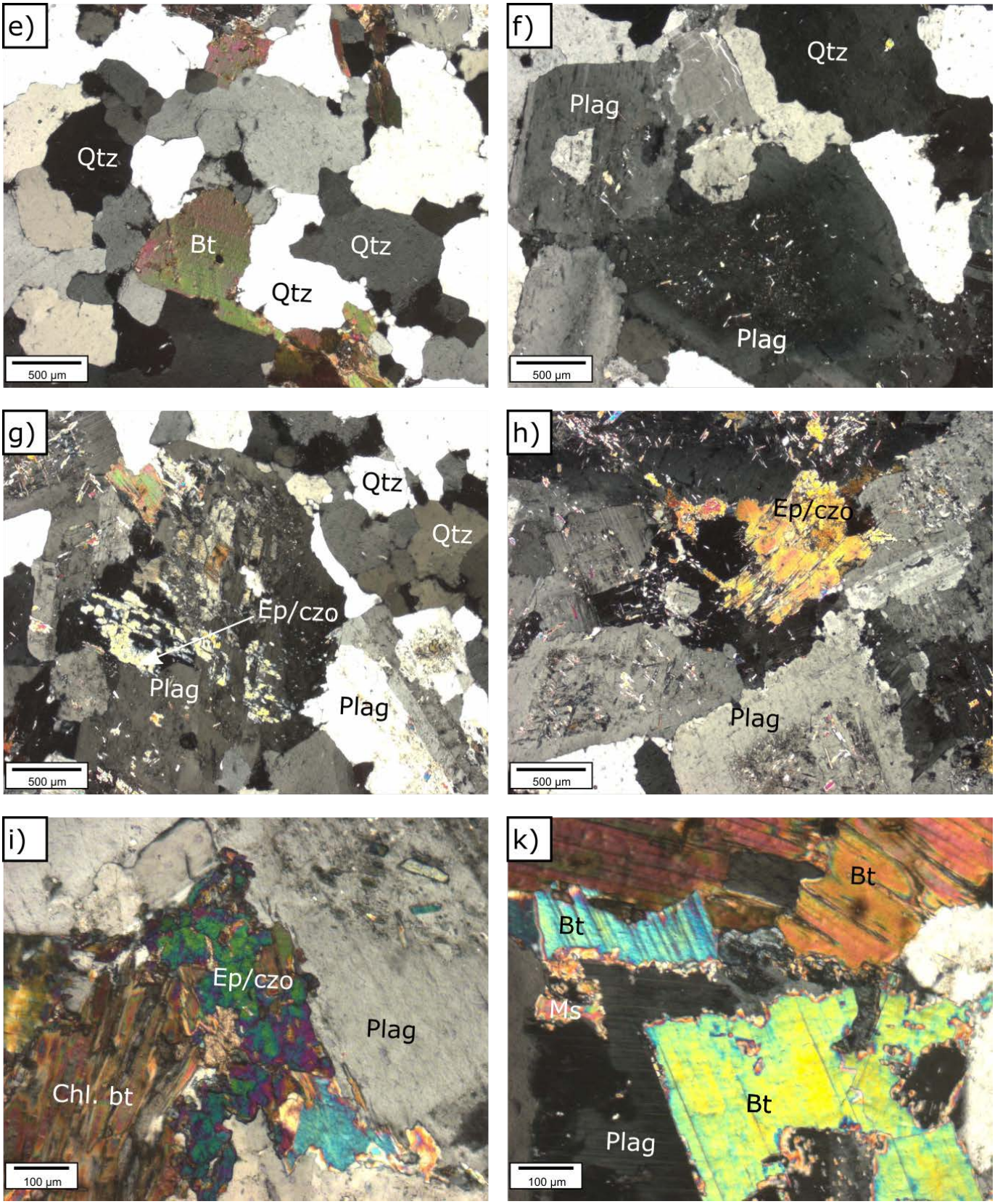

Sample IG_BH03_PW014 (669.2 mbgs (down hole))

Sample IG_BH03_PW014 is a homogenous, equigranular, phaneritic granodiorite. It is mainly composed of fine to medium grained feldspar, quartz and biotite (Figure 10a, b). Plagioclase and alkali feldspar can be distinguished microscopically in the thin section (Figure 10d). Minor amounts of muscovite, sericite and epidote/clinozoisite occur as alteration products (Figure 10c-k). Apatite, zircon and opaque minerals are present as accessories.

Plagioclase makes up to 48 Vol.% and occurs as xenomorphic–hypidiomorphic, fine to coarse grained crystals. The main group of plagioclase is moderately to highly altered and contains fine grained sericite, fine grained stalky and bladed muscovite and/or fine grained granular epidote/clinozoisite (Figure 10e, g, k). In moderately altered plagioclase crystals microfissures in the core are frequently filled with very fine grained needle like sericite, whereas the rim is free of alteration products. Highly altered plagioclase contains very fined grained sericite, stalky and or bladed muscovite and granular epidote/clinozoisite. In few unaltered or weakly altered plagioclase crystals a strong zonation or lamellar twinning is observed (Figure 10i).

Quartz crystals (33 Vol.%) are xenomorphic and mainly fine to medium grained. Few crystals are coarse grained. Quartz frequently occurs in the form of clusters (Figure 10c, e, f).

The main group of biotite (7 Vol.%) is present as xenomorphic, fine to medium grained bladed crystals showing mainly brown and greenish colours/pleochroism (Figure 10c, d, f-h). As in sample IG_BH03_PW011 no alteration of biotite to chlorite is observed. Weakly altered crystals seem to be partially replaced by fine grained epidote/clinozoisite and in association with altered plagioclase epidote/clinozoisite is frequently present at biotite grain boundaries (Figure 10h). Very fine grained opaque minerals apatite and zircon can be observed as inclusions in some unaltered or weakly altered crystals.

Alkali feldspar (9 Vol.%) is present as xenomorphic-hypidiomorphic fine to coarse grained crystals which are unaltered. Some alkali feldspar grains surround fine to medium grained plagioclase and biotite and fine grained epidote/clinozoisite (Figure 10g-i). Some crystals show lamellae of albite (microcline-perthite) or microcline twinning (Figure 10g-i).

Sericite, muscovite and epidote/clinozoisite (3 Vol.%) occur as very fine to fine grained needle-like, bladed or granular inclusions in weakly to highly sericitized plagioclase (Figure 10e-g, k). In association with weakly altered biotite and altered plagioclase epidote/clinozoisite is also frequently present.

The pore space between quartz and feldspar grains is open and free from alteration products (Figure 10e, f, i). Sutural grain boundaries of biotite crystals can not be observed in this rock sample.

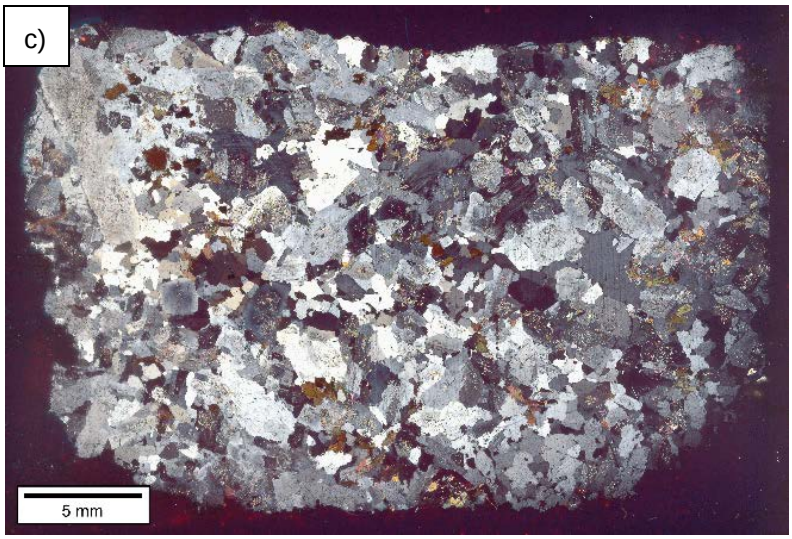

Figure 10: Sample IG_BH03_PW014 (669.2 mbgs (down hole)): a) Macroscopic appearance of the core, b) Macroscopic appearance of the core section PW0014 used for thin section production c) Overview of the mineral assemblage under transmitted, cross-polarized light, d) Overview of the mineral assemblage under transmitted plane-polarized light, e) Unaltered quartz and weakly to moderately altered plagioclase under transmitted, cross-polarized light, f) Sericitized plagioclase, weakly altered biotite partially replaced by epidote/clinozoisite and unaltered alkali feldspar under transmitted, cross-polarized light, g) Weakly altered biotite, and highly altered plagioclase on unaltered alkali feldspar under transmitted, cross-polarized light, h) Unaltered biotite with undefined grain boundaries on unaltered alkali feldspar showing microcline twinning under transmitted, cross-polarized light, i) Weakly to moderately altered plagioclase with strong zonation and unaltered alkali feldspar under transmitted, cross-polarized light, k) Sericitized plagioclase and unaltered alkali feldspar with microcline twinning under transmitted, cross-polarized light.

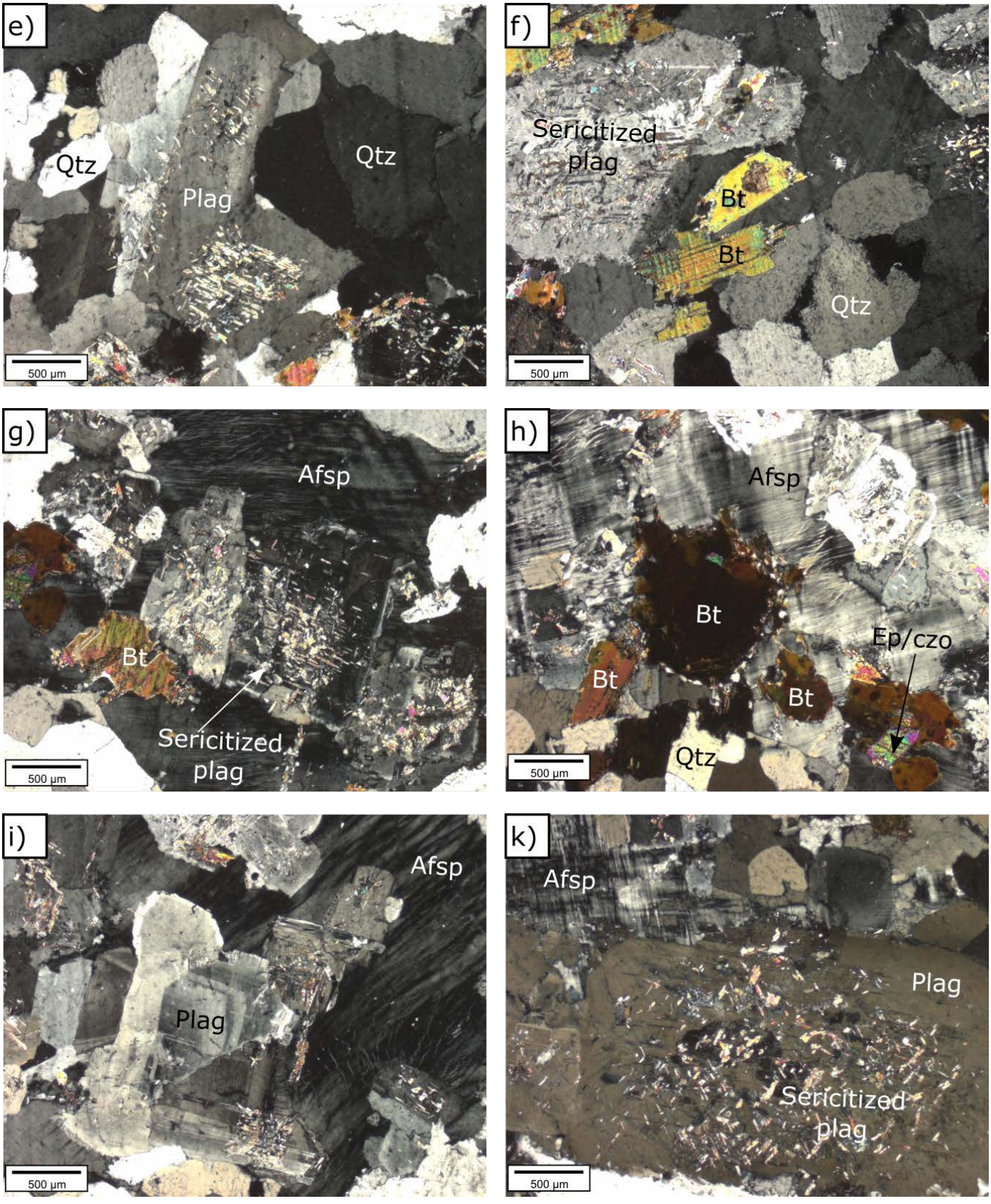

Sample IG_BH03_PW015 (771.6 mbgs (down hole))

Sample IG_BH03_PW015 is a homogenous, equigranular and phaneritic tonalite. Macroscopically, medium to coarse grained feldspar and fine to medium grained quartz and biotite form the bulk of the rock (Figure 11a, b). The red colour of this sample might be due to staining of plagioclase crystals by iron ions replacing calcium ions in the plagioclase crystal lattice. Microscopically, muscovite, sericite and epidote/clinozoisite are observed as alteration products (Figure 11c-h, k). Opaque minerals and hypidiomorphic-idiomorphic very fine to fine grained zircon crystals with pleochroitic haloes, apatite and titanite appear as accessories.

Plagioclase (46 Vol.%) is present as xenomorphic-hypidiomorphic medium grained crystals. The main group of plagioclase is moderately to highly altered and contains fine grained sericite, fine grained stalky and bladed muscovite and/or fine grained granular epidote/clinozoisite (Figure 11e, f, h). Some moderately altered plagioclases contain mainly granular epidote/clinozoisite in the core of the crystal, whereas the rim is free of alteration products. Few weakly altered plagioclases show lamellar twinning.

Quartz makes up to 42 Vol.% of the rock. Xenomorphic, fine to medium grained crystals frequently appear as clusters (Figure 11f, i). Few fine grained opaque minerals are present as accessories between quartz grains.

Biotite (6 Vol.%) is mainly present as xenomorphic, fine to medium grained crystals showing colours/pleochroism in the range of dark brown(ish) to light green(ish) (Figure 11d). Frequently very fine to fine grained granular epidote/clinozoisite and stalky muscovite is observed at grain boundaries to sericitized plagioclase, but in the vicinity of unaltered quartz and alkali feldspar and weakly altered plagioclase biotite shows no alteration products. Only few biotite crystals show alteration to chlorite and a partial replacement of biotite by fine grained epidote/clinozoisite (Figure 11e, k). Very fine grained zircons with pleochroitic haloes, apatite and titanite crystals are observed as inclusions in weakly altered biotite.

A low proportion of alkali feldspar (4 Vol.%) is present as xenomorphic medium grained crystals showing microcline twinning or a microperthite texture. In association with alkali feldspar no alteration products are observed (Figure 11g).

The content of muscovite and epidote/clinozoisite in this sample is about 3 Vol.%. Muscovite occurs as fine grained needle-like inclusions (sericite) or as stalky and bladed crystals in moderately to highly sericitized plagioclase (Figure 11e, f, h). In general, epidote/clinozoisite showing blue/yellow and colourful interferences are associated with weakly altered biotite and moderately to highly altered plagioclase and some biotite crystals seem to be replaced partially by epidote/clinozoisite (Figure 11e, f, h, k).

The pore space between quartz and feldspar crystals is open and not filled with alteration products (Figure 11i). Along sutural altered biotite grains and next to alteration products, a clear grain boundary is generally not observed. In the vicinity of altered minerals, the intergranular pore space also is open.

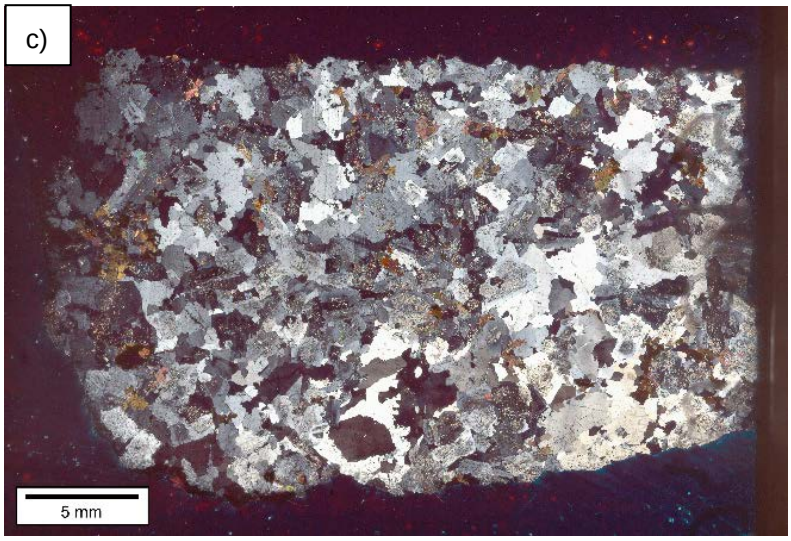

Figure 11: Sample IG_BH03_PW015 (771.6 mbgs (down hole)): a) Macroscopic appearance of the core, b) Macroscopic appearance of the core section PW0015 used for thin section production c) Overview of the mineral assemblage under transmitted, cross-polarized light, d) Overview of the mineral assemblage under transmitted plane-polarized light, e) Highly altered plagioclase in association with biotite and epidote/clinozoisite under transmitted, cross-polarized light, f) Moderately altered plagioclase with mainly granular epidote/clinozoisite in the core, unaltered biotite and epidote/clinzoisite under transmitted, cross-polarized light, g) Unaltered quartz and alkali feldspar with microcline twining and altered plagioclase under transmitted, cross-polarized light, h) Altered plagioclase in association with weakly altered biotite and epidote/clinozoisite under transmitted, cross-polarized light, i) Unaltered biotite and quartz with open grain boundaries under transmitted, cross-polarized light, k) Chloritized biotite partially replaced by epidote/clinozoisite under transmitted, cross-polarized light.

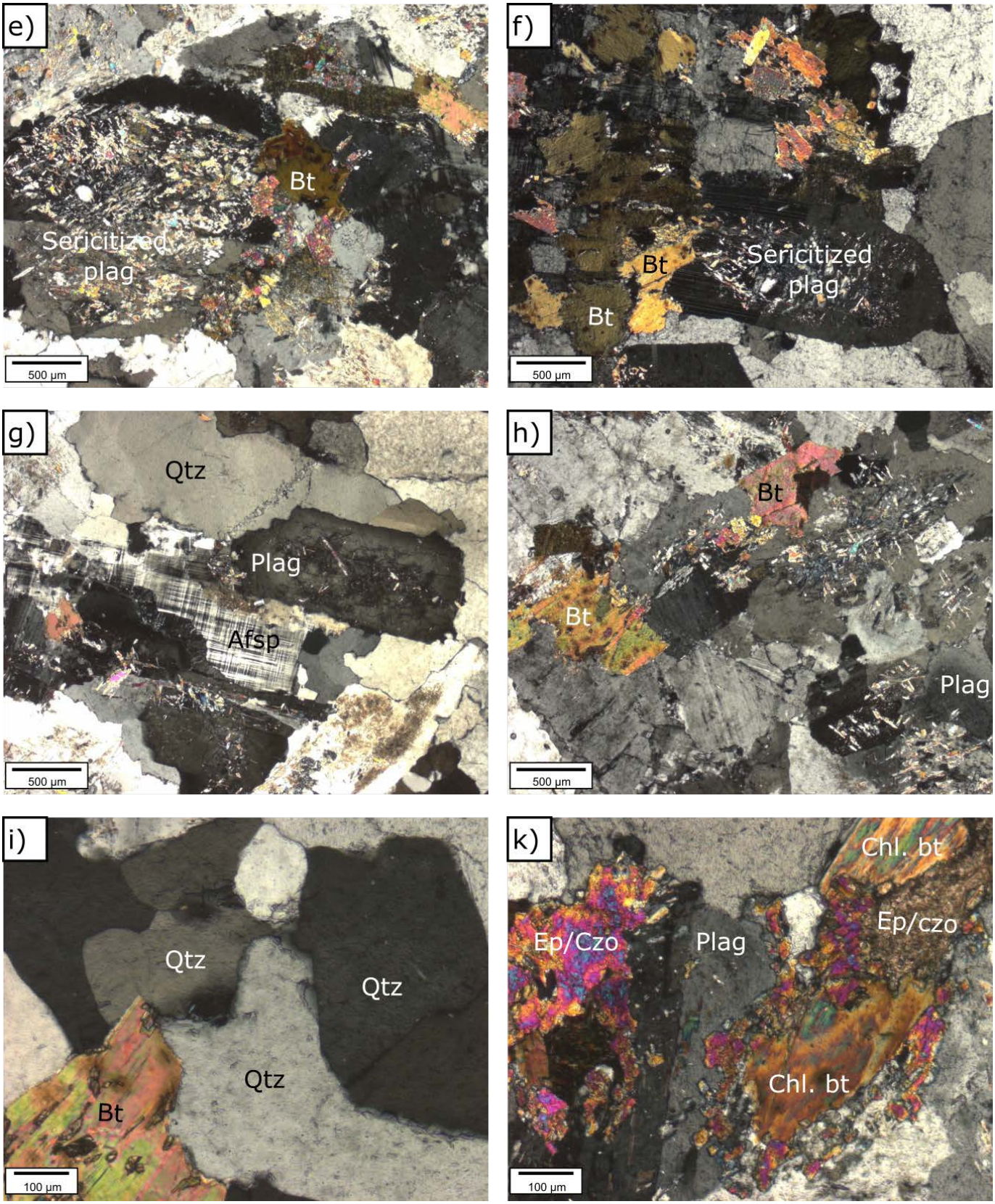

Sample IG_BH03_PW017 (880.4 mbgs (down hole))

Sample IG_BH03_PW017 is a homogenous, equigranular, phaneritic granodiorite (Figure 12a, b). Macroscopically, fine to medium grained feldspar, quartz and biotite can be distinguished (Figure 12b). Minor amounts of muscovite, sericite and epidote/clinozoisite are observed microscopically as alteration products (Figure 12c-k). Apatite, zircon and opaque minerals are present as accessories.

Plagioclase (47 Vol.%) is present as xenomorphic-hypidiomorphic fine to medium grained crystals showing variable degrees of alteration. In moderately to highly altered plagioclase microfissures are often filled with fine grained needle like sericite and/or granular epidote/clinozoisite (Figure 12e, f, h-k). In association with weakly altered biotite fine grained epidote/clinozoisite is frequently present next to plagioclase (Figure 12k). Weakly altered plagioclase crystals that are not associated with biotite contain fine grained bladed muscovite as inclusions and frequently show lamellar twinning (Figure 12g). In few weakly altered plagioclase crystals granular epidote/clinozoisite is present in their core whereas the rim is free of alteration products (Figure 12).

Quartz (29 Vol.%) mainly occurs as xenomorphic-hypidiomorphic fine to medium grained crystals. Quartz is frequently arranged in the shape of clusters and no alteration products can be observed between quartz grains. Few fine grained opaque minerals are observed as accessories between quartz grains (Figure 12d).

Biotite (6 Vol.%) is present as xenomorphic-hypidiomorphic fine to medium grained crystals showing no or a low degree of alteration (Figure 122e, h, k). Weakly altered crystals are associated with granular epidote/clinozoisite and fine grained needle-like muscovite which is present as a margin around weakly altered biotite and at sutural grain boundaries (Figure 12k). Very fine grained zircons with pleochroitic haloes and apatite crystals are observed as inclusions in weakly altered biotite.

The alkali feldspar content (16 Vol.%) is high compared to the other core samples. Alkali feldspar mainly occurs as xenomorphic fine to medium grained crystals showing no alteration products. Few crystals are coarse grained. The main group of alkali feldspar shows microcline twinning or lamellae of albite (Figure 12e, f).

Very fine grained sericite, and very fine to fine grained muscovite and epidote/clinozoisite (2 Vol.%) occur as alteration products in moderately to highly sericitized plagioclase and in association with weakly altered biotite (Figure 12e-k). In association with weakly altered biotite, muscovite is present at sutural grain boundaries of biotite (Figure 12k). Epidote/clinozoisite is also observed as hypidiomorphic granular inclusions in some plagioclase crystals (Figure 12k).

The pore space between quartz grains is open and not filled with alteration products (Figure 12d). In association with weakly altered biotite, the grain boundaries are not defined due to a margin of fine grained needle-like muscovite (Figure 12h, k).

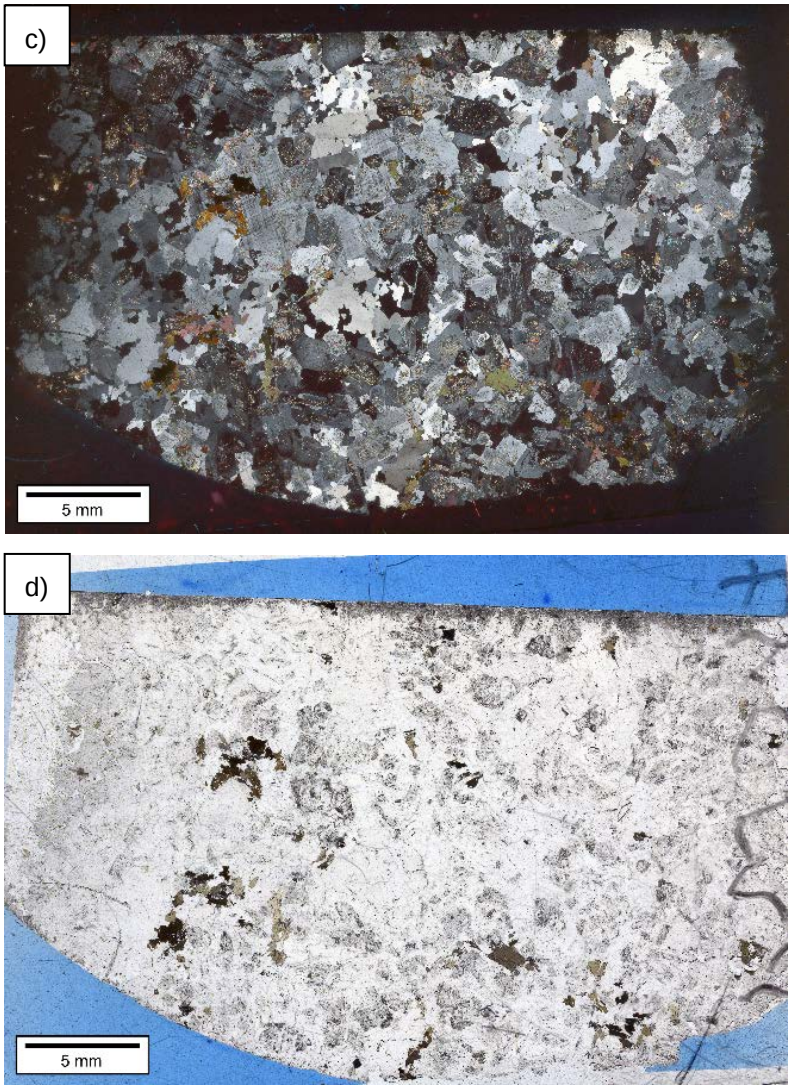

Figure 12: Sample IG_BH03_PW017 (880.4 mbgs (down hole)): a) Macroscopic appearance of the core, b) Macroscopic appearance of the core section PW0017 used for thin section production c) Overview of the mineral assemblage under transmitted, cross-polarized light, d) Overview of the mineral assemblage under transmitted plane-polarized light, e) Altered plagioclase and biotite on unaltered alkali feldspar showing microcline twinning under transmitted, cross-polarized light, f) Weakly altered plagioclase with granular epidote/clinozoisite in the core of the crystal and unaltered alkali feldspar under transmitted, cross-polarized light, g) Weakly altered plagioclase with bladed muscovite inclusions and lamellar twinning under transmitted, cross-polarized light, h) Highly sericitized plagioclase and weakly altered biotite partially replaced by epidote/clinozoisite under transmitted, cross-polarized light, i) Microfissures of plagioclase filled with needle like very fine grained sericite and granular epidote/clinozoisite under transmitted, cross-polarized light, k) Weakly altered biotite with margin of muscovite at sutural grain boundary and epidote/clinzoisite under transmitted, cross-polarized light.

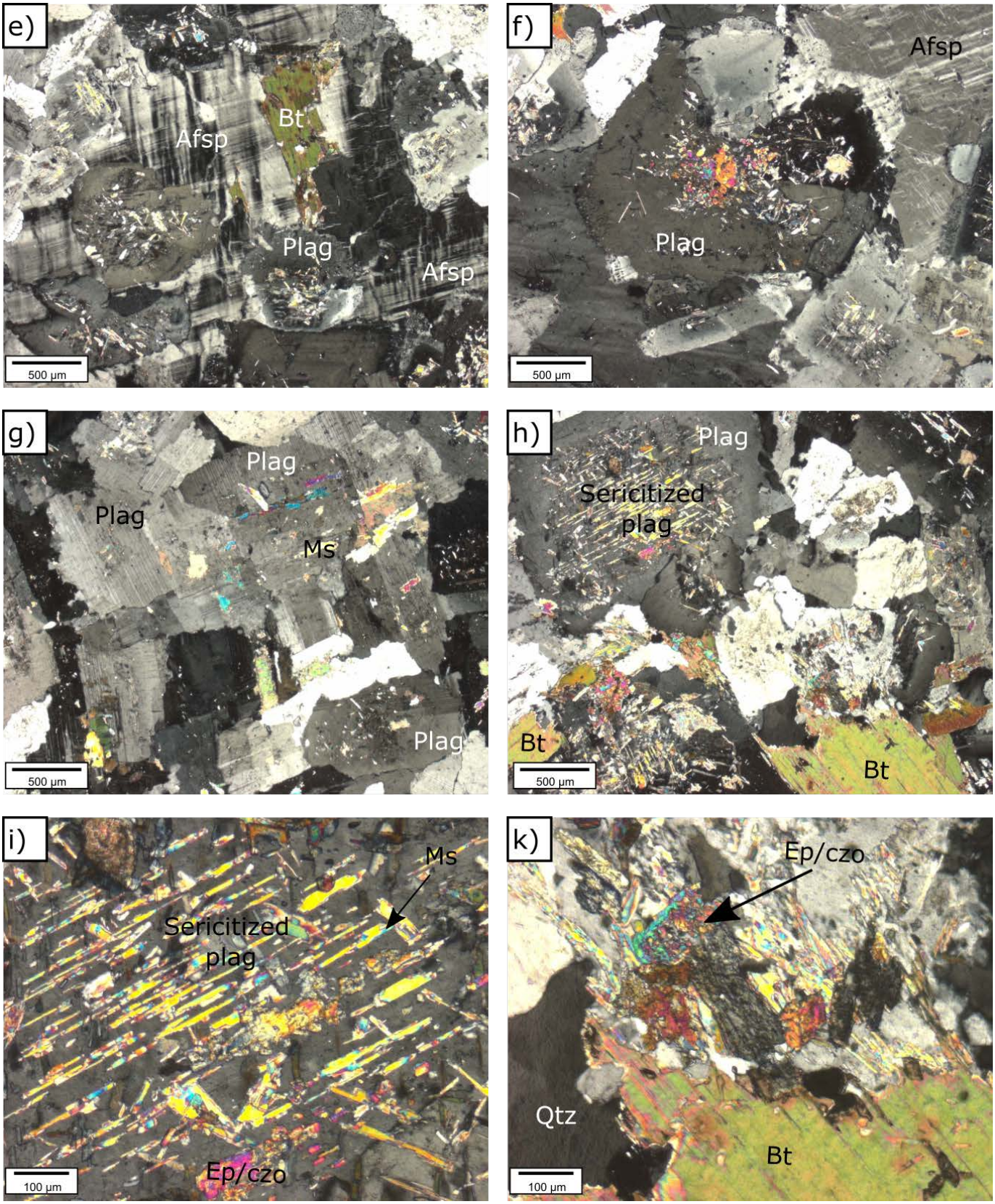

Sample IG_BH03_PW019 (984.7 mbgs (down hole))

Sample IG_BH03_PW019 is a homogenous, equigranular, phaneritic tonalite. It is mainly composed of fine to medium grained feldspar, quartz and biotite (Figure 13a, b). The proportion of alkali feldspar which can be distinguished microscopically from plagioclase is very low in this thin section (Figure 13d). Minor amounts of muscovite, sericite and epidote/clinozoisite occur as alteration products (Figure 13c-k). Apatite, zircon, titanite and opaque minerals are present as accessories.

Plagioclase makes up to 44 Vol.% and occurs as xenomorphic–hypidiomorphic, fine to coarse grained crystals. Few plagioclase crystals are coarse grained. In this rock sample plagioclase shows varying alteration degrees. Some plagioclase crystals are unaltered or weakly altered (Figure 13h, k) and show lamellar twinning. Moderately to highly altered plagioclase contains fine grained sericite, fine grained stalky and bladed muscovite and/or fine grained granular epidote/clinozoisite (Figure 13e-k).

The quartz content (45 Vol.%) is very high in this rock sample. Quartz occurs as xenomorphic and mainly fine to medium grained crystals. Few crystals are coarse grained. Quartz frequently occurs in the form of clusters (Figure 13d, e, i). No alteration products are observed between quartz grains.

The main group of biotite (7 Vol.%) is present as xenomorphic, fine to medium grained bladed crystals showing mainly brown and greenish colours/pleochroism (Figure 13c). In this rock sample no alteration of biotite to chlorite is observed. Weakly altered crystals seem to be partially replaced by fine grained epidote/clinozoisite and in association with altered plagioclase epidote/clinozoisite is frequently present at biotite grain boundaries (Figure 13f, i, k). Very fine grained opaque minerals apatite, zircon and titanite can be observed as inclusions in some unaltered or weakly altered crystals.

The alkali feldspar content is very low compared to the other thin sections (1 Vol.%). Alkali feldspar is present as xenomorphic fine grained crystals which are unaltered. Some crystals show lamellae of albite (microcline-perthite) or microcline twinning (Figure 13e).

Sericite, muscovite and epidote/clinozoisite (3 Vol.%) occur as very fine to fine grained needle-like, bladed or granular inclusions in weakly to highly sericitized plagioclase (Figure 13d-k). In association with weakly altered biotite and altered plagioclase epidote/clinozoisite is also frequently present. It seems that epidote/clinozoisite partially replaces some biotite crystals (Figure 13f, i, k).

The pore space between quartz and feldspar grains is open and free from alteration products (Figure 13d-g, i). Sutural grain boundaries of biotite crystals cannot be observed in this rock sample.

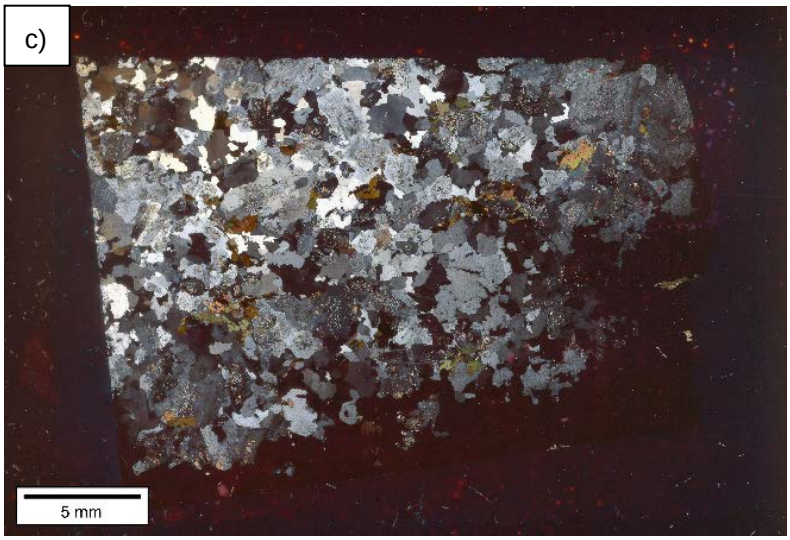

Figure 13: Sample IG_BH03_PW019 (984.7 mbgs (down hole)): a) Macroscopic appearance of the core, b) Macroscopic appearance of the core section PW0019 used for thin section production c) Overview of the mineral assemblage under transmitted, cross-polarized light, d) Overview of the mineral assemblage under transmitted plane-polarized light, e) Altered plagioclase and weakly altered biotite next to unaltered quartz and alkali feldspar showing microcline twinning under transmitted, cross-polarized light, f) Altered plagioclase and biotite in association with granular epidote/clinozoisite in the core of plagioclase and at plagioclase biotite grain boundaries under transmitted, cross-polarized light, g) Plagioclase with lamellar twinning containing alteration products mainly in the core next to weakly altered biotite, epidote/clinozoisite and unaltered quartz under transmitted, cross-polarized light, h) Plagioclase with varying degree of alteration under transmitted, cross-polarized light, i) Biotite in association with highly altered plagioclase partially replaced by epidote/clinozoisite and unaltered quartz under transmitted, cross-polarized light, k) Biotite partially replaced by epidote/clinozoisite and weakly altered plagioclase under transmitted, cross-polarized light.

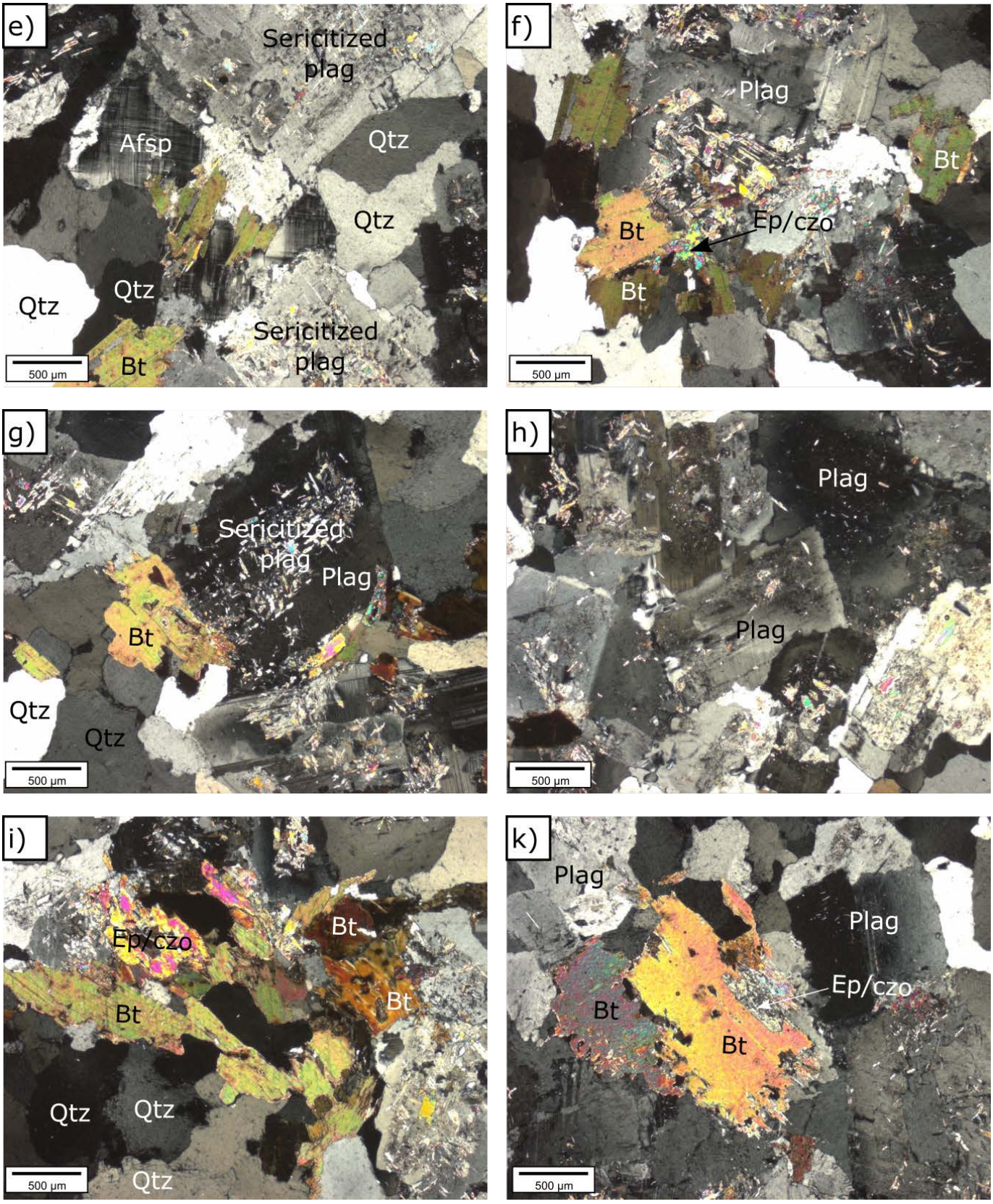

5.0 WATER CONTENT AND WATER-LOSS POROSITY

Water content, bulk density and water-loss porosity were determined on originally saturated segments of the core samples from borehole IG_BH03. The water content was determined by two independent methods, i.e., gravimetrically by drying rock sections at 105 °C to stable weight conditions, and by using the isotope diffusive exchange technique (see Section 3). The gravimetric water content (WC_{grav}) was determined on different segments of the core samples (i.e., on those pieces used for the individual experiments). The initial saturated weight of all these samples was recorded directly after unpacking and preparation of the samples in the laboratory. This ensures that the calculation of the porewater mass is not affected by any possible changes induced during the experiments. Such possible changes were monitored as well by recording the sample weight right after termination of the experiment and before the drying process began. The water loss was calculated using the initial wet weight measured in the lab and the final weight after drying.

The exact determination of the in-situ mass of porewater is of particular importance when using indirect extraction methods, because porewater tracer concentrations are calculated by mass balance equations using the mass of porewater (cf. Section 3). Knowledge of the water-loss porosity (calculated from the water content and density) is further required for the derivation of diffusion coefficients (cf. Section 7).

5.1 Water contents

Gravimetric water contents were determined on the individual core segments used for the specific experiments (cf. Section 3).

5.1.1 Gravimetric water contents determined on aqueous extraction core samples

The gravimetric water contents were determined on different aliquots, with weights between 84 g and 404 g, of the ten AQ samples taken between 238 and 985 mbgs (down hole). These values were further used for the estimation of porewater Cl- and Br-concentrations determined by aqueous extraction experiments (cf. chapter 6.1).

The gravimetric water contents determined on individual aliquots of the AQ samples vary between 0.15 wt.% and 0.30 wt.%, with weighted values ranging between 0.17 ± 0.01 and 0.23 ± 0.05 wt.% (Table 8).

The water contents determined by taking the wet (WC_{wet}) and dry weight (WC_{dry}) are similar within the first two decimal places due to the low water masses in the investigated cores.

The water contents determined on the individual aliquots of the different AQ samples vary significantly, probably due to mineralogical heterogeneities (Table 6).

Table 8: Gravimetric water contents of aliquots of AQ core samples from borehole IG_BH03 used for aqueous extraction experiments using wet (WC_{wet}) and dry masses (WC_{dry}) of the individual core pieces. The weighted values are calculated by using the individual masses

		Aq.ex. subsample A			Aq.ex. subsample B			Aq.ex. subsample C			Aq.ex. subsample D			WC weighted		
Sample	Depth	mass	WCwet	WCdry	mass	WCwet	WCdry	mass	WCwet	WCdry	mass	WCwet	WCdry	WCwet	WCdry	Stdev
	mbgs*	g	wt.%	wt.%	g	wt.%	wt.%	g	wt.%	wt.%	g	wt.%	wt.%	wt.%	wt.%	wt.%
IG_BH03_AQ001	238.8	404.17	0.18	0.18	176.91	0.24	0.24	228.98	0.23	0.23	380.07	0.21	0.21	**0.21**	**0.21**	**0.02**
IG_BH03_AQ002	346.0	191.56	0.19	0.19	121.45	0.22	0.22	149.06	0.24	0.24				**0.21**	**0.21**	**0.02**
IG_BH03_AQ003	460.1	346.66	0.20	0.20	123.25	0.22	0.22	175.28	0.22	0.22				**0.21**	**0.21**	**0.01**
IG_BH03_AQ004	504.2	327.44	0.20	0.20	122.73	0.27	0.27	210.91	0.22	0.22				**0.22**	**0.22**	**0.04**
IG_BH03_AQ005	554.7	310.66	0.20	0.20	153.28	0.30	0.30	96.39	0.21	0.21				**0.23**	**0.23**	**0.05**
IG_BH03_AQ006	608.6	364.20	0.21	0.21	136.45	0.26	0.26	114.20	0.21	0.21				**0.22**	**0.22**	**0.03**
IG_BH03_AQ007	665.9	256.38	0.18	0.18	123.33	0.21	0.21	121.73	0.25	0.25				**0.21**	**0.21**	**0.03**
IG_BH03_AQ008	771.8	367.02	0.19	0.19	150.01	0.20	0.20	185.25	0.22	0.22				**0.20**	**0.20**	**0.01**
IG_BH03_AQ009	880.1	345.38	0.15	0.15	124.15	0.16	0.16	142.76	0.26	0.26				**0.18**	**0.18**	**0.06**
IG_BH03_AQ010	985.0	383.36	0.17	0.17	91.85	0.18	0.18	83.93	0.20	0.20				**0.17**	**0.17**	**0.01**

* mbgs (down hole)

5.1.2 Gravimetric water contents determined on porewater cores

Gravimetric water contents were determined on different aliquots of the ten large sized PW samples taken between 242 and 985 mbgs (down hole).

Gravimetric water contents determined on head pieces

During sample preparation, the head pieces with weights between 133 g and 236 g were cut, weighed and dried at 105 °C to obtain a first estimate about the water contents of the investigated core samples.

The gravimetric water contents determined on the head pieces of the PW core samples vary between 0.16 wt.% and 0.26 wt.%, with weighted WC_{grav} values between 0.16 ± 0.01 wt.% and 0.25 ± 0.02 wt.% (Table 9).

The water contents determined by taking the wet (WC_{wet}) and dry weight (WC_{dry}) are similar within the first two decimal places due to the low water masses in the investigated cores.

The water contents determined on the two head pieces of the different PW samples vary, which is most likely due to mineralogical heterogeneities (Table 6).

Table 9: Gravimetric water contents of head pieces of PW core samples from borehole IG_BH03 using wet (WC_{wet}) and dry masses (WC_{dry}) of the individual core pieces. The weighted values are calculated by using the individual masses.

		Subsample A			Subsample B			WC weighted		
Sample	Depth	mass	WCwet	WCdry	mass	WCwet	WCdry	WCwet	WCdry	Stdev
	mbgs*	g	wt.%	wt.%	g	wt.%	wt.%	wt.%	wt.%	wt.%
IG_BH03_PW002	242.0	160.93	0.23	0.23	193.11	0.23	0.23	**0.23**	**0.23**	**0.01**
IG_BH03_PW003	345.2	174.61	0.18	0.18	181.28	0.23	0.24	**0.21**	**0.21**	**0.04**
IG_BH03_PW005	459.2	201.18	0.21	0.21	178.65	0.23	0.23	**0.22**	**0.22**	**0.02**
IG_BH03_PW007	503.9	206.32	0.19	0.19	223.07	0.24	0.24	**0.22**	**0.22**	**0.03**
IG_BH03_PW009	554.5	211.50	0.23	0.23	198.14	0.24	0.24	**0.23**	**0.23**	**0.01**
IG_BH03_PW011	608.8	198.12	0.26	0.26	220.54	0.24	0.24	**0.25**	**0.25**	**0.02**
IG_BH03_PW014	669.2	233.27	0.19	0.19	196.24	0.17	0.17	**0.18**	**0.18**	**0.01**
IG_BH03_PW015	771.6	212.09	0.19	0.19	236.64	0.20	0.20	**0.19**	**0.19**	**0.01**
IG_BH03_PW017	880.4	128.75	0.17	0.17	201.57	0.16	0.16	**0.16**	**0.16**	**0.01**
IG_BH03_PW019	984.7	221.11	0.19	0.19	133.32	0.17	0.17	**0.18**	**0.18**	**0.02**

* mbgs (down hole)

Gravimetric water contents determined on out-diffusion cores

Gravimetric water contents on large sized 1,444 g to 1,544 g core pieces were determined by the weights taken before and after their long-term immersion in deionised water during out-diffusion experiments. The weight differences of cores before and after out-diffusion experiments are between 0.010 g and 0.196 g (Table 10, Figure 14). Seven of the ten samples have weights between 0.040 g to 0.196 g lower after the experiments than before the experiments, whereas three samples have weights between 0.010 g and 0.087 g higher than before the experiments. The differences result from the determination of the initial weight after surface drying of the cores (as defined in Section 3.2).

The gravimetric water contents determined on the out-diffusion cores vary between 0.17 wt.% and 0.24 wt.% with weighted WC_{grav} values ranging between 0.17 ± 0.01 wt.% and 0.24 ± 0.01 wt.% (Table 10). The weight differences of the core samples determined before (b.e.) and after the experiments (a.e.) result in water content variations of 0.01 wt.% for three samples and 0.02 wt.% for one sample (Table 10, Figure 15). These differences are within the error ranges determined by Gaussian error propagation (Table 10, Figure 15). The water contents determined by taking the wet (WC_{wet}) and dry weight (WC_{dry}) are similar within the first two decimal places due to the low water masses in the investigated cores (Table 10).

Table 10: Gravimetric water contents of out-diffusion core samples from borehole IG_BH03 calculated by the mass of cores determined before (b.e.) and after (a.e.) experiments using wet (WC_{wet}) and dry masses (WC_{dry}) of the individual core pieces; the error of the water content is determined by Gaussian error propagation (Appendix III)

		mass core			mass porewater		$WC_{grav,wet}$		$WC_{grav,dry}$		Error WC_{grav}
Sample	Depth	wet b.e.	wet a.e.	Δm_{core}	m_{core} b.e.	m_{core} a.e.	m_{core} b.e.	m_{core} a.e.	m_{core} b.e.	m_{core} a.e.	
	mbgs*	g	g	g	g	g	wt.%	wt.%	wt.%	wt.%	wt.%
IG_BH03_PW002	242.0	1459.255	1459.099	-0.156	3.249	3.093	0.22	0.21	0.22	0.21	0.01
IG_BH03_PW003	345.2	1444.500	1444.510	0.010	2.799	2.809	0.19	0.19	0.19	0.19	0.01
IG_BH03_PW005	459.2	1480.681	1480.550	-0.131	3.352	3.221	0.23	0.22	0.23	0.22	0.01
IG_BH03_PW007	503.9	1474.450	1474.341	-0.109	3.134	3.025	0.21	0.21	0.21	0.21	0.01
IG_BH03_PW009	554.5	1470.020	1469.899	-0.121	3.482	3.361	0.24	0.23	0.24	0.23	0.01
IG_BH03_PW011	608.8	1489.780	1489.584	-0.196	3.218	3.022	0.22	0.20	0.22	0.20	0.02
IG_BH03_PW014	669.2	1527.808	1527.870	0.062	2.702	2.764	0.18	0.18	0.18	0.18	0.01
IG_BH03_PW015	771.6	1544.553	1544.640	0.087	3.207	3.294	0.21	0.21	0.21	0.21	0.01
IG_BH03_PW017	880.4	1453.355	1453.315	-0.040	2.605	2.565	0.18	0.18	0.18	0.18	0.01
IG_BH03_PW019	984.7	1492.304	1492.244	-0.060	2.531	2.471	0.17	0.17	0.17	0.17	0.01

***** mbgs (down hole)

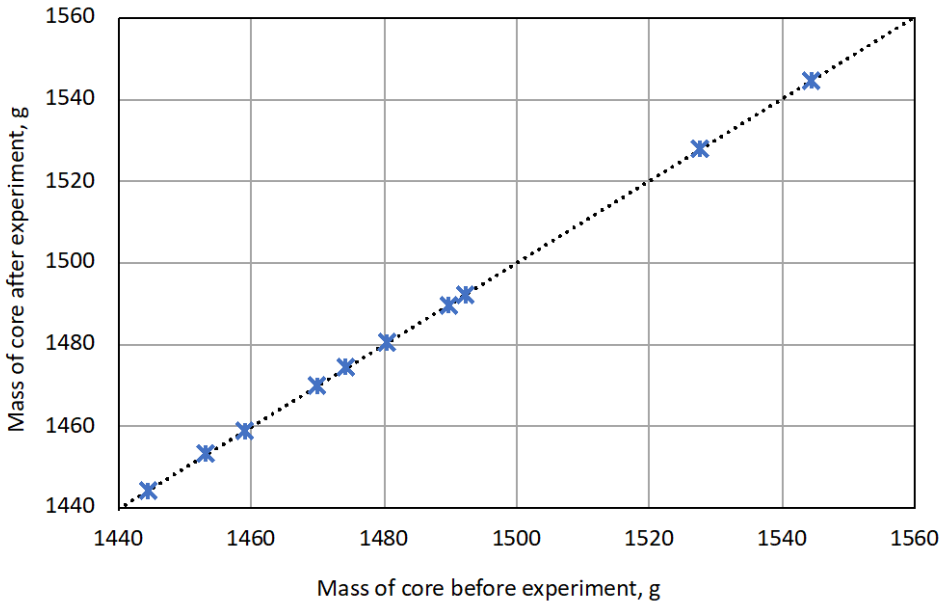

Figure 14: Mass of core samples from borehole IG_BH03 before and after the out-diffusion experiments; the uncertainty of the core mass is ± 0.05 g

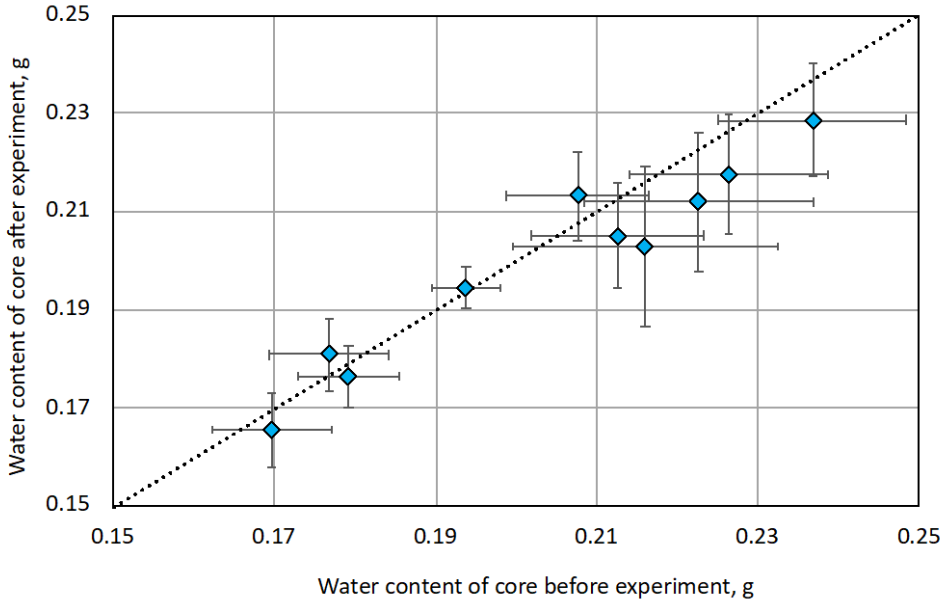

Figure 15: Water content calculated from the wet mass before and after the out-diffusion experiments of core sections from borehole IG_BH03; the error of the water content is determined by Gaussian error propagation (Appendix III)

Water contents determined by isotope diffusive exchange

Gravimetric water contents were determined on crushed core pieces used for the isotope diffusive exchange experiments. The masses of the used rock material are measured before and after the experiments. During the experiments the rocks remain saturated. A weight change of the rocks above the analytical uncertainty of ± 0.05 g (constant total weight) was observed in eight experiments (Table 11). Therefore, the water contents were corrected for the weight loss or gain.

The gravimetric water contents determined on rock pieces used for isotope diffusive exchange experiments ($WC_{IsoEx,grav,corr.}$) vary between 0.14 wt.% and 0.22 wt.% with weighted $WC_{IsoEx,grav}$ values ranging from 0.14 ± 0.01 wt.% to 0.21 ± 0.02 wt.% (Table 11).

The water contents determined by the isotope diffusive exchange technique (WC_{IsoEx}) for core samples from borehole IG_BH03 vary between 0.14 ± 0.01 wt.% and 0.24 ± 0.02 wt.% (Table 12). The water contents are, for most samples, similar to, and within the error range of, the gravimetric values determined on the same core pieces (Table 11 andTable 10, Figure 16). Three samples show slightly lower, and one sample slightly higher, gravimetric water contents than those determined by isotope diffusive exchange. A correlation to any experimental or analytical artefact(s) cannot be observed.

Table 11: Gravimetric water contents determined on core samples from borehole IG_BH03 used for isotope diffusive exchange experiments ($WC_{IsoEx,grav}$); Water contents are corrected for weight changes during the experiments (b.e.=before experiment, a.e. = after experiment); the gravimetric water contents determined on the rock pieces used in the experiments with LAB- and SSI-water are weighted taking their weights into account; the error of the water content is determined by Gaussian error propagation (Appendix III)

	LAB				SSI				
	mass	Δm (a.e.-b.e.)	$WC_{IsoEx,grav}$	$WC_{IsoEx,grav,corr.}$	mass	Δm (a.e.-b.e.)	$WC_{IsoEx,grav}$	$WC_{IsoEx,grav,corr.}$	$WC_{IsoEx,grav}$ weighted
	g	g	wt.%	wt.%	g	g	wt.%	wt.%	wt. %
IG_BH03_PW002	310.2	0.006	0.20	0.20	309.9	0.035	0.22	0.21	**0.20±0.02**
IG_BH03_PW003	298.4	-0.035	0.17	0.18	293.4	0.006	0.18	0.17	**0.18±0.01**
IG_BH03_PW005	383.9	0.035	0.22	0.21	385.7	0.072	0.21	0.19	**0.20±0.02**
IG_BH03_PW007	410.5	-0.133	0.16	0.20	415.3	0.054	0.18	0.17	**0.18±0.02**
IG_BH03_PW009	325.3	0.001	0.20	0.20	327.3	0.076	0.21	0.19	**0.19±0.01**
IG_BH03_PW011	310.8	-0.124	0.18	0.22	305.1	-0.008	0.19	0.19	**0.21±0.02**
IG_BH03_PW014	338.7	-0.051	0.14	0.15	335.6	0.028	0.17	0.16	**0.16±0.02**
IG_BH03_PW015	343.1	-0.013	0.17	0.18	342.6	0.051	0.19	0.17	**0.17±0.01**
IG_BH03_PW017	390.0	0.074	0.16	0.14	396.4	0.198	0.20	0.15	**0.15±0.02**
IG_BH03_PW019	392.0	0.146	0.18	0.14	389.3	0.351	0.23	0.14	**0.14±0.01**

Table 12: Water contents of core samples from borehole IG_BH03 calculated by the isotope diffusive exchange method (cf. eq. 7); the error of the water content is determined by Gaussian error propagation (Appendix III)

	WC_{IsoEx} ($\delta^{18}O$)	WC_{IsoEx} ($\delta^{2}H$)	WC_{IsoEx} average
	wt.%	wt.%	wt.%
IG_BH03_PW002	0.23±0.02	0.22±0.02	0.23±0.02
IG_BH03_PW003	0.25±0.02	0.22±0.02	0.24±0.02
IG_BH03_PW005	0.23±0.01	0.22±0.02	0.22±0.02
IG_BH03_PW007	0.16±0.01	0.17±0.01	0.16±0.01
IG_BH03_PW009	0.21±0.01	0.21±0.02	0.21±0.02
IG_BH03_PW011	0.17±0.01	0.18±0.02	0.17±0.02
IG_BH03_PW014	0.22±0.02	0.20±0.02	0.21±0.02
IG_BH03_PW015	0.22±0.01	0.21±0.02	0.22±0.02
IG_BH03_PW017	0.15±0.01	0.15±0.01	0.15±0.01
IG_BH03_PW019	0.15±0.01	0.14±0.01	0.14±0.01

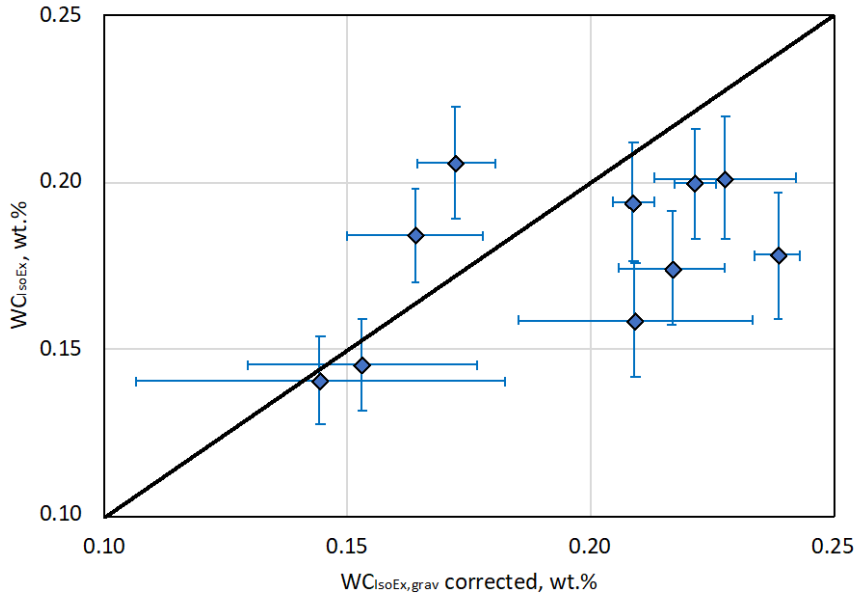

Figure 16: Comparison of water contents determined by isotope diffusive exchange (WC_{IsoEx}) and gravimetrically ($WC_{IsoEx,grav}$, by wet weight, corrected for weight change during experiments) on the same core pieces; the error of the water content is determined by Gaussian error propagation

Summary and depth profiles of water content results

The gravimetric water contents determined on the AQ and PW cores are weighted by the masses of the individual rock pieces (Table 13). The weighted water content represents the entire core, with masses between 462 g and 1,190 g for AQ cores and between 2,392 g and 2,730 g for PW cores. As noted, the water contents of the individual

aliquots vary, which is presumed to be caused by mineralogical heterogeneities. This indicates that water content values cannot be extrapolated.

The weighted gravimetric water contents of the AQ- and PW-core samples taken between 238 and 985 mbgs (down hole) vary between 0.16 wt.% (0.43 Vol.%) and 0.23 wt.% (0,60 Vol.%, Table 13). Between 238 and 771 mbgs (down hole) the water contents are quite constant, ranging between 0.20 wt.% and 0.23 wt.%, with the exception of two PW-core samples taken at 345 and 669 mbgs (down hole) which show slightly lower gravimetric weighted water contents (IG_BH03_PW003 = 0.19 wt.%, IG_BH03_PW014 = 0.17 wt.%, Table 13, Figure 16). In the deepest two sampled intervals at 880 and 985 mbgs (down hole) the determined gravimetric weighted water contents are slightly lower than in the upper bedrock sections, ranging between 0.16 wt.% and 0.18 wt.% (Table 13, Figure 16).

Table 13: Weighted gravimetric water contents of AQ- and PW-core samples in wt.% and Vol.% taken from borehole IG_BH03 and their corresponding total masses; the uncertainties of the water content values are the weighted standard deviations of the individual aliquots showing the diversity of water contents in one entire core sample; the core volume is calculated using the bulk, wet density determined on the out-diffusion and aqueous extraction cores (Table 14).

Sample	Depth	m(rock) tot	WC(grav,weighted)	Bulk,wet density	Volume (core)	WC(grav, weighted)
	mbgs*	g	wt. %	g/ccm	Ccm	Vol.%
IG_BH03_AQ001	238.8	1190.1	0.21±0.02	2.64	450.1	0.55±0.06
IG_BH03_AQ002	346.0	462.1	0.21±0.02	2.64	174.7	0.56±0.07
IG_BH03_AQ003	460.1	645.2	0.21±0.01	2.66	242.9	0.55±0.03
IG_BH03_AQ004	504.2	661.1	0.22±0.04	2.63	251.7	0.58±0.10
IG_BH03_AQ005	554.7	560.3	0.23±0.05	2.64	212.0	0.62±0.14
IG_BH03_AQ006	608.6	614.8	0.22±0.03	2.66	231.6	0.59±0.07
IG_BH03_AQ007	665.9	501.4	0.21±0.03	2.65	189.2	0.55±0.08
IG_BH03_AQ008	771.8	702.3	0.20±0.01	2.65	264.9	0.53±0.04
IG_BH03_AQ009	880.1	612.3	0.18±0.06	2.66	229.9	0.47±0.16
IG_BH03_AQ010	985.0	559.1	0.17±0.01	2.66	210.2	0.46±0.04
IG_BH03_PW002	242.0	2433.6	0.22±0.02	2.64	921.2	0.58±0.04
IG_BH03_PW003	345.2	2392.3	0.19±0.01	2.66	901.0	0.51±0.04
IG_BH03_PW005	459.2	2630.4	0.22±0.01	2.66	988.5	0.58±0.04
IG_BH03_PW007	503.9	2729.9	0.20±0.02	2.67	1023.4	0.55±0.05
IG_BH03_PW009	554.5	2532.3	0.23±0.02	2.66	950.3	0.60±0.06
IG_BH03_PW011	608.8	2524.6	0.22±0.02	2.65	951.0	0.58±0.06
IG_BH03_PW014	669.2	2631.7	0.17±0.01	2.64	996.2	0.46±0.03
IG_BH03_PW015	771.6	2679.1	0.20±0.02	2.65	1011.2	0.52±0.04
IG_BH03_PW017	880.4	2570.1	0.17±0.02	2.66	968.0	0.44±0.05
IG_BH03_PW019	984.7	2628.0	0.16±0.02	2.65	991.8	0.43±0.06

* mbgs (down hole)

5.2 Bulk dry/wet density and water-loss porosity

The bulk dry and wet density is calculated according to equation 1 (Section 3.2) using the dry and wet mass of the full diameter cylindrical cores and the volume of the core samples determined by measuring the height and core diameter by a Vernier Calliper. Bulk wet densities were determined for the cores used for out-diffusion and aqueous extraction experiments before crushing, and bulk dry density was determined only for out-diffusion cores.

Bulk dry and wet density values of the core samples from borehole IG_BH03 are similar, differing by a maximum of 0.01 g/cm^3, due to the low water content of the samples, and vary between 2.63 and 2.67 g/cm^3 (Table 14).

The water-loss (connected) porosity was calculated according to equation 2 (Section 3.2) using the water content calculated by the dry and wet weight and the bulk dry/wet density of the samples. Water-loss porosities are calculated for core sections used for the out-diffusion and aqueous extraction experiments, for which the water content and the bulk dry/wet density were determined. Water-loss porosities calculated using the wet mass and density differ by a maximum of 0.01 Vol.% from those determined by the dry mass and density (Table 14).

Water-loss porosity values of core samples taken between 238 and 985 mbgs (down hole) from borehole IG_BH03 vary between 0.43 ± 0.03 Vol.% and 0.62 ± 0.07 Vol.% (Table 14, Figure 17). Trends in the porosity values for the samples follow the same trends as described by the water contents (Figure 17).

Table 14: Bulk wet and dry density and water-loss (=WL-) porosity determined by water contents calculated for dry ($\Phi_{WL,dry}$) and wet ($\Phi_{WL,wet}$) core samples from borehole IG_BH03; the errors are calculated by Gaussian error propagation (Appendix III).

Sample	Depth	bulk, wet density	bulk, dry density	water-loss porosity $\Phi_{WL,wet}$	water-loss porosity $\Phi_{WL,dry}$
	mbgs*	g/ccm	g/ccm	Vol.%	Vol.%
IG_BH03_PW002	242.0	2.64	2.64	0.58±0.04	0.58±0.04
IG_BH03_PW003	345.2	2.66	2.65	0.51±0.02	0.51±0.02
IG_BH03_PW005	459.2	2.66	2.66	0.58±0.04	0.58±0.04
IG_BH03_PW007	503.9	2.67	2.66	0.55±0.04	0.54±0.04
IG_BH03_PW009	554.5	2.66	2.66	0.60±0.04	0.60±0.04
IG_BH03_PW011	608.8	2.65	2.65	0.58±0.05	0.58±0.05
IG_BH03_PW014	669.2	2.64	2.64	0.46±0.03	0.45±0.03
IG_BH03_PW015	771.6	2.65	2.64	0.52±0.03	0.52±0.03
IG_BH03_PW017	880.4	2.66	2.65	0.44±0.02	0.44±0.02
IG_BH03_PW019	984.7	2.65	2.65	0.43±0.03	0.43±0.03
IG_BH03_AQ001	238.8	2.64		0.55±0.09	
IG_BH03_AQ002	346	2.64		0.56±0.03	
IG_BH03_AQ003	460.1	2.66		0.55±0.05	
IG_BH03_AQ004	504.2	2.63		0.58±0.03	
IG_BH03_AQ005	554.7	2.64		0.62±0.07	
IG_BH03_AQ006	608.6	2.66		0.59±0.06	

Sample	Depth	bulk, wet density	bulk, dry density	water-loss porosity $\Phi_{WL,wet}$	water-loss porosity $\Phi_{WL,dry}$
	mbgs*	g/ccm	g/ccm	Vol.%	Vol.%
IG_BH03_AQ007	665.9	2.65		0.55±0.06	
IG_BH03_AQ008	771.8	2.65		0.53±0.06	
IG_BH03_AQ009	880.1	2.66		0.47±0.03	
IG_BH03_AQ010	985.0	2.66		0.46±0.02	

* mbgs (down hole)

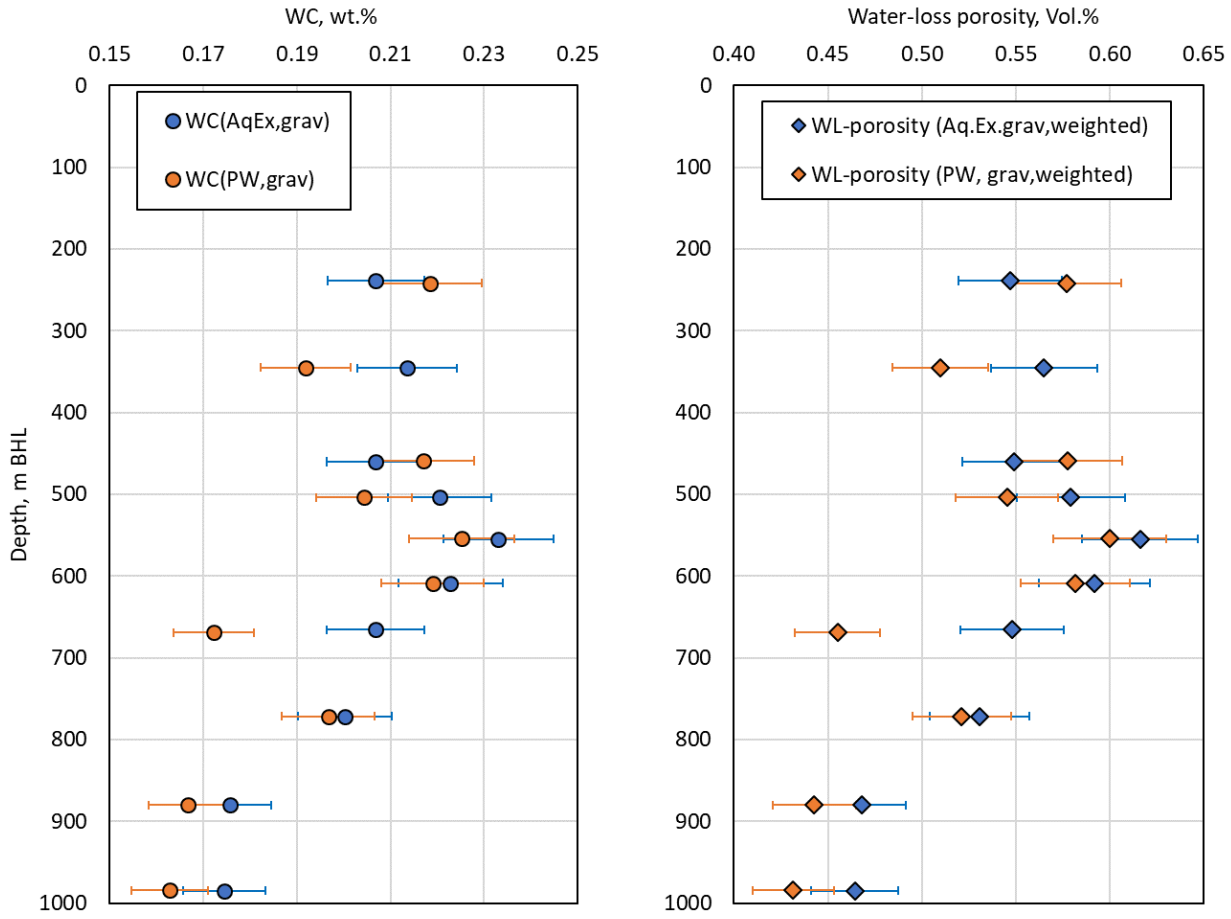

Note: m BHL is equivalent to mbgs (down hole).

Figure 17: Water content and water-loss porosity of core samples from borehole IG_BH03

6.0 CHEMICAL COMPOSITION OF EXPERIMENT SOLUTIONS OF AQUEOUS EXTRACTION AND OUT-DIFFUSION EXPERIMENTS

Out-diffusion and aqueous extraction experiments were performed on ten core samples taken from borehole IG_BH03. In both experiments the investigated rock samples were immersed in test water. The concentrations of dissolved constituents in the test solutions originate from:

a) porewater, which exchanges and mixes with test water;

b) water-rock interactions, releasing reactive elements in the test water; and

c) fluid inclusions (only aqueous extractions), which are liberated during crushing of the rocks.

6.1 Chemical composition of aqueous extraction solutions

The purpose of aqueous extraction experiments is to obtain an initial estimate of the porewater salinity, which is necessary for the adjustment of the ion concentration in the test waters for the indirect porewater extraction methods.

Crushing and grinding of the rock material liberates fluid trapped in mineral fluid inclusions. During leaching, all salts will become dissolved, in addition to the limited dissolution of the original mineral assemblage. The mineralization of a leach solution is therefore the sum of: (i) the constituents originally dissolved in the porewater, (ii) the constituents present in fluid inclusions, and (iii) water-rock interactions during the leaching process. Thus, aqueous leach solutions represent a complex composition in rocks with abundant fluid inclusions and/or rapidly reacting mineral phases.

The aqueous extraction solutions produced by the immersion of crushed cores from borehole IG_BH03 in deionized water (procedure cf. Section 3.3.1) have pH values between 9.4 and 9.8, and a mineralization between 56 and 161 mg/L (sp. electrical conductivity = 56 – 140 µS/cm, Table 15). The dissolved constituents consist predominately of Na, K, Ca, HCO_3, Cl and SO_4 in different concentrations and proportions (Table 15, Figure 18). Minor concentrations of Mg, F and Br could be detected. Concentrations of Sr were below detection limit (Table 15). Silicon and aluminium could be detected in concentrations between 3.3 and 11.8 mg/L (Si) and between 0.43 and 15 mg/L (Al).

The estimated porewater Cl-concentrations of core samples from IG_BH03, extracted by aqueous extraction experiments using the weighted water contents of the AQ samples (cf. Table 8), vary between 2,735 mg/kg_{PW} and 14,599 mg/kg_{PW} (Table 18).

Table 15: Analytical results of the aqueous extraction solutions of crushed core samples from borehole IG_BH03; Test solution types are classified after Jäckli (1970)

Sample		IG_BH03_AQ001	IG_BH03_AQ002	IG_BH03_AQ003	IG_BH03_AQ004	IG_BH03_AQ005	IG_BH03_AQ006	IG_BH03_AQ007	IG_BH03_AQ008	IG_BH03_AQ009	IG_BH03_AQ010
Interval	m BHL	238.8	346.0	460.1	504.2	554.7	608.6	665.9	771.8	880.1	985.0
Hydroisotop No.		331169	331172	331175	331178	331181	331842	331843	331844	333069	333070
MASTER VARIABLES											
pH (lab)	-log(H+)	9.4	9.5	9.6	9.4	9.7	9.8	9.7	9.6	9.5	9.5
Electr. Conductivity	µS/cm	56	61	62	57	61	120	140	108	112	138
Sample Temperature	°C	24.5	24.9	24.4	24.1	24.3	25.2	25.2	25.2	23	23.1
Alkalinity (pH 4,3) Lab.	mmol/l	0.51	0.52	0.53	0.43	0.52	1.1	1.2	1.2	0.50	0.51
Alkalinity (pH 8,2) Lab.	mmol/l	0.22	0.22	0.32	0.22	0.36	0.54	0.52	0.76	0.25	0.28
DOC	mg/l	5.1	5.3	4.0	3.4	3.9	7.8	6.9	6.5	3.4	2.3
DISSOLVED CONSTITUENTS											
CATIONS	mg/l										
Sodium (Na+)	mg/l	12.9	13.2	9.9	9.1	11.9	28.1	27.5	30.0	11.8	13.8
Potassium (K+)	mg/l	3.0	6.0	5.3	5.7	3.8	10.3	14.7	7.7	7.5	9.1
Magnesium (Mg+2)	mg/l	<0.2	<0.2	<0.2	<0.2	<0.2	0.75	0.86	1.1	0.23	0.23
Calcium (Ca+2)	mg/l	1.9	0.97	1.8	1.4	1.9	2.1	2.0	2.2	6.2	7.1
Strontium (Sr+2)	mg/l	<0.01	<0.01	<0.01	<0.01	<0.01	<0.01	<0.01	<0.01	<0.01	<0.01
Silicium (Si+4)	mg/l	3.5	3.9	3.8	3.8	3.3	9.9	11.8	11.6	4.6	5.9
Aluminium (Al+3)	mg/l	1.3	2.5	2.2	2.4	1.9	11.0	11.0	15.0	0.55	0.43
ANIONS											
Fluoride (F-)	mg/l	0.11	0.21	0.22	0.15	0.17	0.47	0.6	0.77	0.1	<0.01
Chloride (Cl-)	mg/l	4.2	4.5	3.0	3.9	3.8	14.7	14.6	12.2	17.6	24.5
Bromide (Br-)	mg/l	0.05	0.07	0.07	0.05	0.03	0.26	0.52	0.64	0.34	0.60
Sulfate (SO4-2)	mg/l	5.2	5.7	2.5	3.4	3.8	3.7	6.4	5.8	0.79	<0.2
Nitrate (NO3-)	mg/l	<0.2	<0.2	<0.2	<0.2	<0.2	<0.2	0.24	0.20	0.26	<0.2
Total Alkalinity as HCO3	mg/l	31.1	31.7	32.3	26.2	31.7	69.6	70.8	73.2	30.5	31.1
PARAMETERS CALCULATED FROM ANALYTICAL DATA											
Sum of analysed constituents	mg/l	63	69	61	56	62	151	161	160	80	93
Charge balance	%	-0.71%	-0.10%	-0.49%	-0.64%	-0.42%	-0.22%	-0.12%	-0.42%	0.33%	-0.10%
Water type		Na-(Ca)-(K)-HCO3-(Cl)-(SO4)	Na-(K)-HCO3-(Cl)-(SO4)	Na-K-HCO3-(Cl)-(SO4)	Na-K-(Ca)-HCO3-(Cl)-(SO4)	Na-(K)-(Ca)-HCO3-(Cl)-(SO4)	Na-(K)-HCO3-(Cl)	Na-K-HCO3-(Cl)	Na-(K)-HCO3-Cl	Na-Ca-(K)-HCO3-Cl	Na-Ca-(K)-Cl-HCO3

Note: m BHL is equivalent to mbgs (down hole).

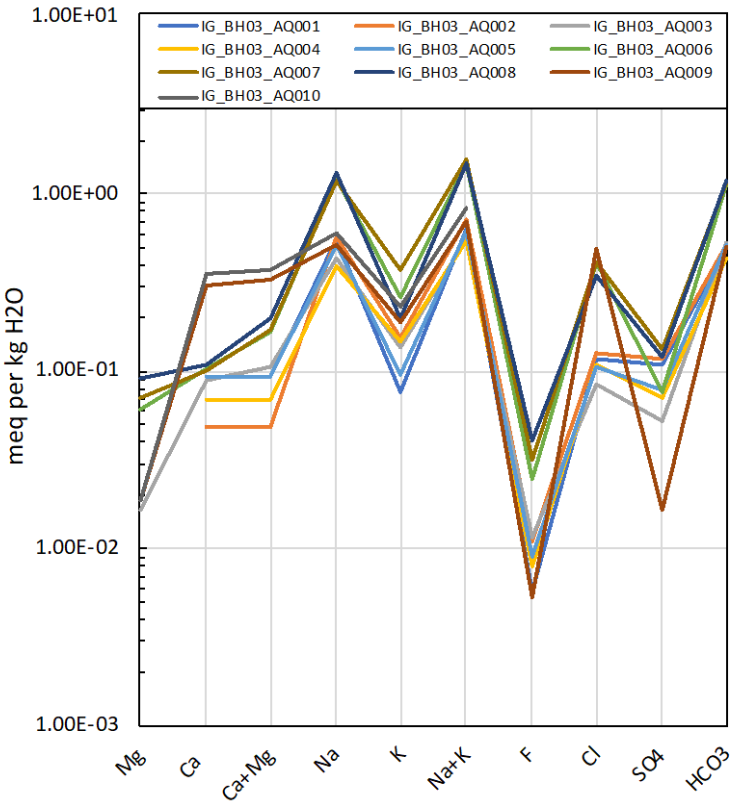

Figure 18: Schoeller diagram of experiment solutions from aqueous extraction experiments conducted with core samples from borehole IG_BH03

6.2 Chemical composition of out-diffusion experiment solutions

Out-diffusion experiments were performed on ten core samples from borehole IG_BH03 to derive the porewater chloride and bromide concentrations, porewater $\delta^{37}Cl$ isotope ratios, and chemical composition of the test solutions - which are the basis for the hydrogeochemical modelling of porewater chemical compositions. The core sections varied in diameter between 60.7 mm and 61.0 mm, with lengths between 187 mm and 199 mm. The corresponding volume of the sections varied between 544 cm^3 and 583 cm^3 and the saturated mass was between 1,444 g and 1,544 g. In the out-diffusion experiments, the mass ratio of experiment solution to rock samples was between 0.085 and 0.098 (Table 16).

During the out-diffusion experiments, a continuous exchange between porewater and test water takes place until equilibrium conditions with respect to conservative, non-reactive compounds are achieved. The exchange appears to occur mainly by diffusion (cf. Section 7). For chemically conservative elements, such as chloride and bromide, for which the porewater is the only source, the porewater concentration can be calculated using the gravimetrically determined porewater mass of the rock sample. For reactive elements and compounds, such as Ca, Mg, Na, K, Sr, Si, Al, SO_4^{2-} and HCO_3^-, the contribution of mineral dissolution reactions during the experiment has to be taken into account. Those reactions are evaluated by the determination of the concentrations of the non-conservative elements taken in time-series (cf. Section 7.1).

In parallel to the out-diffusion experiments, a blank set-up containing only test water, which was sampled at the same frequency as the normal experiments and also finished after 141 days, was conducted. After the experimental period, the “Blank” water, with a pH of 5.8 and a sp. electrical conductivity (EC) of 3 µS/cm, contained 3.1 mg/L dissolved constituents, mainly composed of Ca, Na and HCO_3 (Table 16, Figure 19). The “Blank” test solution has a DOC concentration of 1.7 mg/L and a TIC concentration of 0.51 mg/L. The comparison of the TIC concentration analysed directly (0.51 mg/L) and this calculated from the acid capacity determined by titration (0.48 mg/L) shows that the determination of the HCO_3 concentration by titration is not influenced by organic acids and is reliable.

The pH of the experiment solutions varies between 7.4 and 7.8 with a total mineralization between 111 mg/L and 384 mg/L (EC = 135 - 769 µS/cm, Table 16). It should be noted that the total mineralization obtained for the experiment solutions depends on the water content of the sample and the water/rock ratio used in the experiment (Table 10) and does not directly reflect differences in porewater salinity.

The experimental solutions contain Na (15.7 – 25.4 mg/L), Ca (9.0 – 110 mg/L), K (2.4 – 7.4 mg/L), HCO_3 (31.1 – 109 mg/L), Cl (1.9 – 204 mg/L) and SO_4 (1.9 – 9.7 mg/L) in varying proportions and concentrations (Table 16, Figure 19).

Based on the out-diffusion test solutions, samples are characterized by Na- and HCO_3- dominated water between 242 and 772 mbgs (down hole), and transition to a Ca- and Cl- dominated water below, as observed in samples from 880 and 985 mbgs (down hole), with similar mineralogical composition (Table 16, Figure 19)

Silicon (expressed as Si) is present in concentrations between 7.8 and 10.4 mg/L. Lithium, magnesium, strontium, aluminium, boron, fluoride, bromide and nitrate are below detection limit or present in low or trace concentrations (Table 16).

The concentrations of dissolved organic carbon (DOC) vary between 6.1 and 14.4 mg/L.

The DIC/TIC concentrations (DIC = TIC, because analysed on filtered samples) determined by TIC-analyser vary between 6.1 and 21.4 mg/L. The comparison of the TIC concentrations determined by direct analyses with those determined by acid titration (AC4.3) shows that the total alkalinity is mainly determined by HCO_3. The differences between the TIC values determined by the two methods are between 0.2 and 11 % with higher values determined by titration. The differences are most apparent in test solutions for cores taken between 242 and 555 mbgs (down hole) (ΔTIC = 6.1 – 11.1 %). In the experiments with samples taken between 608 and 985 mbgs (down hole) ΔTIC values are very low, ranging between 0.2 and 0.8 % (Table 16), indicating that the determination of the HCO_3 concentrations by acid titration is reliable (and not influenced to any notable degree by organic acids).

In the experiment, the carbon system of the test water – porewater system is influenced by in- and/or out-gassing of atmospheric CO_2. For all out-diffusion solutions, the CO_2 partial pressure was estimated using the TIC concentrations determined by titration and pH-values of the out-diffusion solutions. The estimated log pCO_2 range between -3.1 and -2.5 and are higher than that of the atmosphere (log pCO_2 ~ -3.5). At the beginning of the experiments the test water was in equilibrium with atmospheric CO_2 and contained only a low concentration of dissolved carbon (~0.19 mmol/L as HCO_3 and CO_2). Therefore, the additional carbon must have been derived from the rock and/or the porewater during the experiments.

The strontium $^{87}Sr/^{86}Sr$ isotope ratios of the out-diffusion test solutions vary between 0.720313 and 0.735476, with Sr-concentrations varying between 0.05 and 1.92 mg/L (Table 16).

Table 16: Analytical results of test solutions of out-diffusion experiments using core samples from borehole IG_BH03

Sample		IG_BH03_Blank	IG_BH03_PW002	IG_BH03_PW003	IG_BH03_PW005	IG_BH03_PW007	IG_BH03_PW009	IG_BH03_PW011	IG_BH03_PW014	IG_BH03_PW015	IG_BH03_PW017	IG_BH03_PW019
Hydroisotop Nr.		338402	338397	338398	338399	338400	338401	340717	340718	340719	340720	340721
Interval	m BHL		242.0	345.2	459.2	503.9	554.5	608.8	669.2	771.6	880.4	984.7
Ratio Exp.Water : Rock	g/g		0.085	0.098	0.091	0.088	0.090	0.091	0.085	0.085	0.090	0.092
Ratio TW:PW	g/g		38	51	40	42	38	42	48	41	50	54
MASTER VARIABLES												
pH (lab), UniBe	-log(H+)	5.8	7.7	7.4	7.7	7.6	7.5	7.8	7.5	7.7	7.5	7.4
Spec.Electr. Conductivity	µS/cm	3	168	135	196	176	178	191	259	233	611	769
Acid Capacity (4.3)	mmol	0.04	1.5	1.2	1.78	1.32	1.42	0.84	0.96	0.88	1.03	0.51
Base Capacity (8.2)	mmol	0.15	0.07	0.11	0.07	0.07	0.1	0.03	0.07	0.04	0.07	0.05
Sample Temperature	ºC	18.8	20.3	19.8	21.3	21.8	20.8	24.2	24.2	24.6	24.2	24.3
DOC	mg/l	1.7	10.8	10.3	14.4	11.2	9.3	9.0	11.1	9.5	10.9	6.1
TIC	mg/l	0.51	16.8	12.8	20.0	14.6	16.0	10.0	11.5	10.5	12.3	6.1
TIC (AC4.3)	mg/l	0.48	18.0	14.4	21.4	15.8	17.0	10.1	11.5	10.6	12.4	6.1
Δ(TIC)	mg/l	-0.03	1.2	1.6	1.4	1.2	1.0	0.1	0.0	0.1	0.1	0.0
DISSOLVED CONSTITUENTS												
CATIONS	mg/l											
Sodium (Na+)	mg/l	0.12	23.2	15.9	19.7	15.7	18.7	18.2	19.1	25.4	22.8	23.3
Potassium (K+)	mg/l	<0.1	2.4	2.5	2.6	3.5	3.2	2.9	4.1	3.6	7.4	6.7
Lithium (Li+)	mg/l	<0.01	0.04	0.03	0.02	0.03	0.014	0.027	0.028	<0.01	0.037	0.018
Calcium (Ca+2)	mg/l	0.49	9.0	12.0	19.7	17.1	16.0	18.5	27.7	20.0	82.2	110
Magnesium (Mg+2)	mg/l	<0.2	<0.2	<0.2	<0.2	<0.2	<0.2	<0.2	0.30	<0.2	0.52	0.35
Strontium (Sr+2)	mg/l	<0.01	0.05	0.07	0.16	0.11	0.12	0.28	0.44	0.37	1.51	1.92
Aluminium (Al+3)	mg/l	<0.01	0.17	0.08	0.08	0.11	0.11	0.14	0.06	0.06	0.05	0.05
Silicium (Si+4)	mg/l	<0.1	7.8	8.1	8.2	8.5	8.1	8.1	10.4	10.3	8.2	9.0
Boron (B)	mg/l	<0.01	0.13	0.073	0.07	0.08	0.06	0.37	0.38	0.70	0.40	0.28
ANIONS												
Fluoride (F-)	mg/l	<0.01	1.5	1.3	2.1	1.4	0.66	1.7	1.2	1.7	1.2	0.92
Chloride (Cl-)	mg/l	0.02	1.9	3.7	2.7	7.9	8.6	22.1	36.7	29.5	139	204
Bromide (Br-)	mg/l	<0.02	0.02	0.15	0.19	0.18	0.16	0.49	0.78	0.91	2.4	4.8
Nitrate (NO3-)	mg/l	<0.2	<0.2	<0.2	<0.2	<0.2	<0.2	0.32	0.31	<0.2	<0.2	<0.2
Sulphate (SO4-2)	mg/l	<0.2	3.8	2.1	1.9	4.0	3.2	3.7	8.2	9.7	5.4	3.4
Total Alkalinity	meq/l	0.04	1.50	1.20	1.78	1.32	1.42	0.84	0.96	0.88	1.03	0.51
Total Alkalinity as HCO3	mg/l	2.4	91.5	73.2	108.6	80.5	86.6	51.2	58.6	53.7	62.8	31.1
PARAMETERS CALCULATED FROM ANALYTICAL DATA												
Sum of Analysed Constituents	mg/l	3.1	133.4	110.9	157.6	130.4	137.3	119.1	157.1	144.9	325.3	386.5
Charge Balance:	%	-15.5	-5.9	-2.3	-2.5	-2.2	-2.0	4.6	2.5	4.5	1.9	2.3
WATER TYPE		Ca-Na-HCO_3	Na-(Ca)-HCO_3	Na-Ca-HCO_3	Na-Ca-HCO_3	Na-Ca-HCO_3-(Cl)	Na-Ca-HCO_3-(Cl)	Na-Ca-HCO_3-Cl	Na-Ca-Cl-HCO_3	Na-Ca-HCO_3-Cl-(SO_4)	Ca-Na-Cl-HCO_3	Ca-Na-Cl
ION-ION RATIOS												
Br*1000/Cl weight			10.5	40.5	70.4	22.8	18.6	22.2	21.3	30.6	17.3	23.5
Br*1000/Cl molal	mol/mol		4.7	18.0	31.2	10.1	8.3	9.8	9.4	13.6	7.7	10.4
Na/Cl molal	mol/mol	9.3	18.8	6.6	11.3	3.1	3.4	1.3	0.8	1.3	0.3	0.2
K/Na molal	mol/mol		0.061	0.092	0.078	0.131	0.101	0.094	0.126	0.083	0.191	0.169
SO4/Cl molal	mol/mol		0.738	0.209	0.260	0.187	0.137	0.062	0.082	0.121	0.014	0.006
Na/(Cl+SO4)	mol/mol	9.3	10.8	5.5	8.9	2.6	2.9	1.2	0.7	1.2	0.2	0.2
ISOTOPE RATIOS												
δ37Cl	pm SMOC		Cl to low	Cl to low	Cl to low	0.68	0.14	0.32	0.45	0.05	0.26	0.45
error δ37Cl	pm SMOC					0.20	0.20	0.20	0.20	0.20	0.20	0.22
87Sr/86Sr			0.735476	0.732913	0.725846	0.731033	0.723266	0.726050	0.727480	0.720313	0.726839	0.723667
error 87Sr/86Sr			0.000050	0.000050	0.000050	0.000050	0.000050	0.000050	0.000050	0.000050	0.000050	0.000050

Note: m BHL is equivalent to mbgs (down hole).

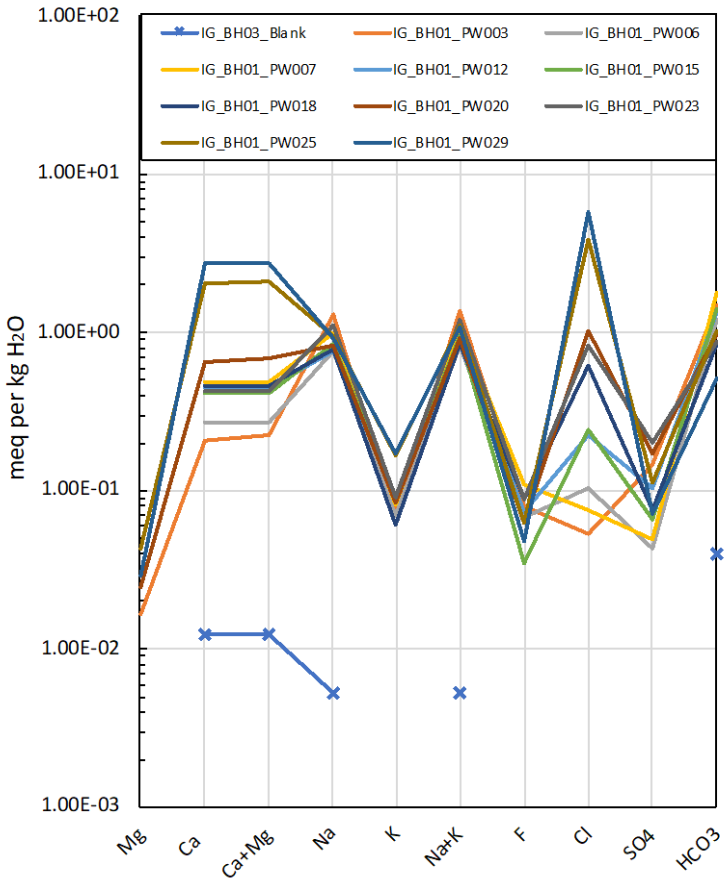

Figure 19: Schoeller diagram of experiment solutions from out-diffusion experiments including the "Blank" set-up conducted with cores from borehole IG_BH03

7.0 ELEMENTAL TIME SERIES AND PORE DIFFUSION COEFFICIENT OF CHLORIDE

7.1 Elemental elution curves

Non-destructive out-diffusion experiments are performed based on the concept of chemical exchange between porewater residing in the rock matrix and a test solution of known composition surrounding the rock sample. The experimental setup is maintained until specific conditions between the two solution reservoirs are attained. Because of the closed system character of out-diffusion experiments, the specific conditions to be achieved between the two solution reservoirs are equilibrium for any solutes for which the porewater is the only source, and which are only subjected to transport processes (i.e., Cl and Br).

For the present study, improved analytical techniques allowed continuous monitoring of all major solute concentrations in the eluate solutions during out-diffusion. This allows definition of mineral reactions and – at a later stage – possible determination of solute specific transport (e.g., ion-specific accessible porosity) in the matrix of crystalline rocks.

Porewater chloride and bromide concentrations are calculated based on the final concentrations in the out-diffusion test solutions and the water content of the individual core samples (cf. Section 3). The approach to equilibrium was monitored by periodically taking sub-samples and analysing them for their Cl and Br concentrations. The criterion for attainment of equilibrium conditions is defined by a difference of less than 5 % in Cl- and Br-concentrations between the last sub-sample and the final test solution at the end of the experiment. This corresponds to the analytical uncertainty of the Cl and Br measurements. Sub-samples were collected as a function of time for all out-diffusion experiments.

Out-diffusion experiments were run for 141 to 159 days. Equilibrium with respect to Cl and Br was attained for all samples with respect to the above mentioned criteria after 45 – 121 days for Cl, and 45 – 91 days for Br, respectively (Figure 20).

It should be noted that the Br concentrations are generally much lower than other constituents. With reference to Figure 20 (IG_BH03_PW002), Br concentrations for the first 120 days were below the detection limit (0.1 mg/L) for the small-volume solutions that are a part of the time-series, and are plotted on the time series as “0 mg/L”. The Br concentration was detectable in the final test solution at 140 days because the larger fluid volume available for testing resulted in a much lower detection limit achieved.

The calculated Br*1000/Cl mass ratios (further expressed as Br/Cl-ratio) of the individual out-diffusion experiments either increase within the first days or weeks of elution or are constant over the entire period of elution (Figure 20). This indicates that there is no significant influence of a diffusional fractionation between bromide and chloride.

Sodium appears to elute in a similar manner as chloride and bromide in the first app. 40 days of the experiments. Different from the conservative elements Cl and Br, Na shows a slight increase later in the experiments (this continues for most samples until the end of the experiments, Figure 20). In several experiments, sodium was in equilibrium after app. 120 days (Figure 20). These trends indicate that the main proportion of sodium in the test solutions originates from porewater, which exchanged by diffusion with the test water, and a low proportion originates from water-rock interactions of Na-bearing plagioclase over the course of the experiments.

Potassium, in contrast, has an elution curve similar to Cl and Br and is for all samples, except for one sample, in equilibrium after few weeks. The potassium concentration in the test solution of sample IG_BH03_PW005 shows a

similar trend as observed for Na with a linear increase between 30 and 140 days during the experiments. The consistent trend of K-elution indicates that, except for sample PW005, there is no influence of interactions of K-bearing alkali feldspar observable from the elution curves. The main proportion of K appears to originate from the diffusive accessible porewater.

The concentrations of Ca are also constant in almost all test solutions after an experimental period of app. 30 to 50 days (Figure 20). An exception of this trend is also sample PW005, which shows a continuous increase in Ca-concentrations until the end of the experiment. The general elution behaviour of Ca in the experiments indicates that there is no main influence of Ca-dissolution reactions of Ca-bearing plagioclase and/or its alteration products on the Ca-contents of the test solutions.

For almost all samples, the sulphate concentrations display a steady increase during the entire elution period (Figure 20). This is reasoned to be caused by the oxidation and elution of sulphide minerals, which are present in the rock as accessories (cf. chapter 4.3).

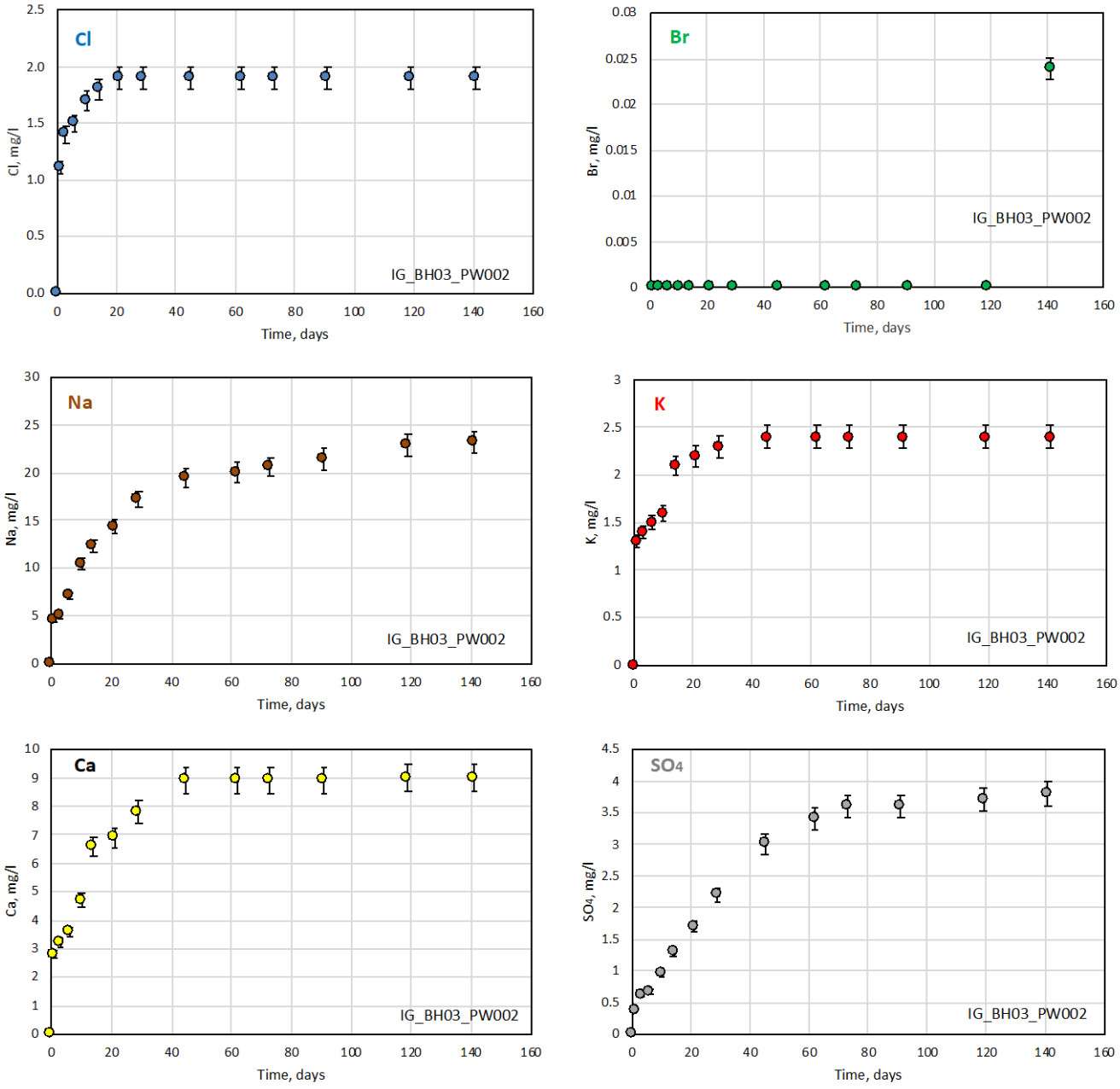

Figure 20: Elution curves of different main anions and cations set-up by the periodic sampling of test solutions of out-diffusion experiments applying core samples from borehole IG_BH03; the errors are the analytical uncertainty of ± 5 %

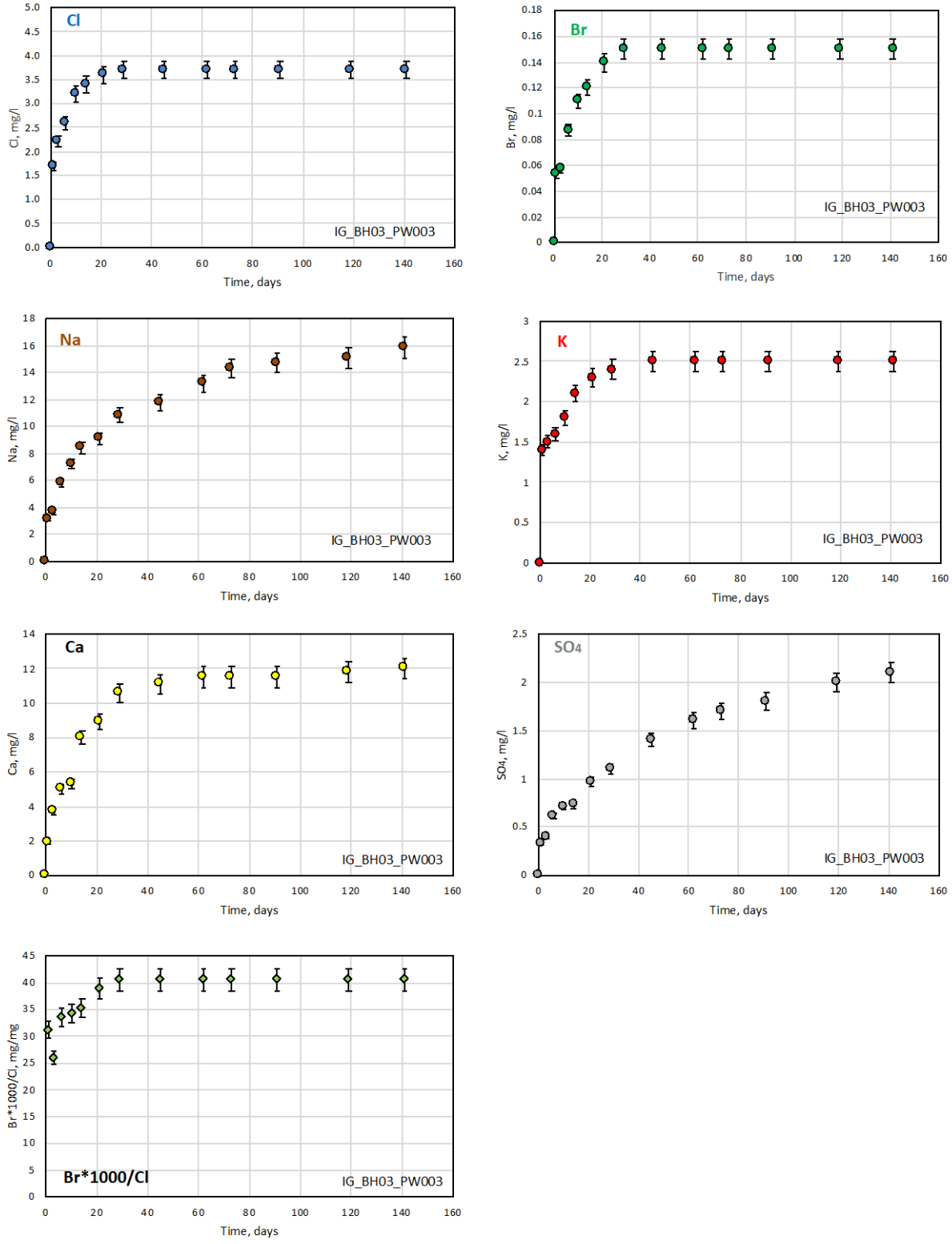

Figure 20 continued

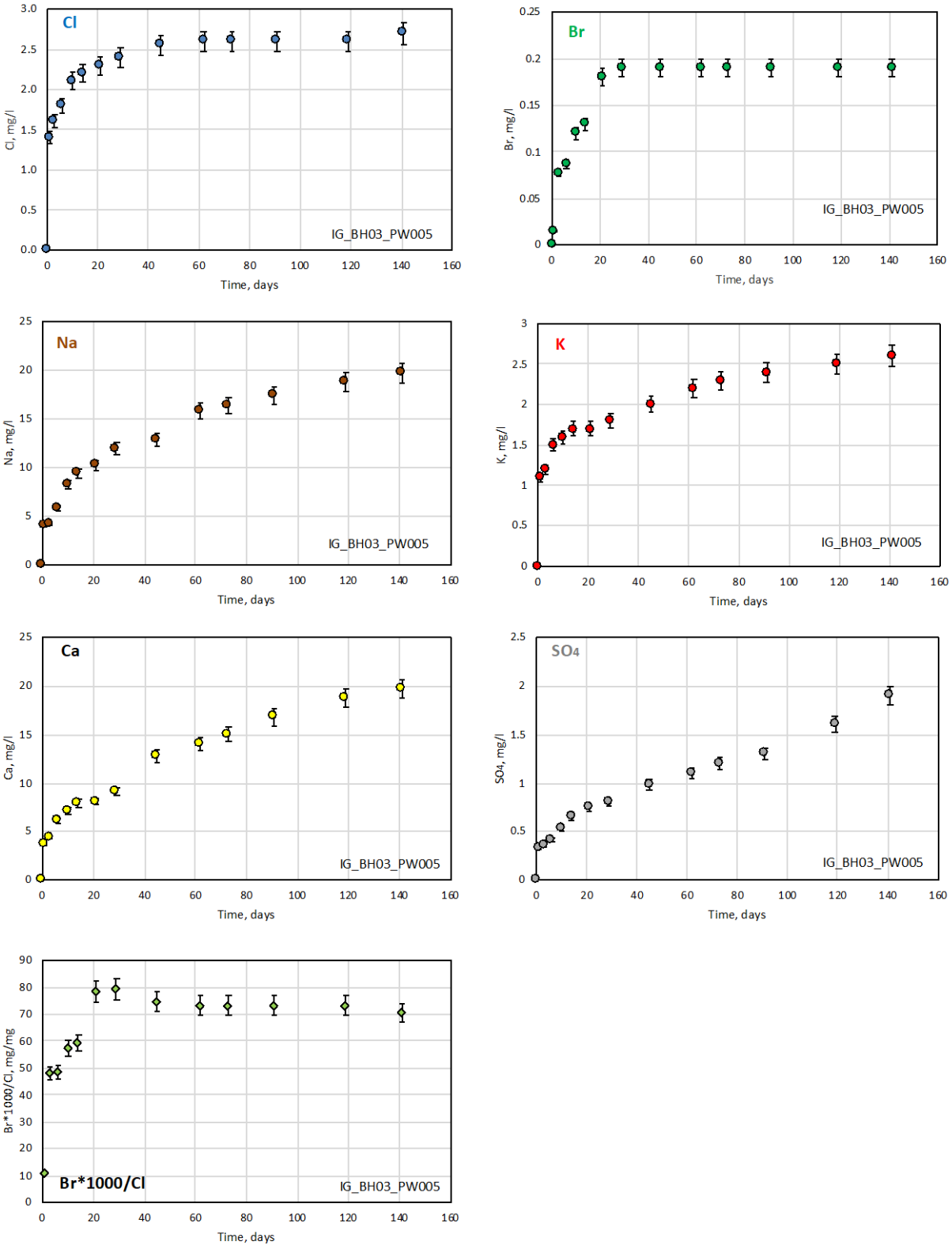

Figure 20 continued

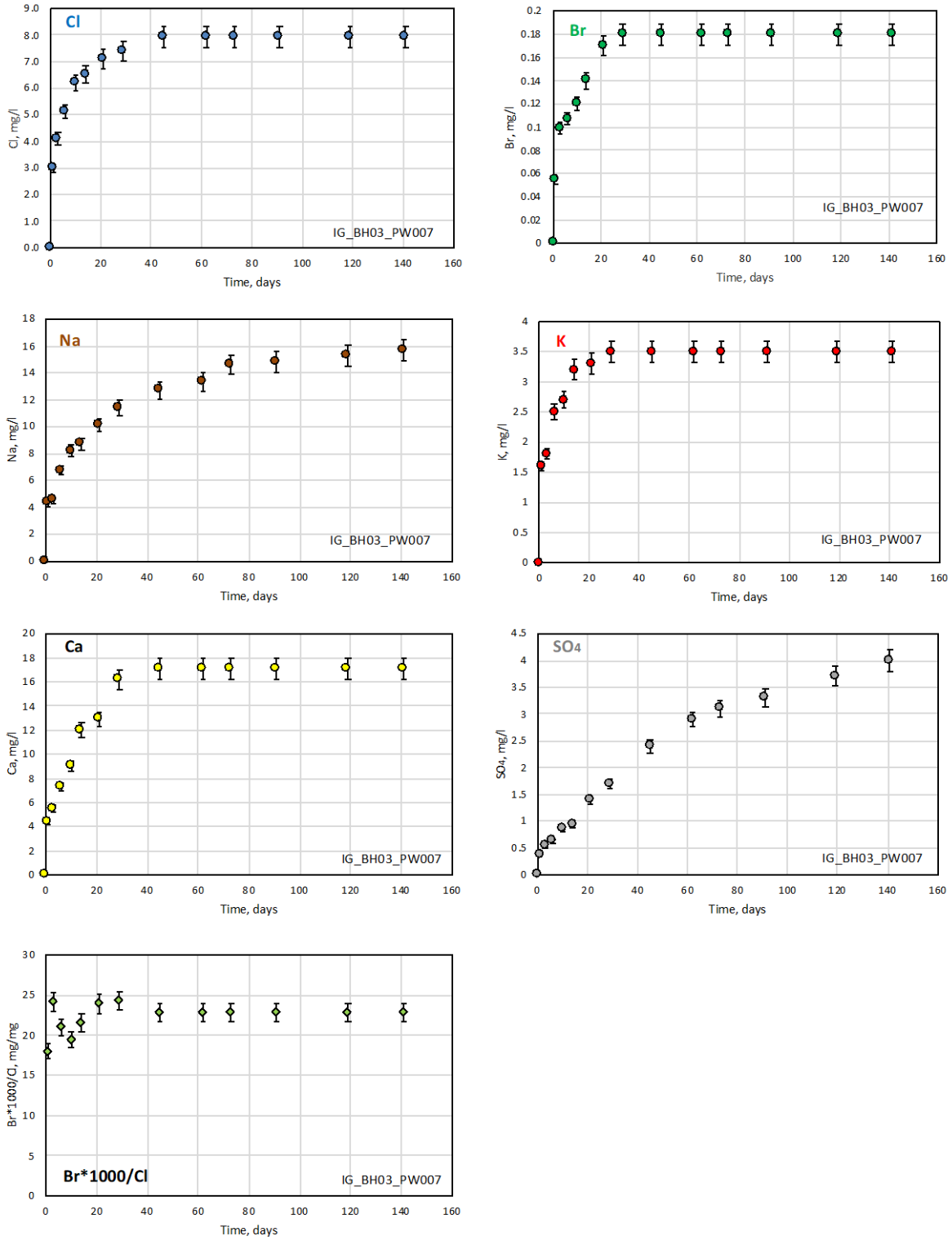

Figure 20 continued

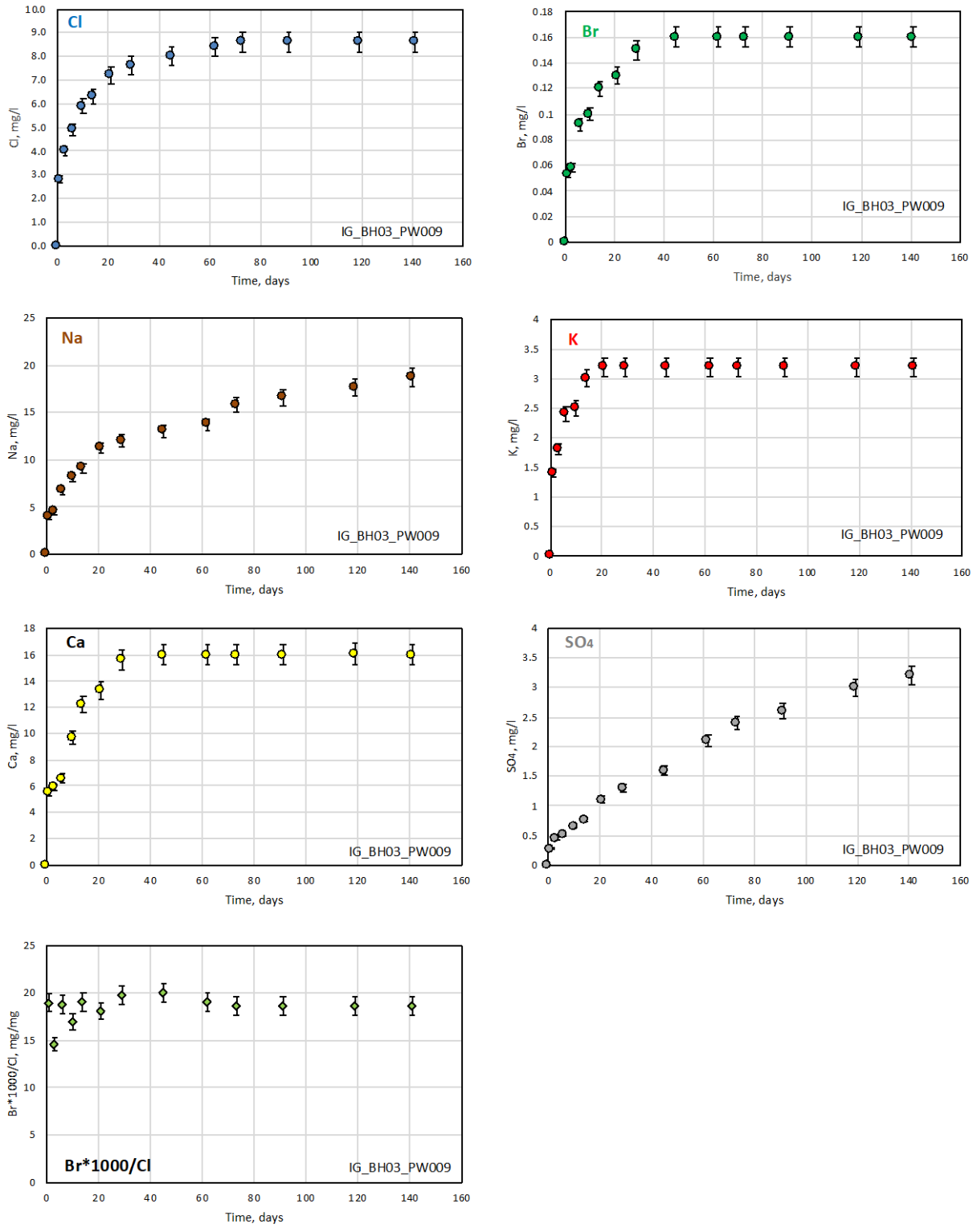

Figure 20 continued

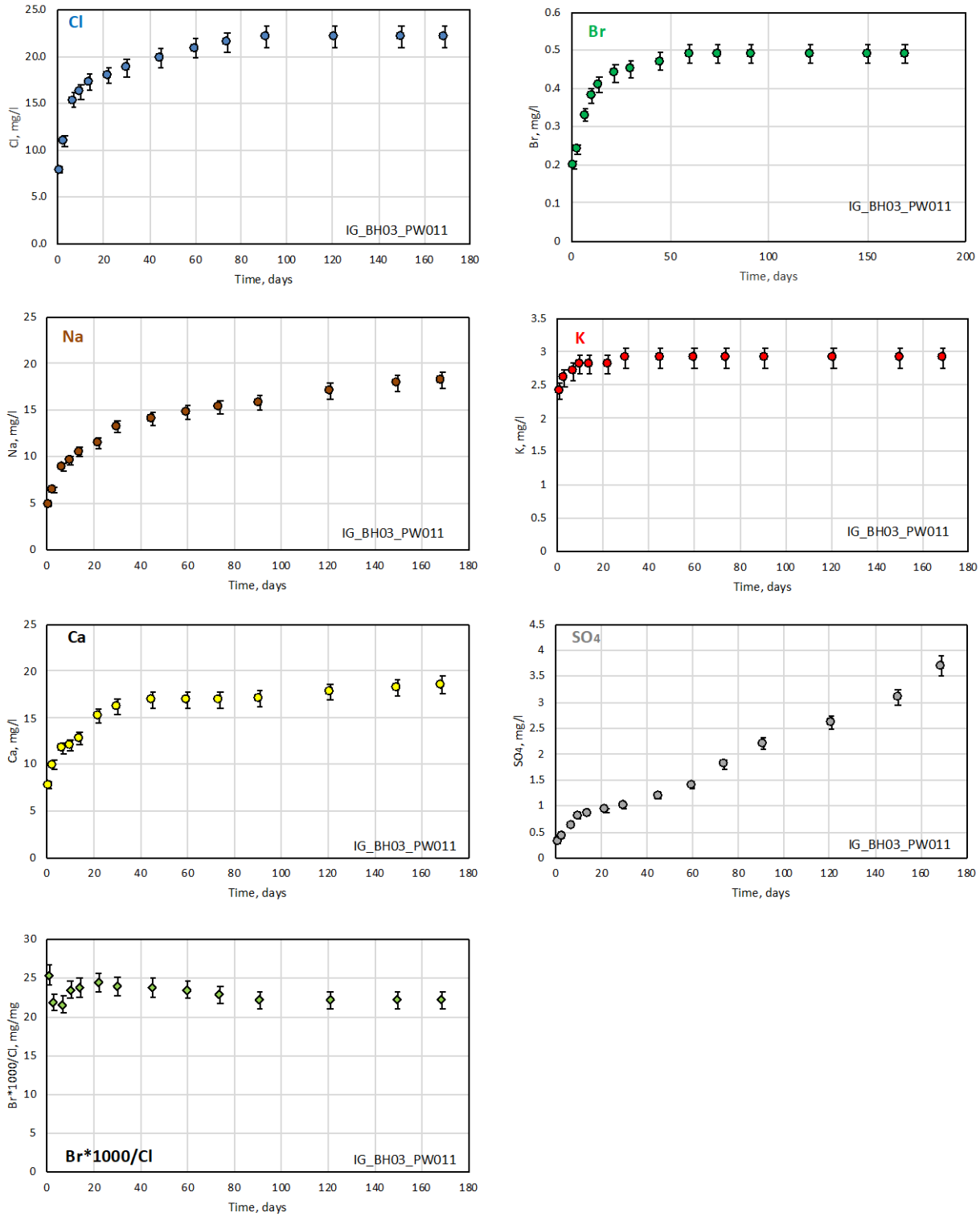

Figure 20 continued

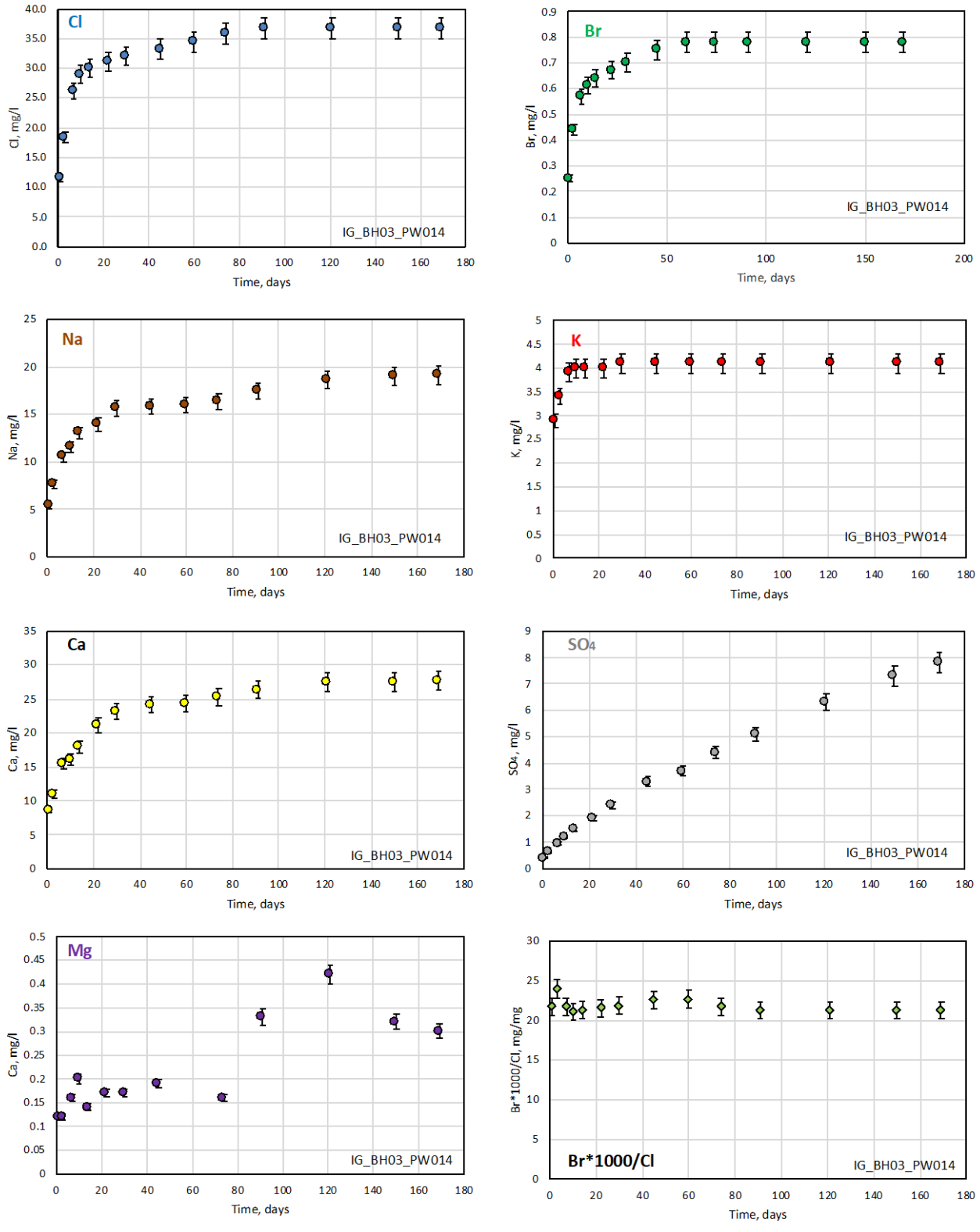

Figure 20 continued

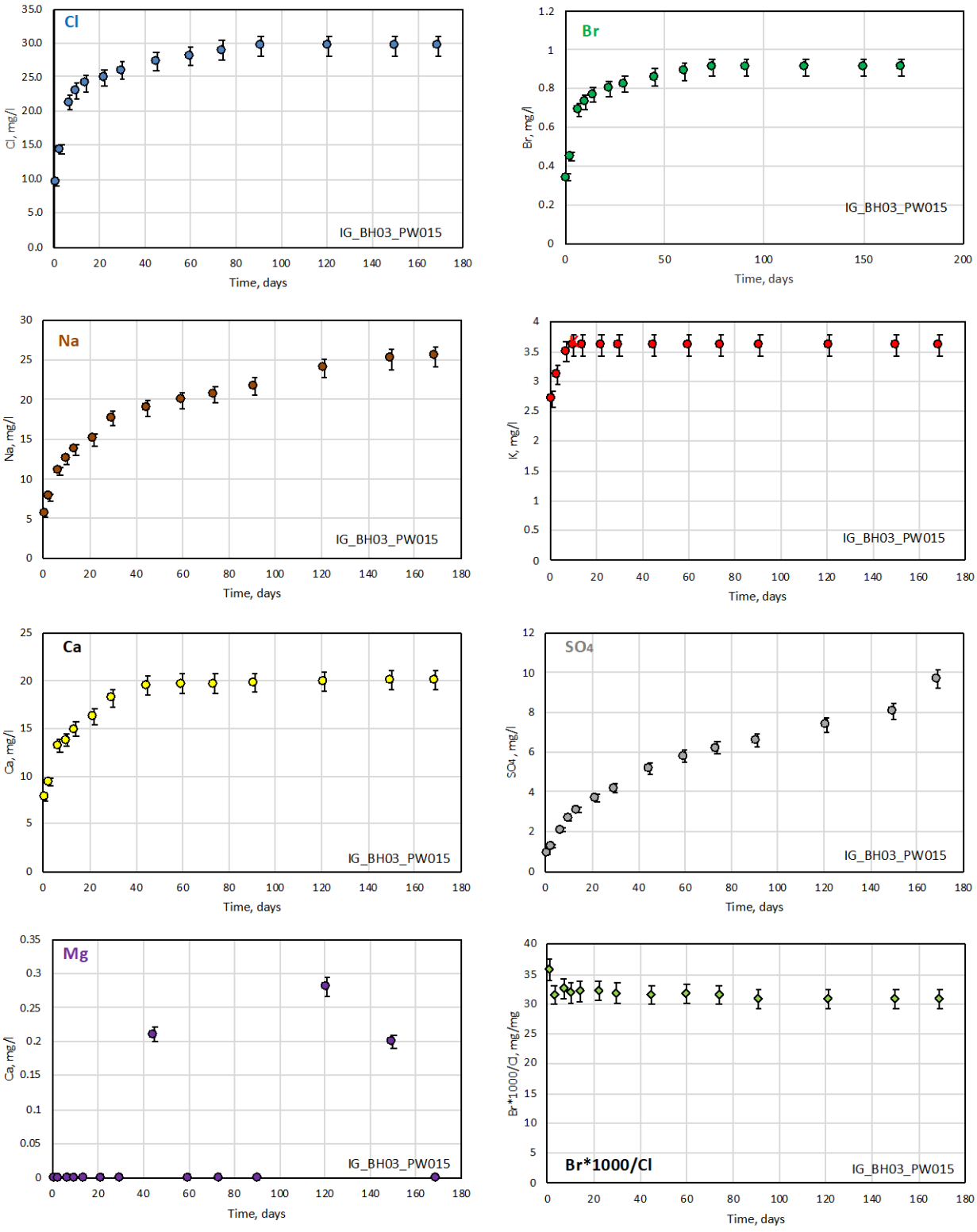

Figure 20 continued

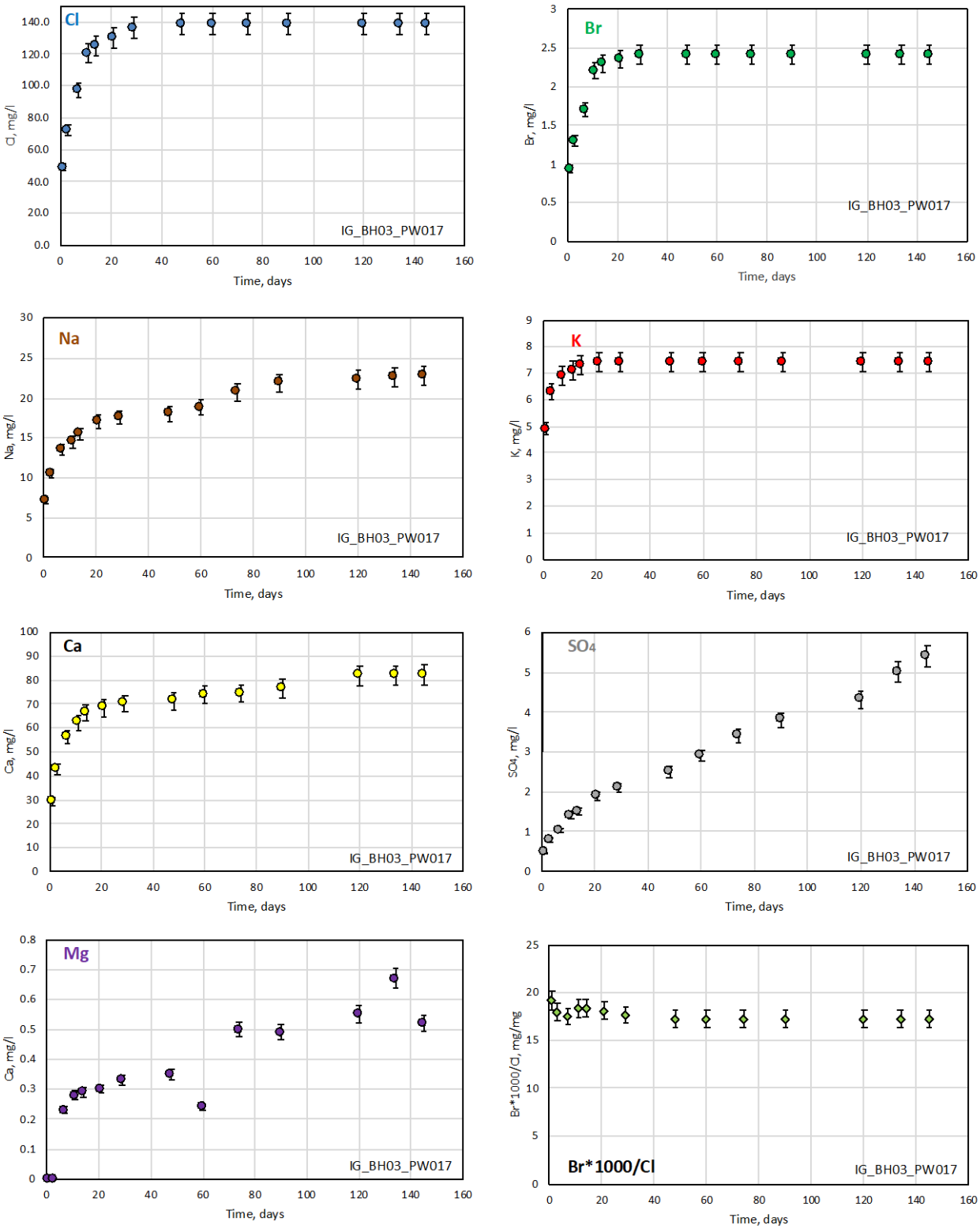

Figure 20 continued

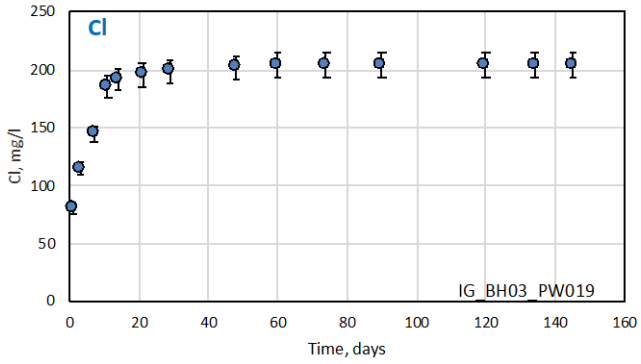

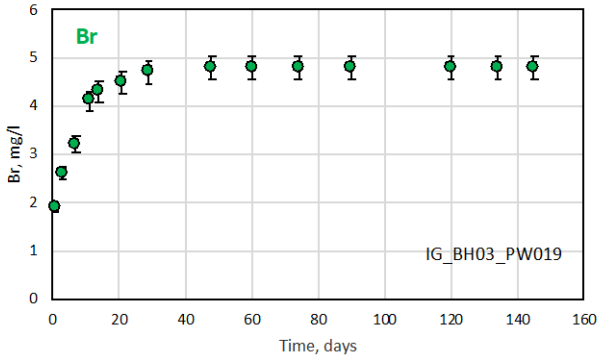

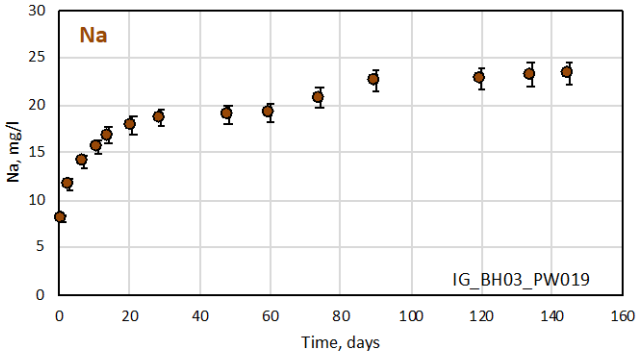

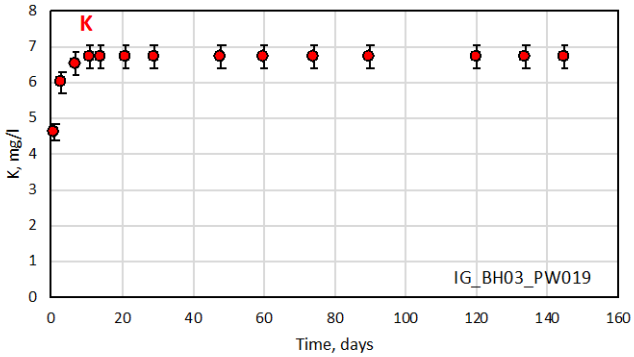

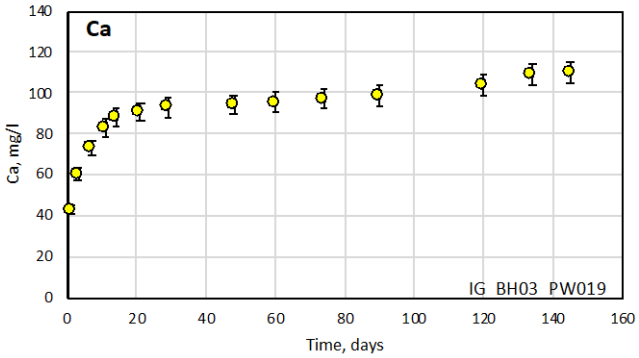

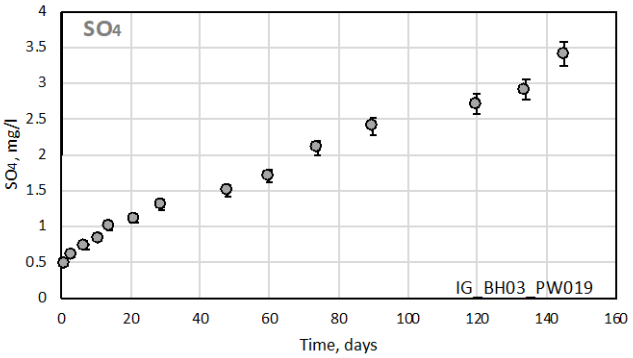

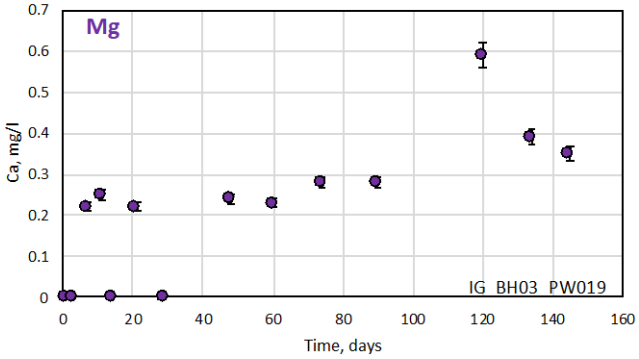

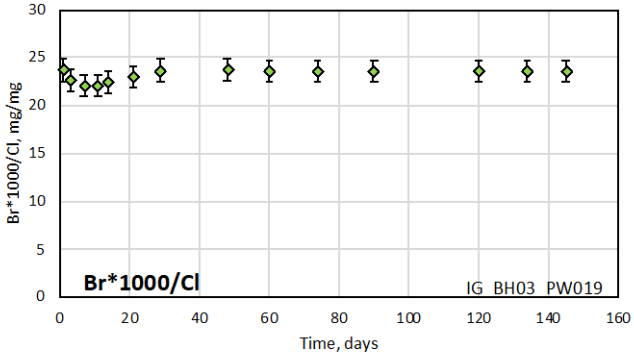

Figure 20 continued

7.2 Modelling of pore diffusion coefficients

Chloride pore diffusion coefficients were derived by modelling the chloride breakthrough curves obtained from the out-diffusion experiments of all ten samples from borehole IG_BH03. The chloride breakthrough curves are deduced from the Cl contents in the small-sized subsamples that were collected periodically during the out-diffusion experiments (cf. Section 3.3.2, 7.1). The pore diffusion coefficient is obtained by fitting the observed data with an analytical solution for one-dimensional radial diffusion out of the cylinder into a well-mixed solution reservoir (Crank 1975). The applied model (T. Gimmi, RWI, University of Bern) is restricted to homogeneous hydraulic properties (porosity, diffusion coefficient) across the core cylinder, and cannot consider heterogeneous properties due to rock anisotropy or induced effects, such as a drilling disturbed zone and/or stress release (Meier et al., 2015).

The pore diffusion coefficient, D_p, of a solute in a geological media mainly depends on the shape and size of water conducting pores (constrictivity) and on the pathways given by the connected pore network (tortuosity, cf. e.g., Ohlsson and Neretnieks 1995). It can be defined as:

$$D_p = D_w \frac{\delta_D}{\tau^2} \qquad \text{Eq. 8}$$

where D_P = pore-diffusion coefficient in m^2/s; D_W = diffusion coefficient in pure water in m^2/s; δ_D = constrictivity; τ = tortuosity; the term δ_D/τ^2 is called the geometry factor.

In a first assumption the pore diffusion coefficient of a given species, D_P, can be converted to the effective diffusion coefficient of this species, D_e, according to:

$$D_e = D_p \Phi_{WC} \qquad \text{Eq. 9}$$

where D_e is the effective diffusion coefficient in m^2/s and Φ_{WC} the species-accessible porosity.

The shape of the Cl elution curves obtained for all core samples from borehole IG_BH03 suggests a heterogeneous transport system from the rim to the centre of the core (Figure 21). The initial slopes are steep (in the transient state) during the first five to ten days of out-diffusion, and become more moderate later in the experiment.

The quality of the D_P fits is controlled by the difference ($\Delta_{meas\text{-}mod}$) of the measured and modelled Cl concentration at equal time and shown graphically by logarithmic plots (Figure 21). To determine the lowest $\Delta_{meas\text{-}mod}$ values, a stepwise adjustment of the single points was conducted and the $\Delta_{meas\text{-}mod}$ values were calculated for every measured point. The determination of the best fits per sampling point indicates a gradual decrease of the modelled pore diffusion coefficients as diffusion progresses deeper into the cores.

The modelled D_P values, which were determined at 45 °C, are additionally converted to 10 °C and 25 °C by the Stoke-Einstein equation (Lide 1994).

For the investigated core samples, the influence of the disturbed zone results in a pore diffusion coefficient that is a factor 1.5 to 6.5 higher than that of the inner core (Table 17, Figure 21).

The average pore diffusion coefficients (D_P) of the ten crystalline core samples vary between 0.7 and $2.3*10^{-10}$ m^2/s (10 °C), resulting in effective diffusion coefficients (D_e) between 0.3 and $1.3*10^{-12}$ m^2/s (10 °C, Table 17, Figure 21).

Considering the depth profile, pore and effective diffusion coefficients of chloride show a decreasing trend between 242 and 554 mbgs (down hole) and subsequently remain almost constant with increasing depth down to 985 mbgs (down hole) (Figure 22).

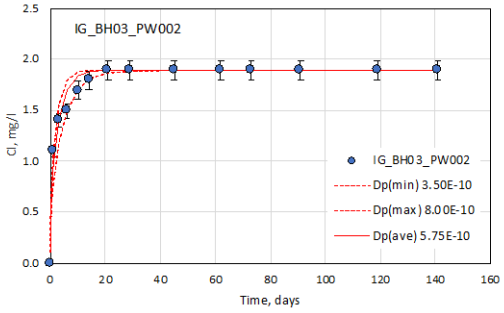

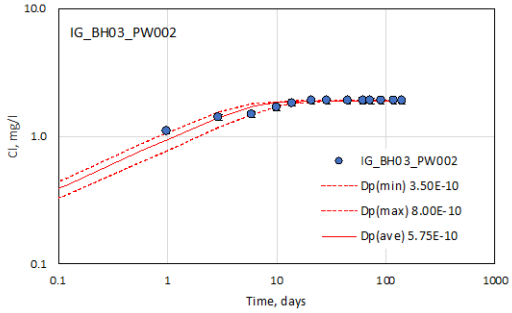

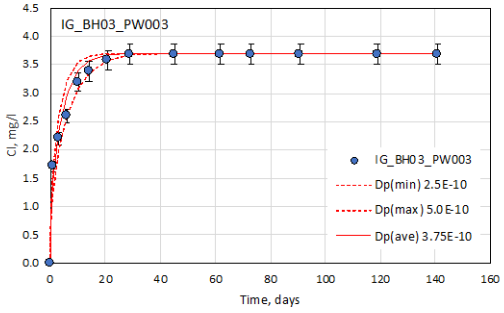

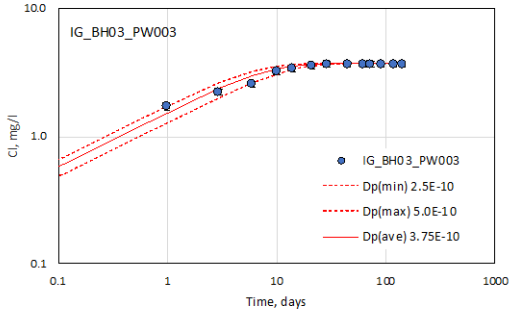

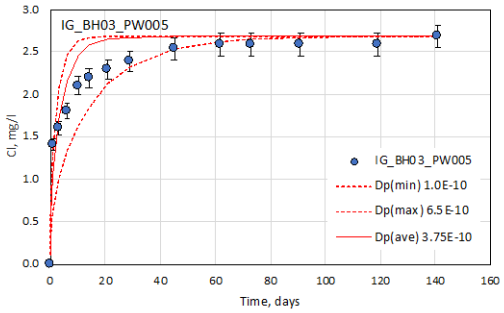

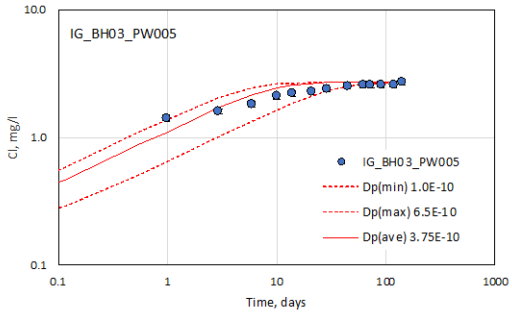

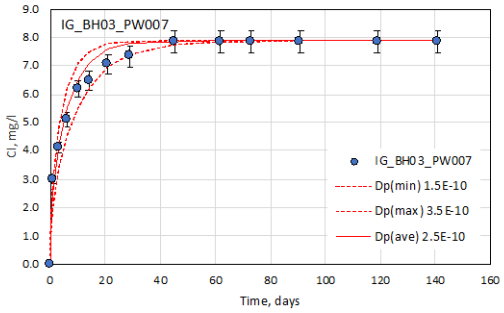

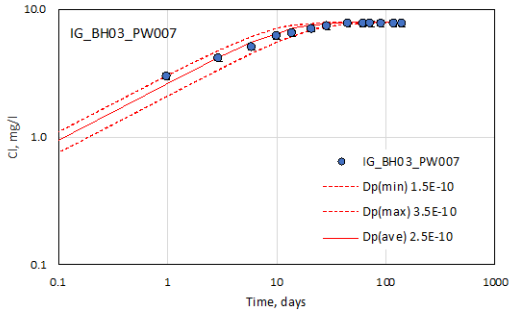

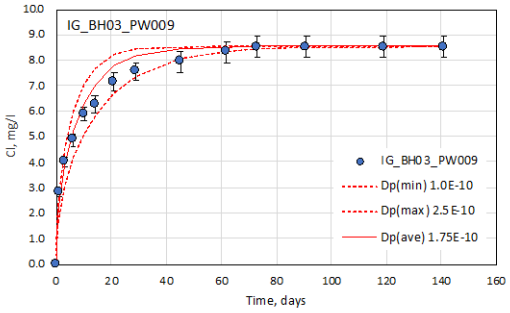

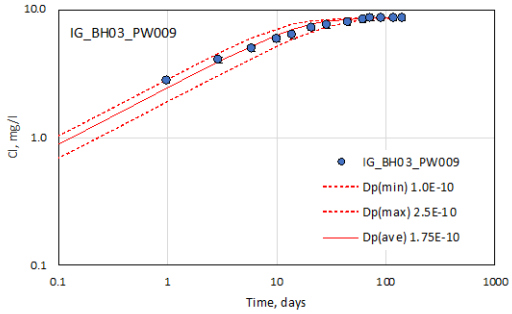

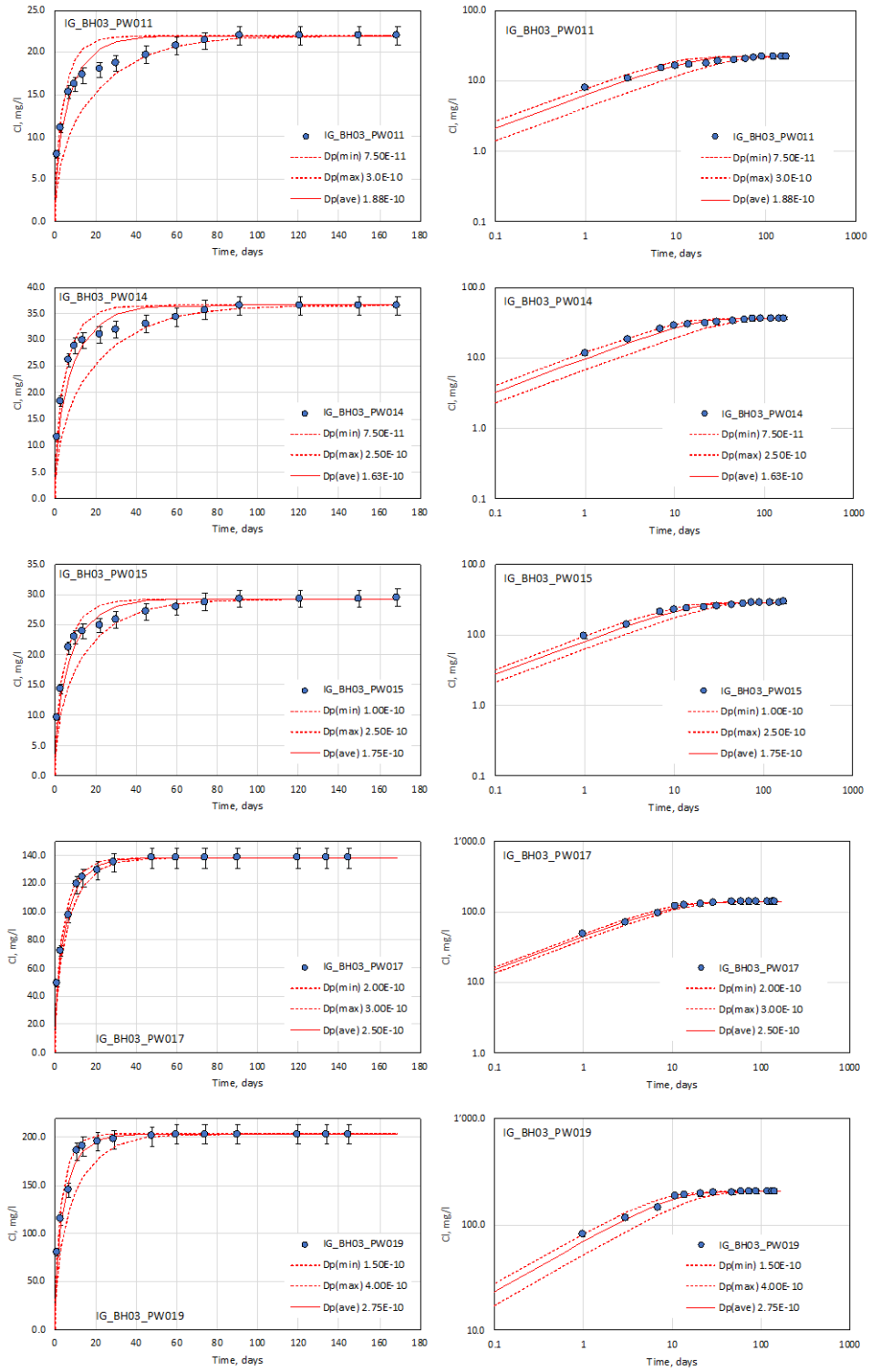

Figure 21: Maximum (Dp(max)) and minimum (Dp(min)) pore diffusion coefficients (45 °C) determined by a best fit of Cl elution curves in linear and logarithmic time and concentration scale; the solid lines mark the average diffusion coefficients (45 °C, Dp(ave))

Table 17: Minimum (min), maximum (max) and average (ave) pore and effective diffusion coefficients determined by 1-dimensional modelling of Cl-elution curves of out-diffusion experiments conducted on core samples from borehole IG_BH03 at 45 °C and calculated by the Stoke-Einstein equation for 10 °C and 25°C

Sample	Depth	WL-Porosity	D_P*10^{-10} (45°C)				D_P*10^{-10} (10°C)				D_e*10^{-12} (10°C)				D_P*10^{-10} (25°C)				D_e*10^{-12} (25°C)		
			max	min	ave		max	min	ave		max	min	ave		max	min	ave		max	min	ave
	mbgs*	Vol.%	m^2/s	m^2/s	m^2/s		m^2/s	m^2/s	m^2/s		m^2/s	m^2/s	m^2/s		m^2/s	m^2/s	m^2/s		m^2/s	m^2/s	m^2/s
IG_BH03_PW002	242.0	0.56	8.0	3.5	5.8		3.2	1.4	2.3		1.8	0.8	1.3		5.0	2.2	3.6		2.8	1.2	2.0
IG_BH03_PW003	345.2	0.52	5.0	2.5	3.8		2.0	1.0	1.5		1.0	0.5	0.8		3.1	1.6	2.4		1.6	0.8	1.2
IG_BH03_PW005	459.2	0.58	6.5	1.0	3.8		2.6	0.4	1.5		1.5	0.2	0.9		4.1	0.6	2.4		2.4	0.4	1.4
IG_BH03_PW007	503.9	0.55	3.5	1.5	2.5		1.4	0.6	1.0		0.8	0.3	0.6		2.2	0.9	1.6		1.2	0.5	0.9
IG_BH03_PW009	554.5	0.61	2.5	1.0	1.8		1.0	0.4	0.7		0.6	0.2	0.4		1.6	0.6	1.1		1.0	0.4	0.7
IG_BH03_PW011	608.8	0.54	3.0	0.8	1.9		1.2	0.3	0.8		0.7	0.2	0.4		1.9	0.5	1.2		1.0	0.3	0.6
IG_BH03_PW014	669.2	0.48	2.5	0.8	1.6		1.0	0.3	0.7		0.5	0.1	0.3		1.6	0.5	1.0		0.7	0.2	0.5
IG_BH03_PW015	771.6	0.56	2.5	1.0	1.8		1.0	0.4	0.7		0.6	0.2	0.4		1.6	0.6	1.1		0.9	0.4	0.6
IG_BH03_PW017	880.4	0.47	3.0	2.0	2.5		1.2	0.8	1.0		0.6	0.4	0.5		1.9	1.3	1.6		0.9	0.6	0.7
IG_BH03_PW019	984.7	0.44	4.0	1.5	2.8		1.6	0.6	1.1		0.7	0.3	0.5		2.5	0.9	1.7		1.1	0.4	0.8

* mbgs (down hole)

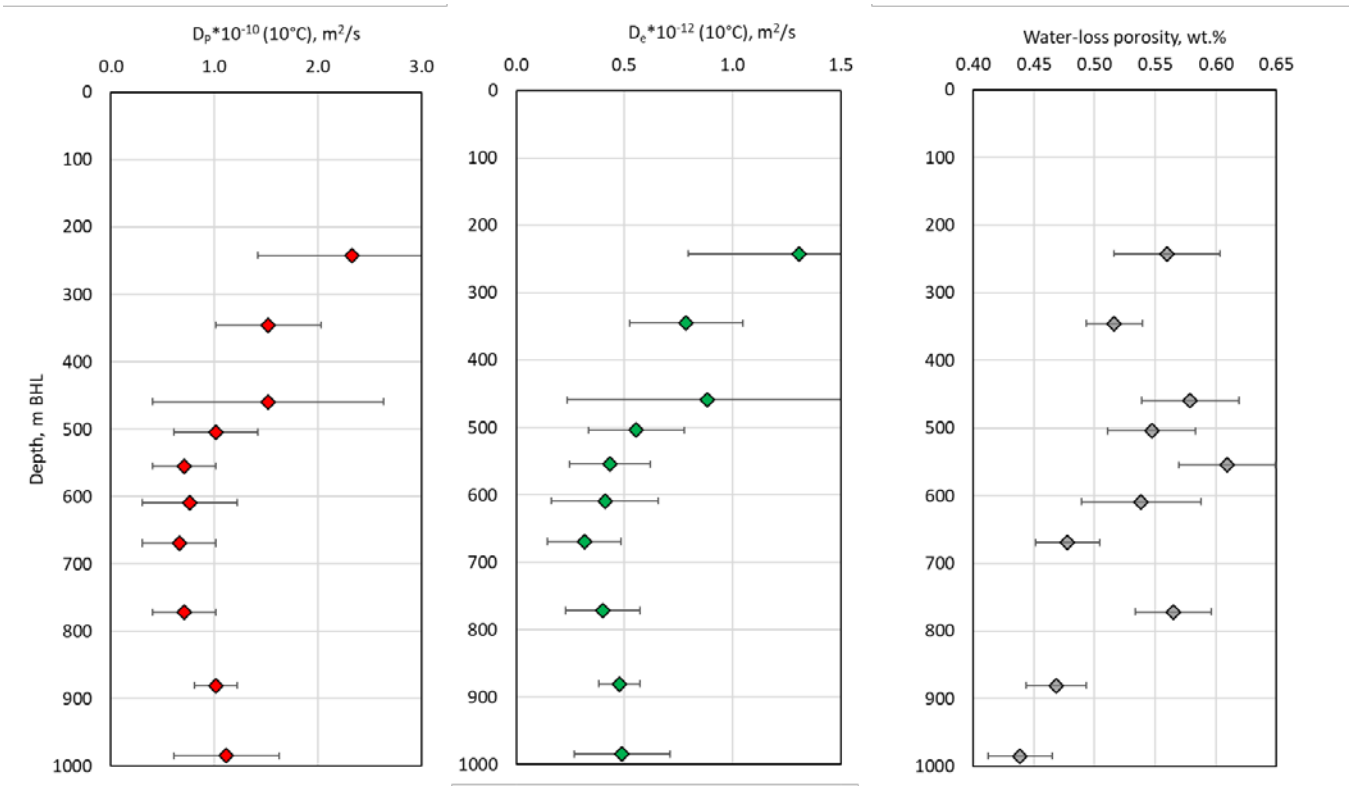

Note: m BHL is equivalent to mbgs (down hole).

Figure 22: Average pore (left) and effective (middle) diffusion coefficients (10 °C) and the corresponding WL-porosity (right) of core samples from borehole IG_BH03 versus depth; the errors are the difference between the average and maximum/minimum values

8.0 CHLORIDE, BROMIDE AND CHLORIDE ISOTOPES IN POREWATER OF BOREHOLE IG_BH03

Chloride and bromide concentrations of porewater were determined by aqueous extraction (cf. Section 3.3.1) and out-diffusion experiments (cf. Section 3.3.2). Aqueous extraction experiments were conducted prior to the other longer lasting out-diffusion and isotope diffusive exchange experiments in order to obtain information about porewater salinities.

8.1 Porewater chloride concentrations estimated by aqueous extraction experiments

Aqueous extraction experiments were conducted on 10 core samples from the individual sampled depth intervals. Approximate estimates of porewater Cl concentrations were calculated according to equation 3 (cf. Section 3.3.1). During crushing of the rock samples, saline fluids from fluid inclusions in quartz and feldspar are released, which contribute to the Cl and Br inventory of the samples. This means that the chloride concentrations determined by aqueous extraction overestimate the actual porewater Cl concentrations.

Estimated porewater Cl concentrations for core samples from borehole IG_BH03 determined by aqueous extraction vary between 2.7 and 14.6 g/kg H_2O (Table 18, Figure 14). Estimated porewater Cl concentrations determined by aqueous extraction are 1.3 to 37 times higher than those determined by out-diffusion (Table 16). The differences in porewater Cl concentrations determined by the two methods decreases with increasing depth and increasing porewater Cl concentrations (Table 18), indicating that porewater is the main Cl source in the deeper, higher salinity samples.

Based on the Cl-concentration range of porewater in core samples taken from borehole IG_BH03 (2.7 - 14.6 g/kg H_2O = 0.08 - 0.42 mol), the chemistry of isotope diffusive exchange experiments was defined at 0.3 mol NaCl.

8.2 Porewater chloride and bromide concentrations and δ^{37}Cl isotope ratios determined by out-diffusion experiments

The conservative behaviour of chloride and bromide, the absence of Cl and Br bearing minerals in the rock and the non-destructive character of the out-diffusion method make the porewater the only source for dissolved Cl and Br in the experimental solution. This allows calculation of the Cl and Br concentration in the porewater using mass balance according to equation 4 (Section 3.3.2), given that equilibrium in the out-diffusion experiments is achieved. As shown by their chloride and bromide elution curves, this latter condition is fulfilled for all samples (cf. Section 7.1).

The mass ratio of the two conservative elements, Cl and Br, serves as tracer of the origin of Cl and Br in porewater and fracture groundwater. The δ^{37}Cl ratio measured for the experiment solutions directly corresponds to the porewater Cl isotope signature. This is because the attained equilibrium in the out-diffusion experiment with respect to total Cl is also expected to result in equilibrium with respect to the Cl isotopes (Gimmi and Waber 2004).

Chloride concentrations of porewater taken between 242 and 985 mbgs (down hole) from borehole IG_BH03 vary between 74 and 11,460 mg/kg H_2O (Table 18, Figure 23). Considering the depth profile, the porewater chloride concentrations increase continuously from 74 mg/kg H_2O at 242 mbgs (down hole) to 11,460 mg/kg H_2O at 985 mbgs (down hole) (Table 18, Figure 23). An exception to this trend is the sample IG_BH03_PW015

(772 mbgs (down hole)), which has a Cl-concentration of 1,190 mg/kg H_2O, which is slightly lower than that of the sample taken above at 669 mbgs (down hole).

Porewater bromide concentrations of core samples from borehole IG_BH03 vary between 0.8 and 270 mg/kg H_2O (Table 18, Figure 23). Along the depth profile, the Br concentrations show almost a similar trend to the porewater Cl concentrations. Porewater Br concentrations increase gradually from 0.8 mg/kg at 242 mbgs (down hole) to 36.6 mg/kg H_2O at 772 mbgs (down hole) and, at greater depths, display a steep increase to 123 mg/kg H_2O at 880 mbgs (down hole) and 270 mg/kg H_2O at 985 mbgs (down hole) (Figure 23).

The Br*1000/Cl mass ratios (=Br/Cl ratio) of porewater from borehole IG_BH03 vary between 11 and 71 (Table 18, Figure 23). From 242 to 459 mbgs (down hole) porewater Br/Cl ratios increase from 11 to 71. The ratios decrease significantly to 23 at 504 mbgs (down hole) and then remain relatively constant, between 19 and 23, down to 669 mbgs (down hole). The ratio increases slightly to 31 at 772 mbgs (down hole), decreases to 17 at 880 mbgs (down hole) and increases again to 24 at 985 mbgs (down hole) (Table 18, Figure 23).

In the bromide versus chloride diagram, porewaters extracted from borehole IG_BH03 cores plot significantly above the seawater dilution line (Br*1000/Cl mass ratio of seawater = 3.4, Figure 24).

Porewater $\delta^{37}Cl$ isotope signatures vary between 0.05 ± 0.20 ‰ and 0.68 ± 0.20 ‰ SMOC along the depth profile between 503 and 985 mbgs (down hole) (Figure 23, Table 18). Porewater stable chlorine isotope signatures do not show a trend with porewater Cl-concentrations (Figure 25).

Table 18: Porewater Cl and Br concentrations and Br*1000/Cl mass ratios and $\delta^{37}Cl$ isotope signatures. Cl concentrations are determined by out-diffusion (o.d.) and estimated using aqueous extraction experiments (aq.ex.); the errors of porewater (o.d.), Br concentrations and Br*1000/Cl mass ratios are calculated by Gaussian error propagation (Appendix III); the errors of $\delta^{37}Cl$ values are the standard deviation of triplicate analyses

Sample	Depth	Cl_{PW} (o.d.)	Estimated Cl_{PW}(aq.ex.)	Br_{PW}	Br*1000/Cl	$\delta^{37}Cl$
	mbgs*	mg/kgH_2O	mg/kgH_2O	mg/kgH2O	mg/mg	‰ SMOC
IG_BH03_PW002	242.0	74±6		0.8±0.1	11±1	-**
IG_BH03_PW003	345.2	185±10		7.5±0.4	41±3	-**
IG_BH03_PW005	459.2	110±8		7.8±0.5	71±7	-**
IG_BH03_PW007	503.9	341±22		7.8±0.5	23±2	0.68±0.20
IG_BH03_PW009	554.5	341±22		6.3±0.4	19±2	0.14±0.20
IG_BH03_PW011	608.8	1000±84		22.2±1.9	22±3	0.32±0.20
IG_BH03_PW014	669.2	1740±100		36.9±2.2	21±2	0.45±0.20
IG_BH03_PW015	771.6	1190±70		36.6±2.2	31±3	0.05±0.20
IG_BH03_PW017	880.4	7140±390		123±7	17±1	0.26±0.20
IG_BH03_PW019	984.7	11460±660		270±15	24±2	0.45±0.22
IG_BH03_AQ001	238.8		2735			
IG_BH03_AQ002	346.0		3916			
IG_BH03_AQ003	460.1		2822			
IG_BH03_AQ004	504.2		4126			

Sample	Depth	Cl_{PW} (o.d.)	Estimated Cl_{PW}(aq.ex.)	Br_{PW}	Br*1000/Cl	$\delta^{37}Cl$
	mbgs*	mg/kgH_2O	mg/kgH_2O	mg/kgH2O	mg/mg	‰ SMOC
IG_BH03_AQ005	554.7		3358			
IG_BH03_AQ006	608.6		8809			
IG_BH03_AQ007	665.9		6135			
IG_BH03_AQ008	771.8		6088			
IG_BH03_AQ009	880.1		11981			
IG_BH03_AQ010	985.0		14599			

* mbgs (down hole)

** Cl-concentrations in out-diffusion test solutions were too low for the determination of chloride isotope signatures

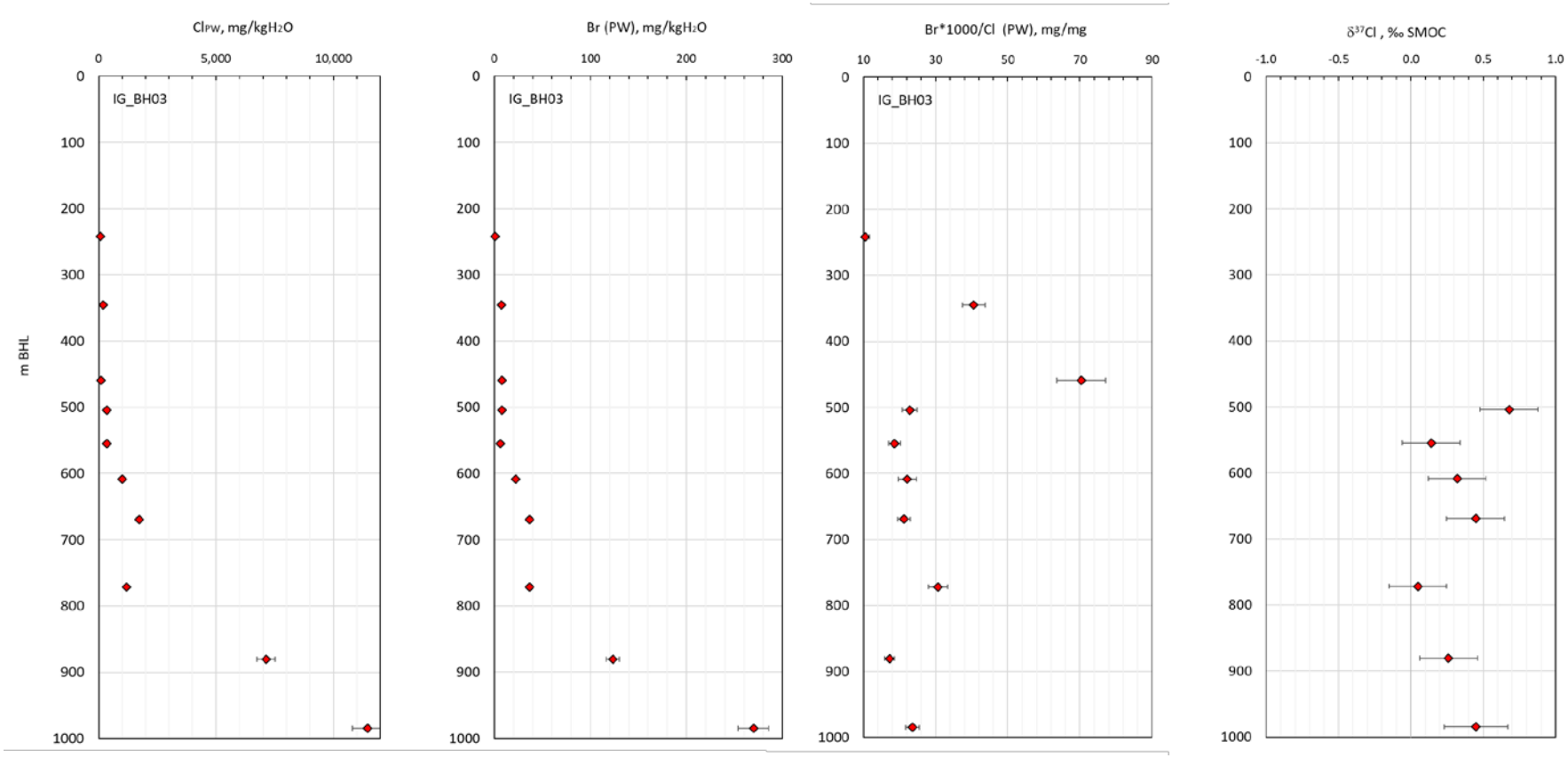

Note: m BHL is equivalent to mbgs (down hole).

Figure 23: Porewater chloride and bromide concentrations (out-diffusion only), Br*1000/Cl mass ratios and $\delta^{37}Cl$ porewater signatures extracted from cores from borehole IG_BH03 as function of depth

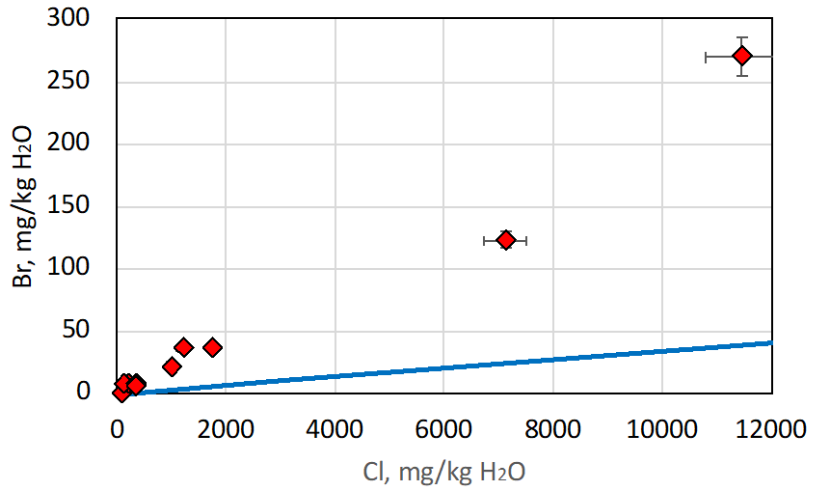

Figure 24: Chloride versus bromide concentrations of porewater from cores from borehole IG_BH03; the blue line indicates the seawater dilution line.

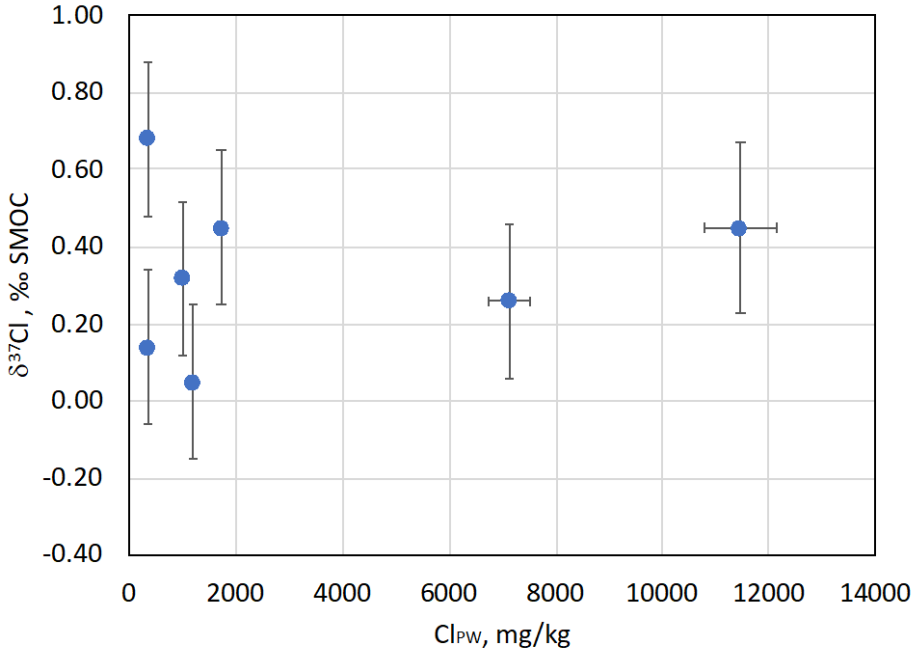

Figure 25: Porewater $\delta^{37}Cl$ isotope signatures versus porewater Cl-concentrations

9.0 $\delta^{18}O$ AND $\delta^{2}H$ OF POREWATER OF CORE SAMPLES FROM BOREHOLE IG_BH03

Isotope diffusive exchange experiments have been carried out on ten core samples (20 individual experiments) from borehole IG_BH03. The $\delta^{18}O$ and $\delta^{2}H$ values of porewater are calculated according to equation 7 (cf. Section 3.3.3), expressed relative to the standard V-SMOW, and are listed in Table 19 and graphically shown in Figure 26 and Figure 27. The calculated porewater isotope signatures, which are based on the isotope analyses of the test waters, are carefully evaluated for potential artefacts, mainly due to evaporation of test water during the experiment, test water storage and handling. Evaporation of porewater during storage and handling was minimized by careful handling of the core samples (cf. Section 3.3.3). These processes might result in large discrepancies between the gravimetric water content and that calculated from isotope mass balance or isotope signatures that are out of any natural range and/or a large error on the calculated porewater isotope signatures. Such differences were not observed in this study (cf. Section 5.1.2).

Evaporation within the experiment was monitored by keeping track of all individual weights before and after the experiments. None of the experiments suffered evaporation > 2 % of the total water mass in the experiments (= mass of porewater determined gravimetrically + mass of test water) during the time of equilibration.

The maximum Cl concentration determined by aqueous extraction prior to the set-up of the isotope diffusive exchange experiments is 14.6 g/kg H_2O, which relates to 0.44 mol $NaCl_{eq}$. Out-diffusion experiments showed a maximum Cl concentration of 11.5 g/kg H_2O, which relates to 0.32 mol $NaCl_{eq}$. Based on the aqueous extraction results, it was decided to adjust the salinity of the test solutions to 0.3 mol NaCl to prevent mass transfer from the test water reservoir to the rocks.

Stable oxygen and hydrogen isotope signatures of porewater extracted from core samples from borehole IG_BH03 vary between -10.82 and -5.97 ‰ for $\delta^{18}O$ and -82.7 and -57.2 ‰ for $\delta^{2}H$ (Table 19, Figure 26). Along the depth profile encountered by borehole IG_BH03, stable water isotope signatures are almost constant within the error range between 242 and 772 mbgs (down hole) showing only minor variations between -10.82 and -9.30 ‰ in $\delta^{18}O$ and between -82.7 and -74.6 ‰ in $\delta^{2}H$, respectively. Exceptions of these trends are the porewaters of the samples IG_BH03_PW012 (504 mbgs (down hole)) and PW018 (613 mbgs (down hole)) which are with -7.18 and -5.97 ‰ for $\delta^{18}O$ and -66.2 and -61.6 ‰ for $\delta^{2}H$. These values are more enriched in ^{18}O and ^{2}H than the other porewaters of core samples taken in this zone (Table 19, Figure 26). The deepest two samples taken at 880 and 985 mbgs (down hole) have $\delta^{18}O$ isotope signature of -8.03 and -7.88 ‰ and $\delta^{2}H$ signatures of -57.2 and -52.7 ‰ and are so more enriched in ^{18}O and ^{2}H than any of the porewater of samples taken above (Table 19, Figure 26).

Porewaters from borehole IG_BH03 of core sample taken between 242 and 772 mbgs (down hole) plot on or slightly to the right of the global meteoric water line (GMWL) on the $\delta^{18}O$-$\delta^{2}H$ diagram (Figure 27). Exceptions of this trend are the porewaters of the samples taken at 504 and 609 mbgs (down hole), which plot to the right of the GMWL above the others sampled in this zone (Figure 27). Porewater of the deepest two samples taken at 880 and 985 mbgs (down hole) plot on the GMWL, above samples taken at lower depths (Figure 27).

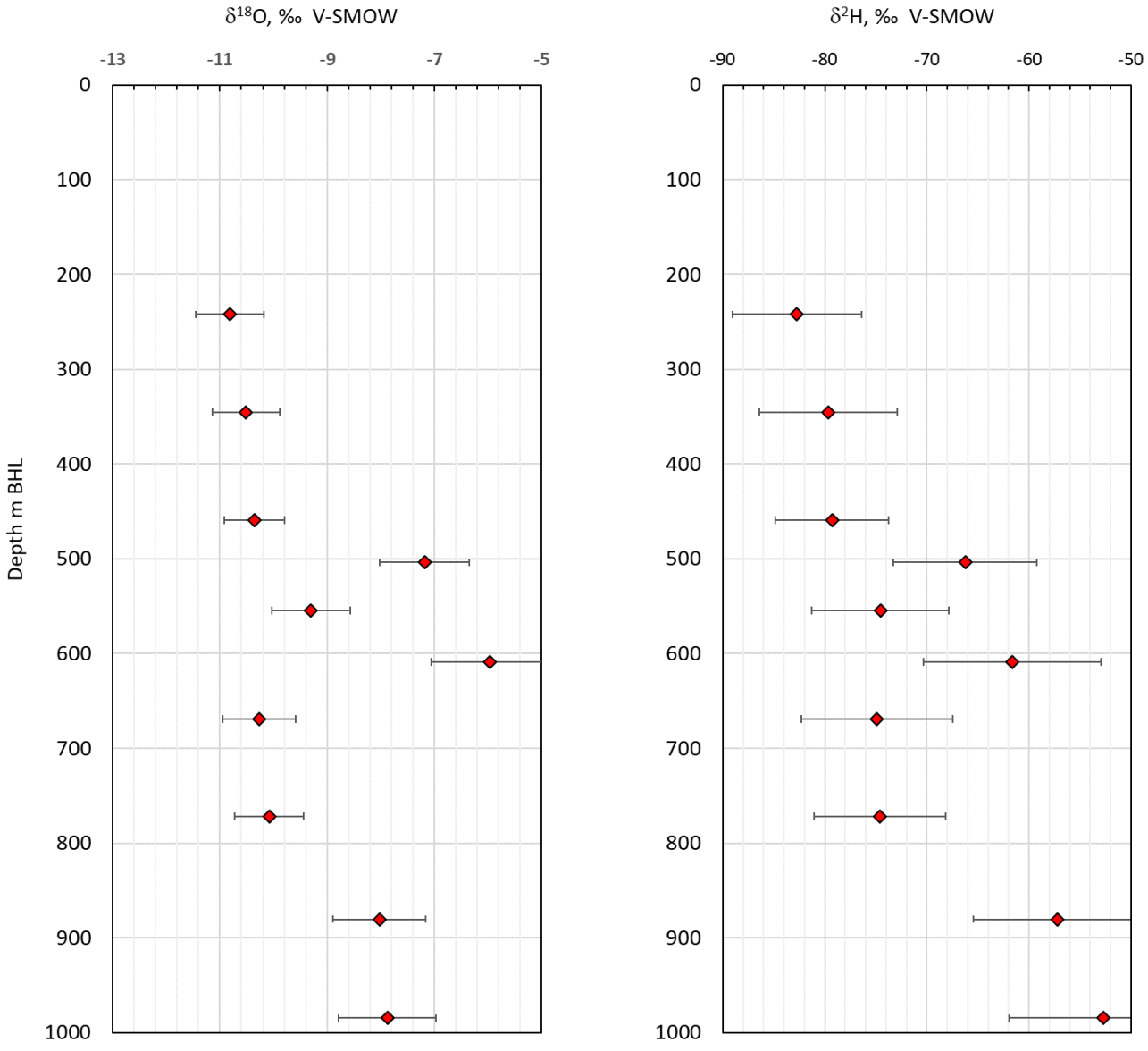

Note: m BHL is equivalent to mbgs (down hole).

Figure 26: $\delta^{18}O$ and $\delta^{2}H$ porewater signatures as function of depth along borehole IG_BH03; errors are calculated by Gaussian error propagation

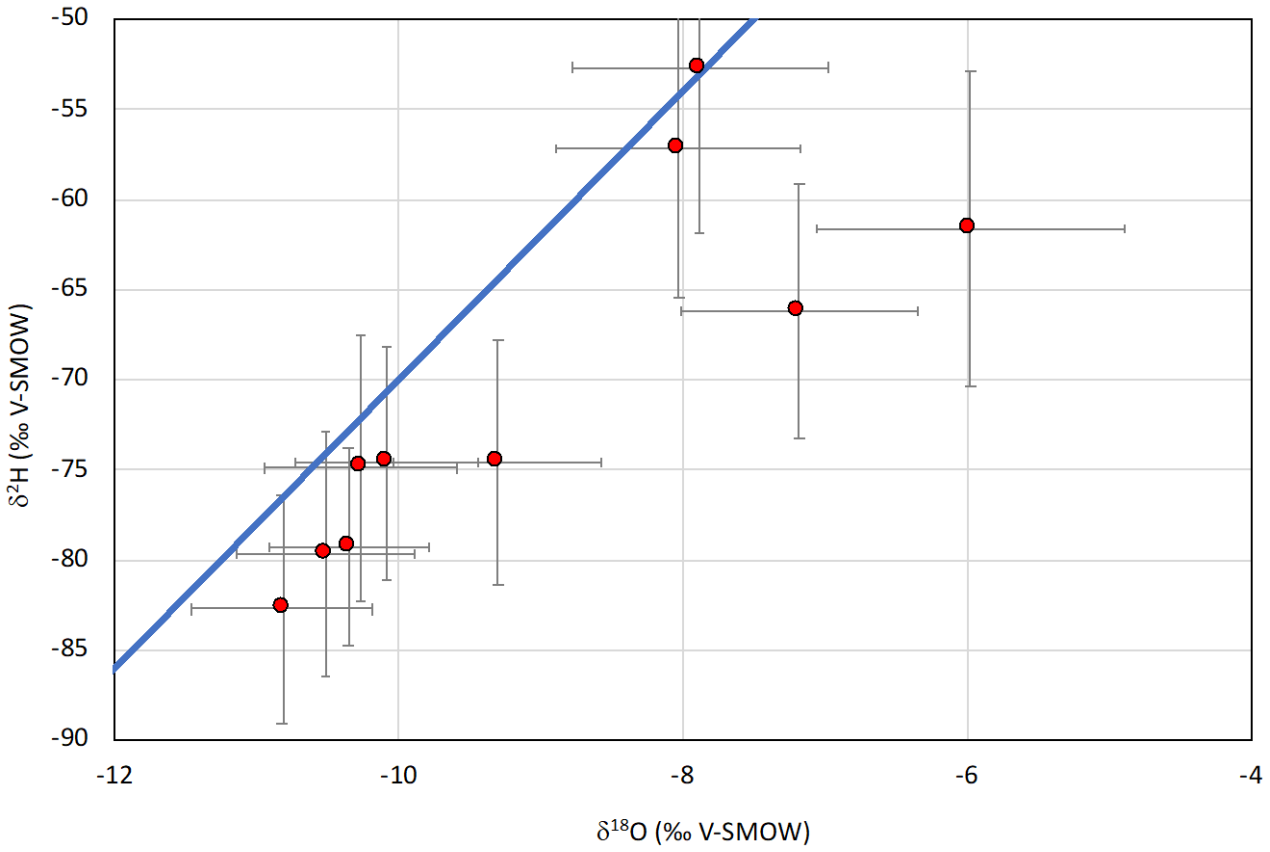

Figure 27: $\delta^{18}O$ versus $\delta^{2}H$ values of porewater; the blue line marks the global meteoric water line; the errors of the stable isotope ratios are calculated by Gaussian error propagation

Table 19: $\delta^{18}O$ and $\delta^{2}H$ values of porewater of core samples from borehole IG_BH03; the errors are calculated by Gaussian error propagation

Sample	Depth	$\delta^{18}O$	Error $\delta^{18}O$	$\delta^{2}H$	Error $\delta^{2}H$
	mbgs*	‰ V-SMOW	‰ V-SMOW	‰ V-SMOW	‰ V-SMOW
IG_BH03_PW002	242.0	-10.82	0.63	-82.7	6.3
IG_BH03_PW003	345.2	-10.51	0.63	-79.6	6.8
IG_BH03_PW005	459.2	-10.35	0.56	-79.3	5.5
IG_BH03_PW0007	503.9	-7.18	0.84	-66.2	7.0
IG_BH03_PW0009	554.5	-9.30	0.73	-74.6	6.7
IG_BH03_PW011	608.8	-5.97	1.09	-61.6	8.7
IG_BH03_PW014	669.2	-10.27	0.67	-74.9	7.4
IG_BH03_PW015	771.6	-10.08	0.64	-74.6	6.5
IG_BH03_PW017	880.4	-8.03	0.86	-57.2	8.3
IG_BH03_PW019	984.7	-7.88	0.90	-52.7	9.3

*mbgs (down hole)

10.0 SUMMARY

Porewater investigations applying different indirect methods were successfully conducted on crystalline core samples taken between 242 and 985 mbgs (down hole) from borehole IG_BH03 drilled in the Revell batholith (RE-B at Ignace, Ontario).

Potential major sampling-, preservation-, preparation-, experimental- and analytical artefacts, were carefully monitored during the investigation, and none were observed.

The investigated ten core samples consisted of macroscopically homogeneous, equigranular granodiorite and tonalite with quartz, plagioclase and biotite as main components, with variable degrees of alteration.

The gravimetrically determined water contents (weighted for the entire core sample) vary along the depth profile between 0.16 and 0.23 wt.%, corresponding to water-loss porosities between 0.43 and 0.62 Vol.%. Gravimetrically determined water contents agreed well with those determined by isotope diffusive exchange experiments. The bulk, wet density values are between 2.63 and 2.67 g/cm^3.

Pore diffusion coefficients were determined by 1-dimensional diffusion modelling based on the fitting of Cl-elution curves, set up by taking periodic sub-samples from out-diffusion experiments. Elution curves could not be fitted by a single pore diffusion coefficient. All cores showed a faster diffusion in the outer rim of the cores and a slower diffusion in the inner parts. The average pore diffusion coefficients (10 °C) vary between $0.7*10^{-10}$ and $2.3*10^{-10}$ m^2/s, corresponding to effective diffusion coefficients between $0.3*10^{-12}$ and $1.3*10^{-12}$ m^2/s.

Aqueous extraction experiments were conducted prior to the set-up of the long-term experiments to obtain first information about porewater salinities, which are necessary for the applied test water concentrations for isotope diffusive exchange experiments.

Out-diffusion experiments ran for more than 140 days. The analyses of time series samples showed that all experiments were in equilibrium with respect to Cl before they were terminated. Test water chemistries are mainly dominated by sodium, calcium, potassium, hydrogen carbonate and chloride in varying proportions and concentrations.

Porewater Cl and Br concentrations were calculated using out-diffusion concentrations and the gravimetrically determined mass of porewater. They vary between 74 and 11,460 mg/kg H_2O for Cl, and 0.8 and 270 mg/kg H_2O for Br, resulting in Br*1000/Cl mass ratios between 11 and 70.

Chlorine isotope signatures of porewater vary along the profile between 0.05 and 0.60 ‰ SMOC and show no correlation to porewater Cl concentrations.

Porewater stable water isotope signatures were determined by isotope diffusive exchange experiments. Along the depth profile encountered by borehole IG_BH03, porewater $\delta^{18}O$ signatures vary between -10.82 and -5.97 ‰ V-SMOW, and δ^2H signatures between -82.7 and -52.7 ‰ V-SMOW.

11.0 REFERENCES

Bas, M.J., Streckeisen, A.L., 1991. The IUGS Systematic of Igneous Rocks. Journal of the Geological Society, London.

Blackburn, C.E. and Hinz, P., 1996. Gold and base metal potential of the northwest part of the Raleigh Lake greenstone belt, northwestern Ontario-Kenora Resident Geologist's District; in Summary of Field Work and Other Activities 1996, Ontario Geological Survey, Miscellaneous Paper 166, p.113-115.

Crank, J., 1975. The Mathematics of Diffusion; Oxford Science Publications; Oxford.

DesRoches, A., Sykes, M., Parmenter, A. and Sykes, E., 2018. Lineament Interpretation of the Revell Batholith and Surrounding Greenstone Belts. Nuclear Waste Management Organization. NWMO Report Number: NWMO-TR-2018-19.

Eichinger, F.L., Waber, H.N., Smellie, J.A.T., 2006. Characterisation of Matrix Porewater at the Olkiluoto Investigation Site, Finland. Posiva Working Report 2006-103, Posiva OY, Olkiluoto Finland.

Golder (Golder Associates Ltd.) and PGW (Paterson Grant and Watson Ltd.), 2017. Phase 2 Geoscientific Preliminary Assessment, Geological Mapping, Township of Ignace and Area, Ontario: APM-REP-01332-0225.

Gimmi, T. and Waber, H.N., 2004. Modelling of Tracer Profiles in Pore Water of Argillaceous Rocks in the Benken Borehole: Stable Water Isotopes, Chloride, and Chlorine Isotopes; Nagra Tech. Rep. 2004-05, Nagra, Wettingen, Switzerland.

Jäckli, H., 1970. Kriterien zur Klassifikation von Grundwasservorkommen. Ecologae geol. Helv., 63 (2), 389-434.

Le Maitre, R.W. (ed.), 2002. IGNEOUS ROCKS A classification and Glossary of Terms. Cambridge University Press, Cambridge, UK.

Lide, D.R., 1994. CRC Handbook of chemistry and physics. 75th ed., CRC Press, Boca Raton, USA.

Meier, D.B., Waber, H.N., Gimmi, T., Eichinger, F., Diamond, L.W., 2015. Reconstruction of in-situ porosity and porewater compositions of low-permeability crystalline rocks: Magnitude of artefacts induced by drilling and sample recovery. Journal of Contaminant Hydrology, 183, 55-71.

OGS (Ontario Geological Survey), 2011. 1:250 000 scale bedrock geology of Ontario, Ontario Geological Survey, Miscellaneous Release Data 126 - Revision 1.

Ohlsson, Y. and Neretnieks, I., 1995. Literature survey of matrix diffusion theory and of experiments and data including natural analogues; SKB Tech. Rep. 95-12, Svensk Kärnbränslehantering AB, Stockholm, Sweden.

Parmenter, A., Waffle, L. and DesRoches, A., 2020. An updated bedrock geology map and geological database for the northern portion of the Revell batholith. Nuclear Waste Management Organization. NWMO Report Number: NWMO-TR-2020-08.

Rogge, T., 1997. Eine molekular-diffusive Methode zur Bestimmung des Porenwassergehaltes und der Zusammensetzung von stabilen Isotopen im Porenwasser von Gestein; unveröffentlichte Diplomarbeit; Heidelberg.

Rübel, A.P., Sonntag, Ch., Lippmann, J., Pearson, F.J. and Gautschi, A., 2002. Solute transport in formations of very low permeability: Profiles of stable isotope and dissolved noble gas contents of pore water in the Opalinus Clay. Mont Terri, Switzerland; Geochim. Cosmochim. Acta, 66, 1311-1321.

Schmid, R., Douglas, Fettes D., Harte, B., Davis, E., Desmons, J., 2007. How to Name a Metamorphic Rock. Recommendations by the IUGS Subcomission on the Systematics of Metamorphic Rocks.

SGL (Sander Geophysics Limited), 2015. Phase 2 Geoscientific Preliminary Assessment, Acquisition, Processing and Interpretation of High-Resolution Airborne Geophysical Data, Township of Ignace, Ontario. NWMO Report Number: APM-REP-06145-0002.

Siivola, J., Schmid, R., 2007. List of Mineral Abbreviations. Recommendations by the IUGS Subcomission on the Systematics of Metamorphic Rocks.

SRK (SRK Consulting, Inc.) and Golder, 2015. Phase 2 Geoscientific Preliminary Assessment, Observation of General Geological Features, Township of Ignace, Ontario. NWMO Report Number: APM-REP-06145-0004.

Streckeisen A.L.,1974. Classification and Nomenclature of Plutonic Rocks. Recommendations of the IUGS Subcommission on the Systematics of Igneous Rocks. International Journal of Earth Sciences 63, 2, 773-786.

Stone, D., 2009. Geology of the Bending Lake Area, Northwestern Ontario; *in* Summary of Field Work and Other Activities 2009. Ontario Geological Survey. Open File Report 6240.

Stone, D., 2010a. Geology of the Stormy Lake Area, Northwestern Ontario; *in* Summary of Field Work and Other Activities 2010. Ontario Geological Survey, Open File Report 6260.

Stone, D., 2010b. Precambrian geology of the central Wabigoon Subprovince area, northwestern Ontario. Ontario Geological Survey, Open File Report 5422.

Stone, D., Halle, J. and Chaloux, E., 1998. Geology of the Ignace and Pekagoning Lake Areas, Central Wabigoon Subprovince; *in* Summary of Field Work and Other Activities 1998, Ontario Geological Survey, Misc. Paper 169.

Stone, D., Davis, D.W., Hamilton, M.A. and Falcon, A., 2010. Interpretation of 2009 Geochronology in the Central Wabigoon Subprovince and Bending Lake Areas, Northwestern Ontario, *in* Summary of Field Work and Other Activities 2010, Ontario Geological Survey, Open File Report 6260.

Waber, H.N. and Smellie, J.A.T., 2005. SKB Site Investigations Forsmark – Borehole KFM06: Characterisation of porewater. Part I: Diffusion experiments; SKB P-Rep. P-05-196, Svensk Kärnbränslehantering AB, Stockholm, Sweden.

Waber, H.N. and Smellie, J.A.T., 2006. Oskarshamn site investigations. Borehole KLX03: Characterisation of porewater. Part 2: Rock properties and diffusion experiments; SKB P-Report P-06-77. Svensk Kärnbränslehantering AB, Stockholm, Sweden.

APPENDIX I

Photo Documentation

Figure A-1: On site documentation of core samples for porewater characterization sent to Hydroisotop (photos provided by Golder); Core samples are packed in the first evacuated and sealed plastic bag

IG_BH03_AQ001: 238.64-238,87 m

IG_BH03_AQ002: 345.03-345.38 m

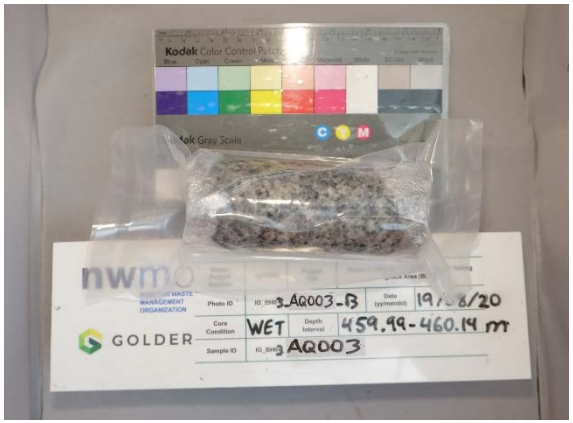

IG_BH03_AQ003: 459.99-459.44 m

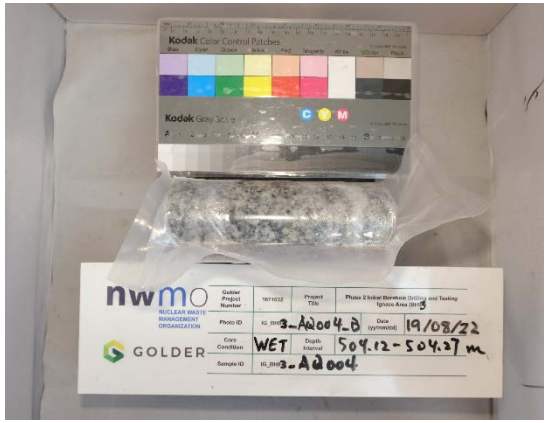

IG_BH03_AQ004: 504.12-504.27 m

IG_BH03_AQ005: 554.64-554.77 m

IG_BH03_AQ006: 608.52-608.66 m

IG_BH03_AQ007: 665.79-665.91 m

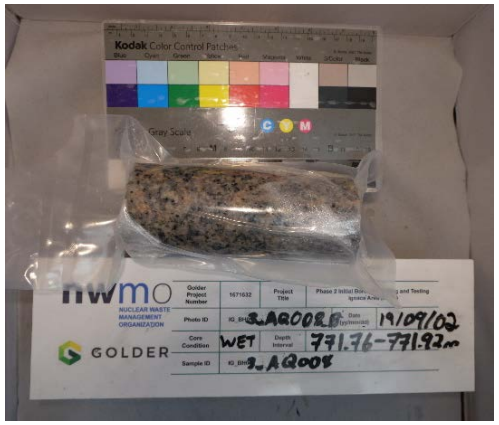

IG_BH03_AQ008: 771.76-771.92 m

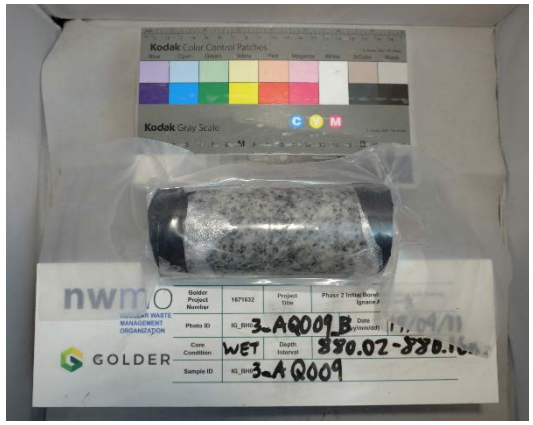

IG_BH03_AQ009: 880.02-880.16 m

IG_BH03_AQ010: 984.89-985.03 m

IG_BH03_PW001: 238.94-239.31 m

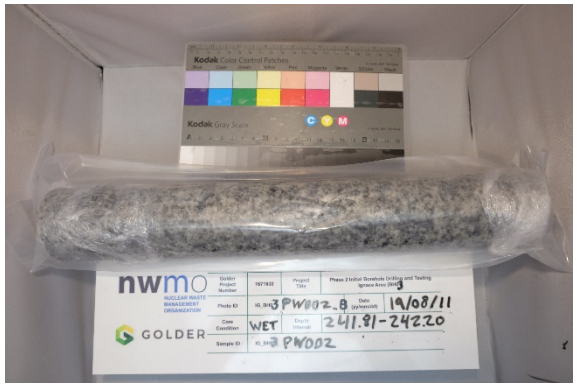

IG_BH03_PW002: 241.81-242.20 m

IG_BH03_PW003: 345.03-345.38 m

IG_BH03_PW004: 347.96-348.34 m

IG_BH03_PW005: 459.01-459.44 m

IG_BH03_PW006: 460.86-4601.26 m

IG_BH03_PW007: 503.72-504.12 m

IG_BH03_PW008: 506.47-506.87 m

IG_BH03_PW009: 554.28-554.64 m

IG_BH03_PW010: 558.53-558.94 m

IG_BH03_PW011: 608.66-609.02 m

IG_BH03_PW012: 612.60-612.98 m

IG_BH03_PW013: 668.55-668.95 m

IG_BH03_PW014: 668.95-669.36 m

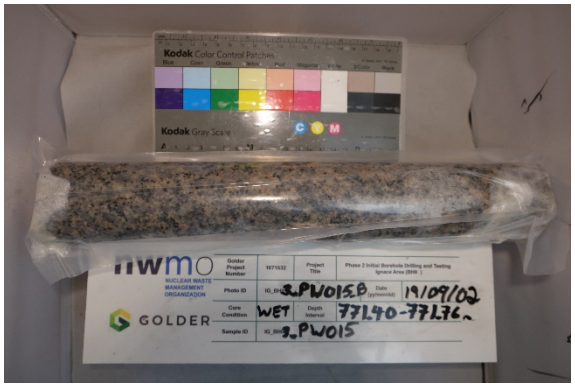

IG_BH03_PW015: 771.40-771.76 m

IG_BH03_PW016: 777.66-778.08 m

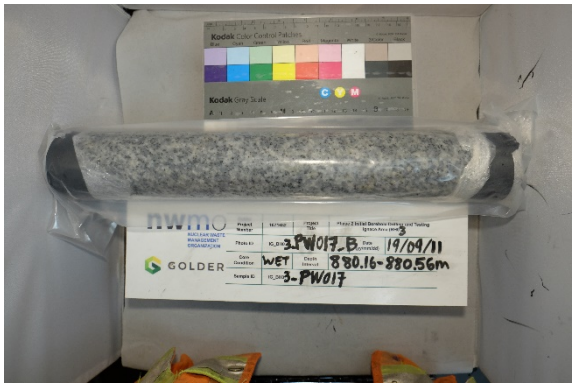

IG_BH03_PW017: 880.16-880.56 m

IG_BH03_PW018: 880.96-881.34 m

IG_BH03_PW019: 984.52-984.89 m

IG_BH03_PW020: 987.32-987.67 m

Figure A-2: Laboratory documentation of core samples for porewater characterization sent to Hydroisotop; photos were taken right after unpacking

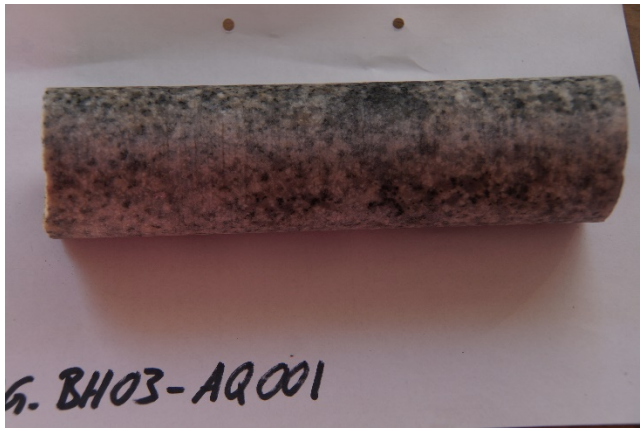

IG_BH03_AQ001: 238.64-238,87 m

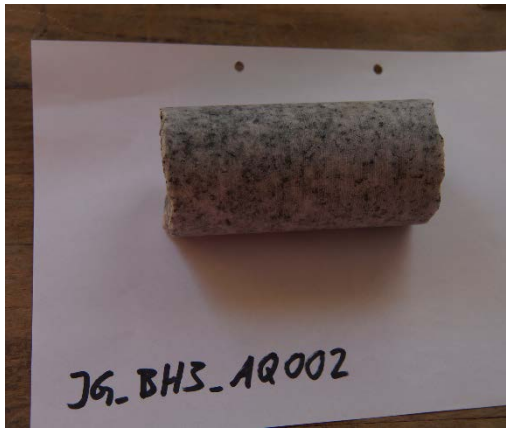

IG_BH03_AQ002: 345.03-345.38 m

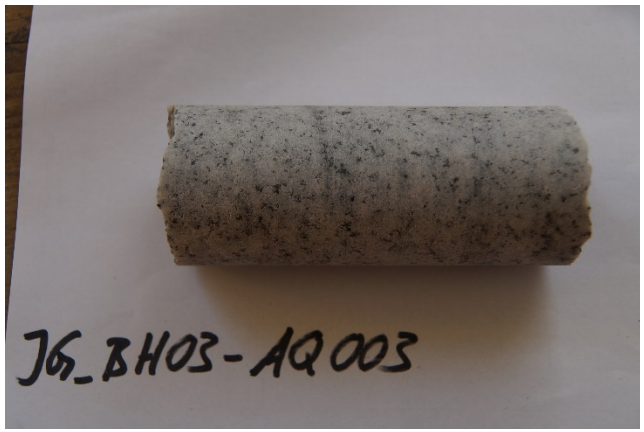

IG_BH03_AQ003: 459.99-459.44 m

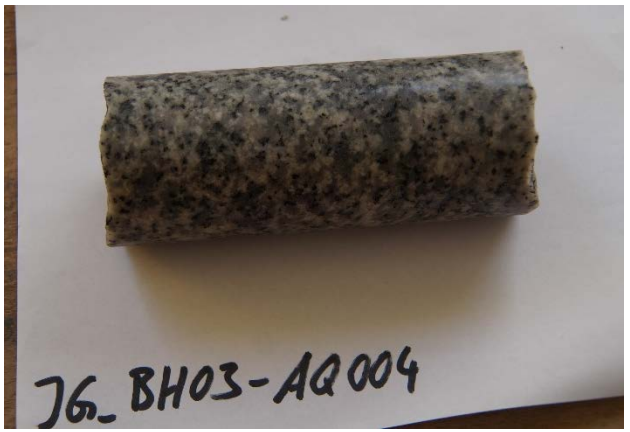

IG_BH03_AQ004: 504.12-504.27 m

IG_BH03_AQ005: 554.64-554.77 m

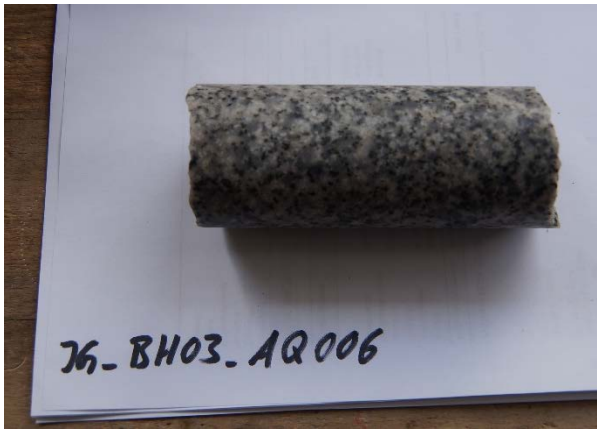

IG_BH03_AQ006: 608.52-608.66 m

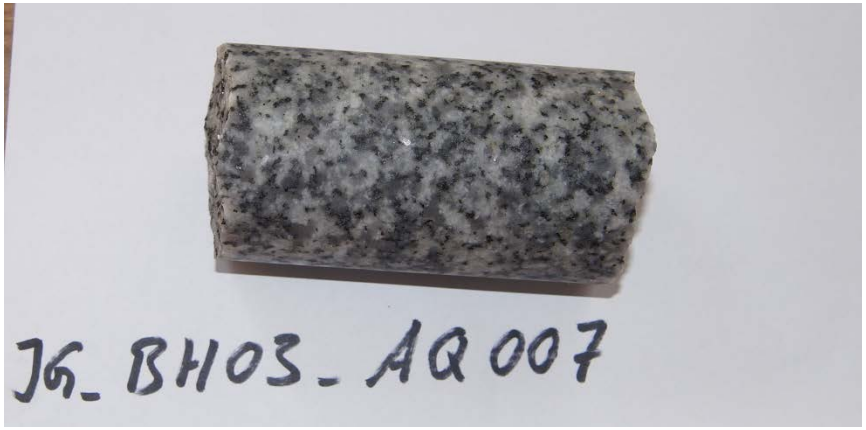

IG_BH03_AQ007: 665.79-665.91 m

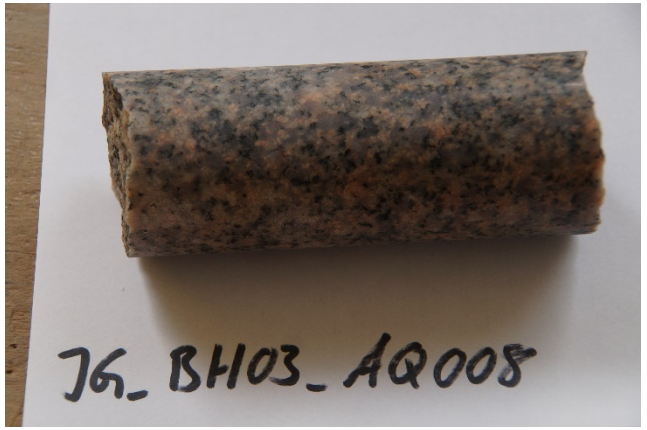

IG_BH03_AQ008: 771.76-771.92 m

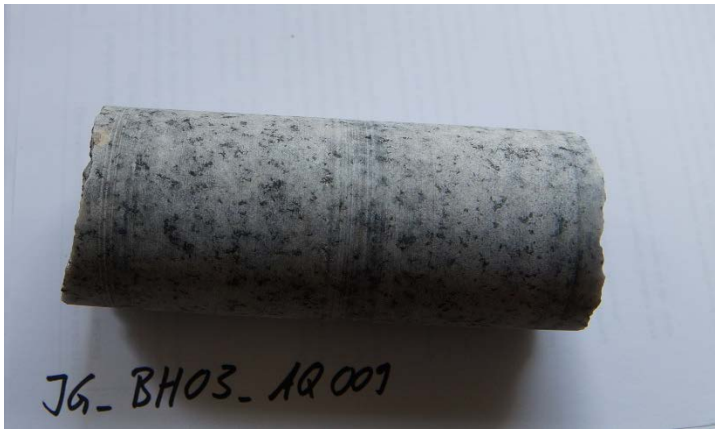

IG_BH03_AQ009: 880.02-880.16 m

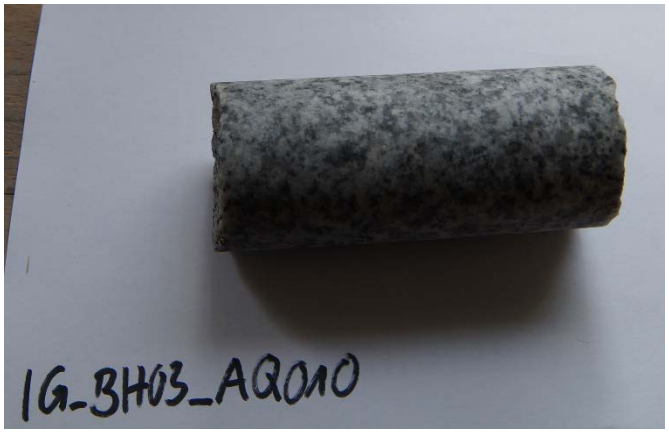

IG_BH03_AQ010: 984.89-985.03 m

IG_BH03_PW002: 241.81-242.20 m

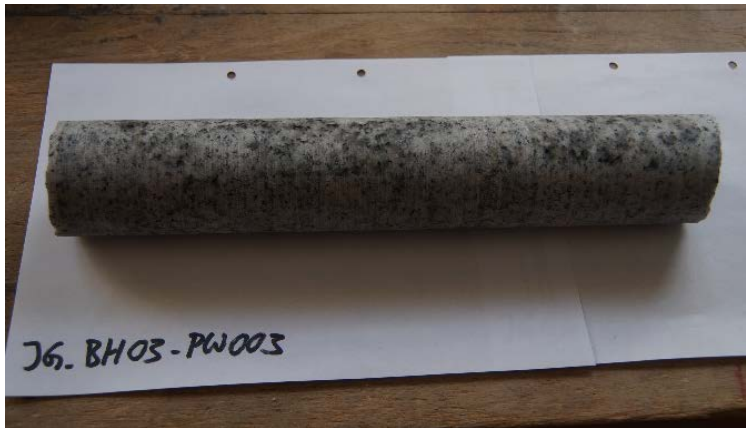

IG_BH03_PW003: 345.03-345.38 m

IG_BH03_PW005: 459.01-459.44 m

IG_BH03_PW007: 503.72-504.12 m

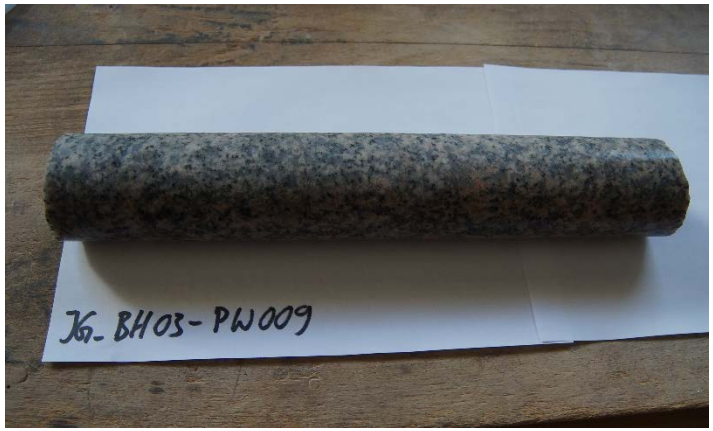

IG_BH03_PW009: 554.28-554.64 m

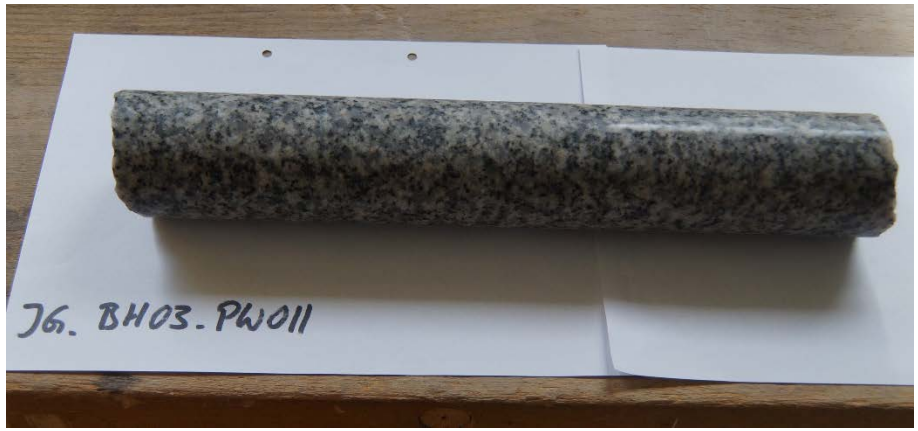

IG_BH03_PW011: 608.66-609.02 m

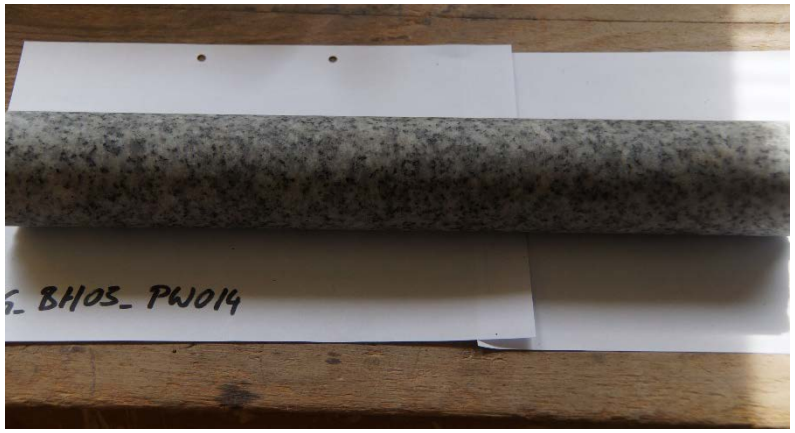

IG_BH03_PW014: 668.95-669.36 m

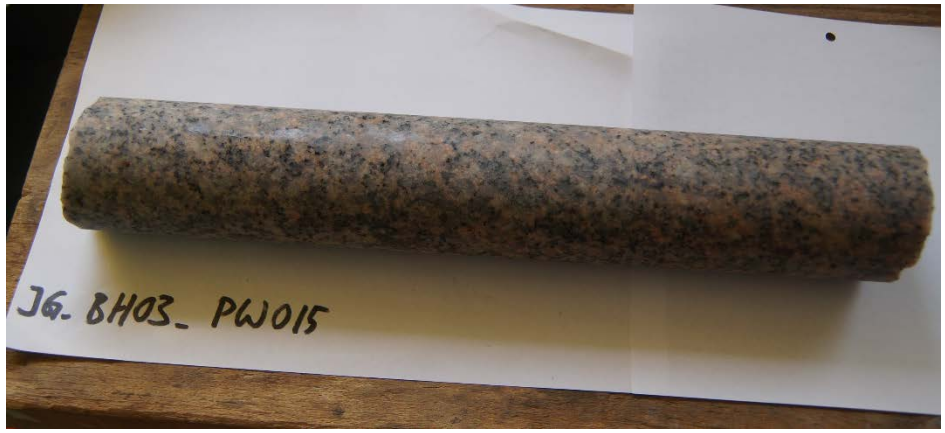

IG_BH03_PW015: 771.40-771.76 m

IG_BH03_PW017: 880.16-880.56 m

IG_BH03_PW019: 984.52-984.89 m

APPENDIX II

Analytical Raw Data

APPENDIX II-1

Calculation of Water Content Values: Raw Data

Table A-1: Determination of gravimetric water content; sample weights, drying times and calculated water contents of core pieces used for aqueous extraction experiments

Sample	Date prepared	m (cryst.dish)	m (cryst+ rock)		10.09.2019	17.09.2019	24.09.2019	30.09.2019	08.10.2019	15.10.2019	24.10.2019	31.10.2019	07.11.2019		Sample	m(rock, wet)	m (rock, dry)
					g	g	g	g	g	g	g	g	g			g	g
IG_BH03_AQ001	03.09.2019	86,407	490,575		489,848	489,840	489,839								IG_BH03_AQ001	404,168	403,432
IG_BH03_AQ002	03.09.2019	87,596	279,156		278,797	278,793	278,793								IG_BH03_AQ002	191,56	191,197
IG_BH03_AQ003	03.09.2019	87,188	433,849		433,174	433,167	433,167								IG_BH03_AQ003	346,661	345,979
IG_BH03_AQ004	03.09.2019	90,364	417,808		417,166	417,160	417,158								IG_BH03_AQ004	327,444	326,794
IG_BH03_AQ005	03.09.2019	91,021	401,680		401,046	401,045									IG_BH03_AQ005	310,659	310,024
IG_BH03_AQ006	16.09.2019	87,214	451,415				450,639	450,638							IG_BH03_AQ006	364,201	363,424
IG_BH03_AQ007	16.09.2019	92,975	349,352				348,893	348,89	348,879	348,883					IG_BH03_AQ007	256,377	255,904
IG_BH03_AQ008	16.09.2019	89,012	456,034				455,324	455,333							IG_BH03_AQ008	367,022	366,312
IG_BH03_AQ009	10.10.2019	90,676	436,053							435,548	435,541	435,54			IG_BH03_AQ009	345,377	344,864
IG_BH03_AQ010	10.10.2019	86,938	470,297							469,674	469,665	469,652	469,651		IG_BH03_AQ010	383,359	382,713
		m (wet surf)			10.09.2019	17.09.2019	24.09.2019	01.10.2019	08.10.2019	15.10.2019	24.10.2019	31.10.2019	07.11.2019				
IG_BH03_AQ001-A	03.09.2019	176,910			176,516	176,504	176,489	176,488							IG_BH03_AQ001-A	176,910	176,488
IG_BH03_AQ002-A	03.09.2019	121,450			121,19	121,186	121,182	121,181							IG_BH03_AQ002-A	121,450	121,181
IG_BH03_AQ003-A	03.09.2019	123,249			122,982	122,98									IG_BH03_AQ003-A	123,249	122,98
IG_BH03_AQ004-A	03.09.2019	122,727			122,414	122,407	122,398	122,394	122,392	122,393					IG_BH03_AQ004-A	122,727	122,392
IG_BH03_AQ005-A	03.09.2019	153,280			152,875	152,836	152,828	152,825	152,815	152,820					IG_BH03_AQ005-A	153,280	152,815
IG_BH03_AQ001-B	03.09.2019	228,975			228,469	228,466	228,46	228,458							IG_BH03_AQ001-B	228,975	228,458
IG_BH03_AQ002-B	03.09.2019	149,060			148,716	148,711	148,705	148,705							IG_BH03_AQ002-B	149,060	148,705
IG_BH03_AQ003-B	03.09.2019	175,283			174,911	174,906	174,9	174,9							IG_BH03_AQ003-B	175,283	174,9
IG_BH03_AQ004-B	03.09.2019	210,912			210,453	210,45	210,439	210,439							IG_BH03_AQ004-B	210,912	210,439
IG_BH03_AQ005-B	03.09.2019	96,387			96,186	96,182	96,181								IG_BH03_AQ005-B	96,387	96,181
IG_BH03_AQ001-C	03.09.2019	380,070			379,297	379,293	379,284	379,283							IG_BH03_AQ001-C	380,070	379,283
IG_BH03_AQ006-A	16.09.2019	136,445					136,106	136,099	136,094	136,094					IG_BH03_AQ006-A	136,445	136,094
IG_BH03_AQ007-A	16.09.2019	114,195					113,966	113,961	113,953	113,954					IG_BH03_AQ007-A	114,195	113,953
IG_BH03_AQ008-A	16.09.2019	123,330					123,067	123,067							IG_BH03_AQ008-A	123,330	123,067
IG_BH03_AQ006-B	16.09.2019	121,734					121,448	121,444	121,435	121,433					IG_BH03_AQ006-B	121,734	121,433
IG_BH03_AQ007-B	16.09.2019	150,010					149,726	149,722	149,717	149,718					IG_BH03_AQ007-B	150,010	149,717
IG_BH03_AQ008-B	16.09.2019	185,254					184,853	184,851							IG_BH03_AQ008-B	185,254	184,851
IG_BH03_AQ009-A	10.10.2019	124,146								123,956	123,951	123,949			IG_BH03_AQ009-A	124,146	123,949
IG_BH03_AQ010-A	10.10.2019	142,76								142,404	142,4	142,394	142,394		IG_BH03_AQ010-A	142,760	142,394
IG_BH03_AQ009-B	10.10.2019	91,853								91,696	91,693	91,687	91,687		IG_BH03_AQ009-B	91,853	91,687
IG_BH03_AQ010-B	10.10.2019	83,925								83,763	83,761				IG_BH03_AQ010-B	83,925	83,761

Table A-2: Determination of gravimetric water content; sample weights, drying times and calculated water contents of rim core pieces of samples used for out-diffusion and isotope diffusive exchange experiments

	Set-up date	m(ini)		10.09.2019	17.09.2019	24.09.2019	01.10.2019	08.10.2019	15.10.2019	23.10.2019	31.10.2019	07.11.2019	14.11.2019	27.11.2019	05.12.2019	Sample	m wet	m dry
				g	g	g	g	g	g	g	g	g	g	g	g		g	g
IG_BH03_PW002-A	03.09.2019	160,926		160,554	160,554											IG_BH03_PW002-A	160,926	160,554
IG_BH03_PW002-B	03.09.2019	193,108		192,678	192,673	192,666	192,662	192,661								IG_BH03_PW002-B	193,108	192,661
IG_BH03_PW003-A	03.09.2019	174,610		174,297	174,297											IG_BH03_PW003-A	174,610	174,297
IG_BH03_PW003-B	03.09.2019	181,277		180,861	180,857	180,852	180,851									IG_BH03_PW003-B	181,277	180,851
IG_BH03_PW005-A	03.09.2019	201,180		200,789	200,783	200,773	200,769	200,767								IG_BH03_PW005-A	201,180	200,767
IG_BH03_PW005-B	03.09.2019	178,649		178,257	178,252	178,245	178,243									IG_BH03_PW005-B	178,649	178,243
IG_BH03_PW007-A	03.09.2019	206,317		205,927	205,918	205,916										IG_BH03_PW007-A	206,317	205,916
IG_BH03_PW007-B	03.09.2019	223,070		222,569	222,557	222,547	222,545									IG_BH03_PW007-B	223,070	222,545
IG_BH03_PW009-A	03.09.2019	211,496		211,028	211,025	211,016	211,012	211,010								IG_BH03_PW009-A	211,496	211,01
IG_BH03_PW009-B	03.09.2019	198,143		197,676	197,675											IG_BH03_PW009-B	198,143	197,675
IG_BH03_PW011-A	16.09.2019	198,118				197,625	197,61	197,601	197,596	197,595						IG_BH03_PW011-A	198,118	197,595
IG_BH03_PW011-B	16.09.2019	220,541				220,043	220,036	220,03	220,022	220,02						IG_BH03_PW011-B	220,541	220,02
IG_BH03_PW014-A	16.09.2019	233,273				232,873	232,865	232,845	232,842	232,84						IG_BH03_PW014-A	233,273	232,84
IG_BH03_PW014-B	16.09.2019	196,243				195,926	195,922	195,916	195,916							IG_BH03_PW014-B	196,243	195,916
IG_BH03_PW015-A	16.09.2019	212,092				211,692	211,697									IG_BH03_PW015-A	212,092	211,692
IG_BH03_PW015-B	16.09.2019	236,635				236,168	236,169									IG_BH03_PW015-B	236,635	236,168
IG_BH03_PW017-A	10.10.2019	128,753							128,549	128,545	128,54	128,538				IG_BH03_PW017-A	128,753	128,538
IG_BH03_PW017-B	10.10.2019	201,573							201,262	201,257	201,251	201,25				IG_BH03_PW017-B	201,573	201,25
IG_BH03_PW019-A	10.10.2019	221,109							220,730	220,718	220,712	220,705	220,698	220,685	220,685	IG_BH03_PW019-A	221,109	220,685
IG_BH03_PW019-B	10.10.2019	133,318							133,104	133,099	133,094	133,092				IG_BH03_PW019-B	133,318	133,092

Table A-3: Determination of gravimetric water content; sample weights, drying times and calculated water contents of core pieces used for isotope diffusive exchange experiments

Sample	Date start drying	Drying times (days)	m (cryst.dish)	m (cryst+ rock)	15.11.2019	29.11.2019	06.12.2019	17.12.2019	07.01.2020	21.01.2020	04.02.2020	Mass dry	m rock wet	m rock dry
IG_BH03_PW002 LAB	07.11.2019	75	93,930	404,161	403,585	403,548		403,575	403,563	403,564		403,548	310,231	309,618
IG_BH03_PW002 SSI	07.11.2019	75	87,823	397,726	397,110	397,049		397,116	397,100	397,098		397,049	309,903	309,226
IG_BH03_PW003 LAB	07.11.2019	75	93,452	391,812	391,340	391,305		391,339	391,331	391,333		391,305	298,36	297,853
IG_BH03_PW003 SSI	07.11.2019	75	89,513	382,928	382,438	382,410		382,455	382,422	382,424		382,410	293,415	292,897
IG_BH03_PW005 LAB	07.11.2019	75	87,548	471,479	470,691	470,647		470,692	470,659	470,661		470,647	383,931	383,099
IG_BH03_PW005 SSI	07.11.2019	75	84,033	469,768	469,003	468,956		469,008	468,971	468,972		468,956	385,735	384,923
IG_BH03_PW007 LAB	07.11.2019	75	92,889	503,370	502,732	502,694		502,740	502,703	502,705		502,694	410,481	409,805
IG_BH03_PW007 SSI	07.11.2019	75	93,453	508,776	508,052	508,010		508,050	508,017	508,019		508,010	415,323	414,557
IG_BH03_PW009 LAB	07.11.2019	75	88,048	413,367	412,752	412,707		412,744	412,732	412,734		412,707	325,319	324,659
IG_BH03_PW009 SSI	07.11.2019	75	88,084	415,352	414,708	414,668		414,718	414,691	414,693		414,668	327,268	326,584
IG_BH03_PW011 LAB	19.11.2019	77	90,808	401,654			401,114	401,131	401,107	401,099	401,100	401,099	310,846	310,291
IG_BH03_PW011 SSI	19.11.2019	77	86,034	391,158			390,578	390,612	390,583	390,579	390,580	390,578	305,124	304,544
IG_BH03_PW014 LAB	19.11.2019	28	87,227	425,947			425,480	425,478				425,478	338,72	338,251
IG_BH03_PW014 SSI	19.11.2019	63	90,724	426,316			425,743	425,750	425,739	425,737		425,737	335,592	335,013
IG_BH03_PW015 LAB	19.11.2019	77	85,907	429,020			428,429	430,574	430,537	430,551	430,554	428,429	343,113	342,522
IG_BH03_PW015 SSI	19.11.2019	77	86,940	429,541			428,912	428,906	428,905	428,898	428,898	428,898	342,601	341,958
IG_BH03_PW017 LAB	09.12.2019	43	94,758	484,796				484,174	484,162	484,160		484,160	390,038	389,402
IG_BH03_PW017 SSI	09.12.2019	43	86,228	482,627				481,892	481,848	481,850		481,848	396,399	395,620
IG_BH03_PW019 LAB	09.12.2019	57	88,615	480,571				479,908	479,884	479,876	479,878	479,876	391,956	391,261
IG_BH03_PW019 SSI	09.12.2019	57	87,600	476,891				476,012	475,997	475,991	475,992	475,991	389,291	388,391

Table A-4: Determination of gravimetric water content; sample weights, drying times and calculated water contents of core pieces used for out-diffusion experiments

		before experiment (b.e.)		after experiment (a.e.)											
Sample	**Date start drying**	**m wet surface**	**m dry surface**	**m wet surf**	**m (2 min)**	**m dry surf**	**05.02.2020**	**19.02.2020**	**04.03.2020**	**17.03.2020**	**18.03.2020**	**01.04.2020**	**15.04.2020**	**28.04.2020**	**12.05.2020**
		g	**g**	**g**	**g**	**g**	**g**	**g**	**g**	**g**	**g**	g	g	g	
Drying time (days)															
IG_BH03_PW002	22.01.2020	1459,406	1459,255	1459,405	1459,221	1459,099	1456,074	1456,059	1456,040		1456,026	1456,009	1456,006	1456,017	1456,025
IG_BH03_PW003	22.01.2020	1444,603	1444,5	1444,816	1444,621	1444,51	1441,770	1441,749	1441,733		1441,718	1441,703	1441,701		
IG_BH03_PW005	22.01.2020	1480,911	1480,681	1480,802	1480,601	1480,55	1477,521	1477,428	1477,388		1477,365	1477,337	1477,329	1477,338	1477,332
IG_BH03_PW007	22.01.2020	1474,680	1474,45	1474,652	1474,455	1474,341	1471,425	1471,386	1471,365		1471,342	1471,327	1471,316	1471,33	1471,324
IG_BH03_PW009	22.01.2020	1470,089	1470,02	1470,163	1469,967	1469,899	1466,723	1466,649	1466,623		1466,603	1466,556	1466,538	1466,561	1466,554
IG_BH03_PW011	03.03.2020	1489,921	1489,78	1489,89	1489,697	1489,584				1486,610		1486,592	1486,562	1486,585	1486,566
IG_BH03_PW014	03.03.2020	1527,899	1527,808	1528,306	1527,930	1527,87				1525,139		1525,123	1525,106	1525,112	1525,092
IG_BH03_PW015	03.03.2020	1544,612	1544,553	1544,894	1544,656	1544,64				1541,387		1541,373	1541,346	1541,372	1541,362
IG_BH03_PW017	03.03.2020	1453,360	1453,355	1453,71	1453,330	1453,315				1450,797		1450,777	1450,750	1450,766	1450,750
IG_BH03_PW019	03.03.2020	1492,320	1492,304	1492,276	1492,276	1492,244				1489,826		1489,798	1489,773	1489,793	1489,774

Sample	**m (dry)**	**m(PW) b.e.**	**m(PW) a.e.**
	g	**g**	**g**
IG_BH03_PW002	1456,006	3,249	3,093
IG_BH03_PW003	1441,701	2,799	2,809
IG_BH03_PW005	1477,329	3,352	3,221
IG_BH03_PW007	1471,316	3,134	3,025
IG_BH03_PW009	1466,538	3,482	3,361
IG_BH03_PW011	1486,562	3,218	3,022
IG_BH03_PW014	1525,092	2,716	2,778
IG_BH03_PW015	1541,346	3,207	3,294
IG_BH03_PW017	1450,750	2,605	2,565
IG_BH03_PW019	1489,773	2,531	2,471

APPENDIX II-2

Determination of Bulk Wet and Dry Density: Raw Data

Table A-5: Determination of bulk wet and dry density; sample dimensions, weights and density results

Sample	m (core) wet	diameter core	height core	Volume core	bulk, wet density
	g	cm	cm	cm^3	g/cm^3
IG_BH03_AQ001	451,92	6,12	5,81	170,91	2,64
IG_BH03_AQ002	406,769	6,09	5,28	153,80	2,64
IG_BH03_AQ003	404,613	6,09	5,23	152,34	2,66
IG_BH03_AQ004	405,695	6,08	5,32	154,46	2,63
IG_BH03_AQ005	392,703	6,09	5,1	148,56	2,64
IG_BH03_AQ006	408,148	6,1	5,26	153,72	2,66
IG_BH03_AQ007	254,074	6,11	3,27	95,88	2,65
IG_BH03_AQ008	413,148	6,09	5,35	155,84	2,65
IG_BH03_AQ009	369,282	6,09	4,76	138,65	2,66
IG_BH03_AQ010	379,19	6,08	4,91	142,55	2,66

Sample	m (core a.e.) wet	m (core a.e.) dry	diameter core	height core	Volume core	bulk, wet density	bulk, dry density
	g	g	cm	cm	cm3	g/cm^3	g/cm^3
IG_BH03_PW002	1459,099	1456,006	6,10	18,9	552,35	2,64	2,64
IG_BH03_PW003	1444,51	1441,701	6,07	18,8	544,03	2,66	2,65
IG_BH03_PW005	1480,55	1477,329	6,09	19,1	556,36	2,66	2,66
IG_BH03_PW007	1474,341	1471,316	6,07	19,1	552,71	2,67	2,66
IG_BH03_PW009	1469,899	1466,538	6,08	19	551,63	2,66	2,66
IG_BH03_PW011	1489,584	1486,562	6,10	19,2	561,11	2,65	2,65
IG_BH03_PW014	1527,87	1525,092	6,10	19,79	578,36	2,64	2,64
IG_BH03_PW015	1544,64	1541,346	6,10	19,95	583,03	2,65	2,64
IG_BH03_PW017	1453,315	1450,75	6,10	18,73	547,38	2,66	2,65
IG_BH03_PW019	1492,244	1489,773	6,10	19,27	563,16	2,65	2,65

APPENDIX II-3

Aqueous Extraction Experiments: Raw Data

Table A-6: Experimental data of aqueous extraction experiments

Sample	Depth	Grain size	m (bottle)	m (bottle + rock)	m (rock)	m (b+r+H2O)	m (H2O)	water:rock
	m a.b.		g	g	g		g	
IG_BH03_AQ001	238,8	< 1mm	18,512	95,735	77,223	165,308	69,573	0,90
IG_BH03_AQ001		1 - 2 mm	19,255	88,913	69,658	179,627	90,714	1,30
IG_BH03_AQ001		2 - 4 mm	18,563	97,992	79,429	181,940	83,948	1,06
IG_BH03_AQ002	346,0	< 1mm	18,491	86,176	67,685	153,407	67,231	0,99
IG_BH03_AQ002		1 - 2 mm	18,528	68,066	49,538	154,279	86,213	1,74
IG_BH03_AQ002		2 - 4 mm	19,278	86,929	67,651	170,771	83,842	1,24
IG_BH03_AQ003	460,1	< 1mm	18,793	78,745	59,952	148,694	69,949	1,17
IG_BH03_AQ003		1 - 2 mm	19,035	63,362	44,327	146,765	83,403	1,88
IG_BH03_AQ003		2 - 4 mm	18,714	80,714	62,000	162,064	81,350	1,31
IG_BH03_AQ004	504,2	< 1mm	17,885	77,771	59,886	152,670	74,899	1,25
IG_BH03_AQ004		1 - 2 mm	17,893	61,005	43,112	152,235	91,230	2,12
IG_BH03_AQ004		2 - 4 mm	17,92	76,251	58,331	158,295	82,044	1,41
IG_BH03_AQ005	554,7	< 1mm	19,255	79,65	60,395	153,01	73,360	1,21
IG_BH03_AQ005		1 - 2 mm	17,891	70,413	52,522	163,229	92,816	1,77
IG_BH03_AQ005		2 - 4 mm	18,626	76,028	57,402	162,39	86,362	1,50
IG_BH03_AQ006	608,6	< 2 mm	18,643	88,168	69,525	171,494	83,326	1,20
IG_BH03_AQ007	665,9	< 2 mm	17,855	101,31	83,455	171,444	70,134	0,84
IG_BH03_AQ008	771,8	< 2 mm	17,83	90,85	73,02	163,724	72,874	1,00
IG_BH03_AQ009	880,1	< 2 mm	18,575	77,008	58,433	156,56	79,552	1,36
IG_BH03_AQ010	985	< 2 mm	18,604	79,216	60,612	151,453	72,237	1,19

APPENDIX II-4

Isotope Diffusive Exchange Experiments: Raw Data

Table A-7: Experimental data of isotope diffusive exchange experiments

Sample		Date Experiment Start	Date Experiment End	Standard	Weight container	Weight container and rock	Cryst. dish	Cryst Dish + H2O	Total weight container	Weight rock	Weight test solution	Total weight container after experiment	Weight test solution after experiment	Weight container and rock after experiment	Weight test solution after experiment	Weight rock after experiment	mass (PW)	mass TW+PW after exp.	Δ total weight before & after	Δ weight rock before & after	Δ weight test solution before & after	Δ weight rock and test solution	Δ weight rock and test solution - Δ total weight before and after	Δ weight rock and test solution	Δ water loss (total weight)	remaining water fraction
					g	g	g	g	g	g	g	g	g	g	g	g	g	g	g	g	g	g	g	% of TW	% of TW+PW	
IG_BH03_PW002	LAB	03.09.2019	07.11.2019	IG03-LAB	524,781	835,692	13,271	15,087	850,770	310,911	1,816	850,755	15,050	835,698	1,779	310,917	0,613	2,392	-0,015	0,006	-0,037	-0,031	-0,016	1,7	0,6	0,99
IG_BH03_PW003	LAB	03.09.2019	07.11.2019		524,966	823,574	12,967	14,808	838,375	298,608	1,841	838,349	14,802	823,539	1,835	298,573	0,507	2,342	-0,026	-0,035	-0,006	-0,041	-0,015	2,2	1,1	0,99
IG_BH03_PW005	LAB	03.09.2019	07.11.2019	0.3 n NaCl	526,067	910,327	13,176	14,998	925,307	384,260	1,822	925,293	14,922	910,362	1,746	384,295	0,832	2,578	-0,014	0,035	-0,076	-0,041	-0,027	2,3	0,5	0,99
IG_BH03_PW007	LAB	03.09.2019	07.11.2019		523,433	946,548	13,567	15,451	961,978	423,115	1,884	961,967	15,551	946,415	1,984	422,982	0,676	2,660	-0,011	-0,133	0,100	-0,033	-0,022	1,8	0,4	1,00
IG_BH03_PW009	LAB	03.09.2019	07.11.2019		523,525	850,766	15,277	17,114	867,868	327,241	1,837	867,855	17,075	850,767	1,798	327,242	0,66	2,458	-0,013	0,001	-0,039	-0,038	-0,025	2,1	0,5	0,99
IG_BH03_PW011	LAB	16.09.2019	19.11.2019		524,567	835,998	14,274	16,095	852,077	311,431	1,821	852,040	16,162	835,874	1,888	311,307	0,555	2,443	-0,037	-0,124	0,067	-0,057	-0,020	3,1	1,5	0,98
IG_BH03_PW014	LAB	16.09.2019	19.11.2019		521,004	867,670	14,819	16,844	884,503	346,666	2,025	884,465	16,853	867,619	2,034	346,615	0,469	2,503	-0,038	-0,051	0,009	-0,042	-0,004	2,1	1,5	0,98
IG_BH03_PW015	LAB	16.09.2019	19.11.2019		523,447	866,733	14,743	16,588	883,314	343,286	1,845	883,283	16,562	866,720	1,819	343,273	0,591	2,410	-0,031	-0,013	-0,026	-0,039	-0,008	2,1	1,3	0,99
IG_BH03_PW017	LAB	10.10.2019	09.12.2019		524,638	914,657	14,757	16,596	931,249	390,019	1,839	931,215	16,475	914,731	1,718	390,093	0,636	2,354	-0,034	0,074	-0,121	-0,047	-0,013	2,6	1,4	0,99
IG_BH03_PW019	LAB	10.10.2019	09.12.2019		523,497	915,440	14,659	16,481	931,897	391,943	1,822	931,876	16,285	915,586	1,626	392,089	0,695	2,321	-0,021	0,146	-0,196	-0,050	-0,029	2,7	0,9	0,99
IG_BH03_PW002	SSI	03.09.2019	07.11.2019	IG03-SSI	525,997	836,668	15,958	17,776	854,438	310,671	1,818	854,418	17,710	836,703	1,752	310,706	0,677	2,429	-0,020	0,035	-0,066	-0,031	-0,011	1,7	0,8	0,99
IG_BH03_PW003	SSI	03.09.2019	07.11.2019		525,984	821,179	14,914	16,727	837,893	295,195	1,813	837,864	16,664	821,185	1,750	295,201	0,518	2,268	-0,029	0,006	-0,063	-0,057	-0,028	3,1	1,3	0,99
IG_BH03_PW005	SSI	03.09.2019	07.11.2019	0.3 n NaCl	525,189	911,293	15,255	17,072	928,367	386,104	1,817	928,337	16,965	911,365	1,710	386,176	0,812	2,522	-0,030	0,072	-0,107	-0,035	-0,005	1,9	1,2	0,99
IG_BH03_PW007	SSI	03.09.2019	07.11.2019		523,113	945,289	13,235	15,110	960,375	422,176	1,875	960,379	15,027	945,343	1,792	422,230	0,766	2,558	0,004	0,054	-0,083	-0,029	-0,033	1,5	-0,2	1,00
IG_BH03_PW009	SSI	03.09.2019	07.11.2019		523,192	850,694	13,579	15,528	866,207	327,502	1,949	866,185	15,408	850,770	1,829	327,578	0,684	2,513	-0,022	0,076	-0,120	-0,044	-0,022	2,3	0,9	0,99
IG_BH03_PW011	SSI	16.09.2019	19.11.2019		523,431	832,408	14,801	16,735	849,130	308,977	1,934	849,090	16,686	832,400	1,885	308,969	0,58	2,465	-0,040	-0,008	-0,049	-0,057	-0,017	2,9	1,6	0,98
IG_BH03_PW014	SSI	16.09.2019	19.11.2019		521,961	868,599	14,294	16,283	884,873	346,638	1,989	884,835	16,209	868,627	1,915	346,666	0,579	2,494	-0,038	0,028	-0,074	-0,046	-0,008	2,3	1,5	0,98
IG_BH03_PW015	SSI	16.09.2019	19.11.2019		523,519	866,359	14,691	16,507	882,852	342,840	1,816	882,825	16,416	866,410	1,725	342,891	0,643	2,368	-0,027	0,051	-0,091	-0,040	-0,013	2,2	1,1	0,99
IG_BH03_PW017	SSI	10.10.2019	09.12.2019		523,508	919,797	14,919	16,728	936,515	396,289	1,809	936,480	16,478	919,995	1,559	396,487	0,779	2,338	-0,035	0,198	-0,250	-0,052	-0,017	2,9	1,5	0,99
IG_BH03_PW019	SSI	10.10.2019	09.12.2019		523,909	912,927	15,001	16,807	929,712	389,018	1,806	929,690	16,411	913,278	1,410	389,369	0,9	2,310	-0,022	0,351	-0,396	-0,045	-0,023	2,5	1,0	0,99

Table A-8: Analytical raw data of isotope diffusive exchange experiments

Sample	Test water	Initial $\delta^{18}O$ TW	Initial $\delta^{2}H$ TW	Final $\delta^{18}O$ TW	Final $\delta^{2}H$ TW
		‰ VSMOW	‰ VSMOW	‰ VSMOW	‰ VSMOW
IG_BH03_PW002	LAB	-10,41	-73,1	-10,52	-75,8
IG_BH03_PW003	LAB	-10,41	-73,1	-10,44	-74,9
IG_BH03_PW005	LAB	-10,41	-73,1	-10,39	-75,1
IG_BH03_PW007	LAB	-10,41	-73,1	-9,56	-71,2
IG_BH03_PW009	LAB	-10,41	-73,1	-10,11	-73,5
IG_BH03_PW011	LAB	-10,42	-73,1	-9,44	-70,4
IG_BH03_PW014	LAB	-10,42	-73,1	-10,38	-73,6
IG_BH03_PW015	LAB	-10,42	-73,1	-10,32	-73,5
IG_BH03_PW017	LAB	-10,47	-73,6	-9,87	-69,5
IG_BH03_PW019	LAB	-10,47	-73,6	-9,85	-68,7
IG_BH03_PW002	SSI	-29,72	-233,0	-24,34	-191,5
IG_BH03_PW003	SSI	-29,72	-233,0	-24,10	-192,1
IG_BH03_PW005	SSI	-29,72	-233,0	-23,45	-184,3
IG_BH03_PW007	SSI	-29,72	-233,0	-23,79	-187,0
IG_BH03_PW009	SSI	-29,72	-233,0	-24,44	-191,7
IG_BH03_PW011	SSI	-29,75	-233,7	-24,77	-195,5
IG_BH03_PW014	SSI	-29,75	-233,7	-24,29	-193,4
IG_BH03_PW015	SSI	-29,75	-233,7	-23,97	-188,1
IG_BH03_PW017	SSI	-29,91	-234,0	-24,45	-189,3
IG_BH03_PW019	SSI	-29,91	-234,0	-24,62	-191,5

APPENDIX II-5

Out-diffusion Experiments: Raw Data

Table A-9: Experimental data of out-diffusion experiments

Sample		IG_BH03_Blank	IG_BH03_PW002	IG_BH03_PW003	IG_BH03_PW005	IG_BH03_PW007	IG_BH03_PW009	IG_BH03_PW011	IG_BH03_PW014	IG_BH03_PW015	IG_BH03_PW017	IG_BH03_PW019
Depth	m		242,0	345,2	459,2	503,9	554,5	608,8	669,2	771,6	880,4	984,7
start experiment		03.09.2019	03.09.2019	03.09.2019	03.09.2019	03.09.2019	03.09.2019	16.09.2019	16.09.2019	16.09.2019	10.10.2019	10.10.2019
Initial Rock Mass (as received, +/- mountain wet)	g		1459,406	1444,603	1480,911	1474,680	1470,089	1489,921	1527,899	1544,612	1453,360	1492,327
Initial Rock Mass (start experiment)	g		1459,255	1444,500	1480,681	1474,450	1470,020	1489,780	1527,808	1544,553	1453,355	1492,304
Final Rock Mass (resaturated, wet surf.)			1459,405	1444,816	1480,802	1474,652	1470,163	1489,890	1528,306	1544,894	1453,710	1492,593
Final Rock Mass (resaturated, 2 min.)			1459,221	1444,621	1480,601	1474,455	1469,967	1489,697	1527,930	1544,656	1453,330	1492,276
Final Rock Mass (resaturated, dry surf.)	g		1459,099	1444,510	1480,550	1474,341	1469,899	1489,584	1527,870	1544,640	1453,315	1492,244
Uptake of water	g		-0,31	-0,09	-0,36	-0,34	-0,19	-0,34	-0,03	0,03	-0,04	-0,08
Saturation	%		100,021	100,006	100,024	100,023	100,013	100,023	100,002	99,998	100,003	100,006
Core Diametre	cm		6,10	6,07	6,09	6,07	6,08	6,10	6,10	6,10	6,10	6,10
Core Length	cm		18,9	18,8	19,1	19,1	19,0	19,2	19,79	19,95	18,73	19,27
Volume of Rock Sample	cm3		552,35	544,03	556,36	552,71	551,63	561,11	578,36	583,03	547,38	563,16
Density (calculated from volume & mass)	g/cm3		2,64	2,66	2,66	2,67	2,66	2,66	2,64	2,65	2,66	2,65
Mass of Rock (calculated from volume and density)			1459,41	1444,60	1480,91	1474,68	1470,09	1489,92	1527,90	1544,61	1453,36	1492,33
Masses before experiment												
Mass cylinder	g	356,319	358,194	357,612	356,751	357,040	356,832	357,925	356,608	356,994	357,342	356,272
Mass cylinder + core	g		1817,500	1802,881	1837,515	1831,590	1826,939	1847,584	1884,397	1901,489	1810,740	1848,589
Mass cylinder + core + H2O	g	921,227	1942,187	1944,124	1971,844	1961,627	1959,517	1983,090	2013,705	2032,144	1940,735	1985,763
Mass tot start	g	921,227	1942,187	1944,124	1971,844	1961,627	1959,517	1983,090	2013,705	2032,144	1940,735	1985,763
Initial Water Mass	ml	564,908	124,687	141,243	134,329	130,037	132,578	135,506	129,308	130,655	129,995	137,174
Ratio Exp.Water : Rock			0,085	0,098	0,091	0,088	0,090	0,091	0,085	0,085	0,089	0,092
End Experiment		22.01.2020	22.01.2020	22.01.2020	22.01.2020	22.01.2020	22.01.2020	03.03.2020	03.03.2020	03.03.2020	03.03.2020	03.03.2020
Mass cylinder + core + H2O final	g		1932,886	1936,674	1965,067	1954,645	1952,739	1975,283	2006,147	2024,357	1933,147	1978,499
Final Water Mass (measured, not all recoverable)	ml	112,774	131,742	124,775	120,020	122,429	124,981	118,814	119,923	119,622	127,287	0,000
Time Experiment	days	141	141	141	141	141	141	169	169	169	145	145
Volume of samples for Cl-measurements												
sample A	ml	0,5	0,9	0,5	0,6	0,5	0,5	0,5	0,5	0,5	0,5	0,5
sample B	ml	0,5	0,6	0,5	0,5	0,5	0,5	0,5	0,5	0,5	0,5	0,5
sample C	ml	0,5	0,5	0,5	0,5	0,5	0,5	0,5	0,5	0,5	0,5	0,5
sample D	ml	0,5	0,5	0,5	0,5	0,5	0,5	0,5	0,5	0,5	0,5	0,5
sample E	ml	0,5	0,5	0,5	0,5	0,5	0,5	0,5	0,5	0,5	0,5	0,5
sample F	ml	0,5	0,5	0,5	0,5	0,5	0,5	0,5	0,5	0,5	0,5	0,5
sample G	ml	0,5	0,5	0,5	0,5	0,5	0,5	0,5	0,5	0,5	0,5	0,5
sample H	ml	0,5	0,5	0,5	0,5	0,5	0,5	0,5	0,5	0,5	0,5	0,5
sample I	ml	0,5	0,5	0,5	0,5	0,5	0,5	0,5	0,5	0,5	0,5	0,5
sample K	ml	0,5	0,5	0,5	0,5	0,5	0,5	0,5	0,5	0,5	0,5	0,5
sample L	ml	0,5	0,5	0,5	0,5	0,5	0,5	0,5	0,5	0,5	0,5	0,5
sample M	ml	0,5	1,5	0,5	0,5	0,5	0,5	0,5	0,5	0,5	0,5	0,5
sample N								0,5	0,5	0,5	0,5	0,5
total volume subsamples	ml	6,0	7,5	6,0	6,1	6,0	6,0	6,5	6,5	6,5	6,5	6,5
Volumen TS calculated cyl (ini-final)	ml		9,30	7,45	6,78	6,98	6,78	7,81	7,56	7,79	7,59	7,26
Difference V(ss) - V(calc)	ml		1,80	1,45	0,68	0,98	0,78	1,31	1,06	1,29	1,09	0,76
Difference % of TS	%		1,4	1,0	0,5	0,8	0,6	1,0	0,8	1,0	0,8	0,6

Table A-10: Chemical composition of time series samples taken during out-diffusion experiments

Sample			IG_BH03_PW002											IG_BH03_PW003									
Sub-samples	Time	Date	Na	K	Ca	Mg	Sr	F	Cl	SO4	NO3	Br	Br/Cl	Na	K	Ca	Mg	Sr	F	Cl	SO4	NO3	Br	Br/Cl
	days		mg/l	mg/l	mg/l	mg/l	mg/l	mg/l	mg/l	mg/l	mg/l	mg/l		mg/l	mg/l	mg/l	mg/l	mg/l	mg/l	mg/l	mg/l	mg/l	mg/l	
Preparation		03.09.2019																						
A	1	04.09.2019	4,5	1,3	2,8	<0,2	<1	<1	1,1	0,38	1,9	<0,1		3,1	1,4	1,9	<0,2	<1	<1	1,7	0,33	1,3	<0,1	
B	3	06.09.2019	4,9	1,4	3,2	<0,2	<1	<1	1,4	0,62	0,43	<0,1		3,7	1,5	3,7	<0,2	<1	<1	2,2	0,4	0,25	<0,1	
C	6	09.09.2019	7,1	1,5	3,6	<0,2	<1	<1	1,5	0,67	0,37	<0,1		5,8	1,6	5	<0,2	<1	<1	2,6	0,61	1,7	<0,1	
D	-2	01.09.2019	10,4	1,6	4,7	<0,2	<1	<1	1,7	0,95	1,8	<0,1		7,2	1,8	5,3	<0,2	<1	<1	3,2	0,71	0,39	0,11	34
E	14	17.09.2019	12,3	2,1	6,6	<0,2	<1	<1	1,8	1,3	<0,2	<0,1		8,4	2,1	8	<0,2	<1	<1	3,4	0,73	0,31	0,12	35
F	21	24.09.2019	14,3	2,2	6,9	<0,2	<1	<1	1,9	1,7	<0,2	<0,1		9,1	2,3	8,9	<0,2	<1	<1	3,6	0,97	0,15	0,14	39
G	29	02.10.2019	17,2	2,3	7,8	<0,2	<1	<1	1,9	2,2	<0,2	<0,1		10,8	2,4	10,6	<0,2	<1	<1	3,7	1,1	0,16	0,15	41
H	45	18.10.2019	19,5	2,4	8,9	<0,2	<1	<1	1,9	3	<0,2	<0,1		11,8	2,5	11,1	<0,2	<1	<1	3,7	1,4	0,32	0,15	41
I	62	04.11.2019	20	2,4	8,9	<0,2	<1	<1	1,9	3,4	<0,2	<0,1		13,2	2,5	11,5	<0,2	<1	<1	3,7	1,6	<0,2	0,15	41
K	73	15.11.2019	20,6	2,4	8,9	<0,2	<1	<1	1,9	3,6	<0,2	<0,1		14,3	2,5	11,5	<0,2	<1	<1	3,7	1,7	<0,2	0,15	41
L	91	03.12.2019	21,4	2,4	8,9	<0,2	<1	<1	1,9	3,6	<0,2	<0,1		14,7	2,5	11,5	<0,2	<1	<1	3,7	1,8	<0,2	0,15	41
M	119	31.12.2019	22,8	2,4	9	<0,2	<1	<1	1,9	3,7	<0,2	<0,1		15,1	2,5	11,8	<0,2	<1	<1	3,7	2	<0,2	0,15	41
Final	141	22.01.2020	23,2	2,4	9	<0,2	0,05	1,5	1,9	3,8	<0,2	0,024		15,9	2,5	12	<0,2	0,07	1,3	3,7	2,1	<0,2	0,15	41
Sample			IG_BH03_PW005											IG_BH03_PW007									
Sub-samples	Time	Date	Na	K	Ca	Mg	Sr	F	Cl	SO4	NO3	Br	Br/Cl	Na	K	Ca	Mg	Sr	F	Cl	SO4	NO3	Br	Br/Cl
	days		mg/l	mg/l	mg/l	mg/l	mg/l	mg/l	mg/l	mg/l	mg/l	mg/l		mg/l	mg/l	mg/l	mg/l	mg/l	mg/l	mg/l	mg/l	mg/l	mg/l	
Preparation		03.09.2019																						
A	1	04.09.2019	4	1,1	3,7	<0,2	<1	<1	1,4	0,33	0,63	<0,1		4,3	1,6	4,4	<0,2	<1	<1	3	0,36	0,63	<0,1	
B	3	06.09.2019	4,2	1,2	4,4	<0,2	<1	<1	1,6	0,36	0,29	<0,1		4,5	1,8	5,5	<0,2	<1	<1	4,1	0,53	<0,2	<0,1	
C	6	09.09.2019	5,8	1,5	6,1	<0,2	<1	<1	1,8	0,41	0,51	<0,1		6,7	2,5	7,3	<0,2	<1	<1	5,1	0,63	0,72	0,1	20
D	-2	01.09.2019	8,2	1,6	7,1	<0,2	<1	<1	2,1	0,53	0,74	0,12	57	8,2	2,7	9	<0,2	<1	<1	6,2	0,85	<0,2	0,12	19
E	14	17.09.2019	9,4	1,7	7,9	<0,2	<1	<1	2,2	0,65	0,33	0,15	68	8,7	3,2	12	<0,2	<1	<1	6,5	0,92	<0,2	0,14	22
F	21	24.09.2019	10,2	1,7	8,1	<0,2	<1	<1	2,3	0,75	0,27	0,18	78	10,1	3,3	12,9	<0,2	<1	<1	7,1	1,4	<0,2	0,17	24
G	29	02.10.2019	11,9	1,8	9,1	<0,2	<1	<1	2,4	0,8	0,29	0,19	79	11,4	3,5	16,2	<0,2	<1	<1	7,4	1,7	<0,2	0,18	24
H	45	18.10.2019	12,8	2	12,8	<0,2	<1	<1	2,55	0,98	<0,2	0,19	75	12,7	3,5	17,1	<0,2	<1	<1	7,9	2,4	<0,2	0,18	23
I	62	04.11.2019	15,8	2,2	14	<0,2	<1	<1	2,6	1,1	<0,2	0,19	73	13,3	3,5	17,1	<0,2	<1	<1	7,9	2,9	<0,2	0,18	23
K	73	15.11.2019	16,3	2,3	15	<0,2	<1	<1	2,6	1,2	<0,2	0,19	73	14,6	3,5	17,1	<0,2	<1	<1	7,9	3,1	<0,2	0,18	23
L	91	03.12.2019	17,4	2,4	16,8	<0,2	<1	<1	2,6	1,3	<0,2	0,19	73	14,8	3,5	17,1	<0,2	<1	<1	7,9	3,3	<0,2	0,18	23
M	119	31.12.2019	18,8	2,5	18,8	<0,2	<1	<1	2,6	1,6	<0,2	0,19	73	15,3	3,5	17,1	<0,2	<1	<1	7,9	3,7	<0,2	0,18	23
N	141	22.01.2020	19,7	2,6	19,7	<0,2	0,16	2,1	2,7	1,9	<0,2	0,19	70	15,7	3,5	17,1	<0,2	0,11	1,4	7,9	4	<0,2	0,18	23
Sample			IG_BH03_PW009																					
Sub-samples	Time	Date	Na	K	Ca	Mg	Sr	F	Cl	SO4	NO3	Br	Br/Cl											
	days		mg/l	mg/l	mg/l	mg/l	mg/l	mg/l	mg/l	mg/l	mg/l	mg/l												
Preparation		03.09.2019																						
A	1	04.09.2019	3,9	1,4	5,5	<0,2	<1	<1	2,8	0,27	1,1	0,053	19											
B	3	06.09.2019	4,5	1,8	5,9	<0,2	<1	<1	4	0,45	0,16	0,058	15											
C	6	09.09.2019	6,7	2,4	6,6	<0,2	<1	<1	4,9	0,52	0,46	0,092	19											
D	-2	01.09.2019	8,1	2,5	9,7	<0,2	<1	<1	5,9	0,65	<0,2	0,1	17											
E	14	17.09.2019	9,1	3	12,2	<0,2	<1	<1	6,3	0,77	<0,2	0,12	19											
F	21	24.09.2019	11,3	3,2	13,3	<0,2	<1	<1	7,2	1,1	<0,2	0,13	18											
G	29	02.10.2019	12	3,2	15,6	<0,2	<1	<1	7,6	1,3	<0,2	0,15	20											
H	45	18.10.2019	13	3,2	16	<0,2	<1	<1	8	1,6	<0,2	0,16	20											
I	62	04.11.2019	13,7	3,2	16	<0,2	<1	<1	8,4	2,1	<0,2	0,16	19											
K	73	15.11.2019	15,8	3,2	16	<0,2	<1	<1	8,6	2,4	<0,2	0,16	19											
L	91	03.12.2019	16,6	3,2	16	<0,2	<1	<1	8,6	2,6	<0,2	0,16	19											
M	119	31.12.2019	17,6	3,2	16,1	<0,2	<1	<1	8,6	3	<0,2	0,16	19											
N	141	22.01.2020	18,7	3,2	16	<0,2	0,12	0,66	8,6	3,2	<0,2	0,16	19											

Table A-10: continued

Sample			IG_BH03_PW011											IG_BH03_PW014										
Sub-samples	Time	Date	Na	K	Ca	Mg	Sr	F	Cl	SO4	NO3	Br	Br/Cl	Na	K	Ca	Mg	Sr	F	Cl	SO4	NO3	Br	Br/Cl
	days		mg/l	mg/l	mg/l	mg/l	mg/l	mg/l	mg/l	mg/l	mg/l	mg/l		mg/l	mg/l	mg/l	mg/l	mg/l	mg/l	mg/l	mg/l	mg/l	mg/l	
Preparation		16.09.2019																						
A	1	17.09.2019	4,9	2,4	7,8	<0,2	<1	<1	7,9	0,3	0,31	0,2		5,3	2,9	8,6	0,12	<1	<1	11,5	0,41	0,2	0,25	
B	16	19.09.2019	6,4	2,6	9,9	<0,2	<1	<1	11	0,42	0,29	0,24		7,6	3,4	11	0,12	<1	<1	18,4	0,63	0,2	0,44	
C	20	23.09.2019	8,9	2,7	11,8	<0,2	<1	<1	15,3	0,62	0,29	0,33	22	10,5	3,9	15,5	0,16	<1	<1	26,2	0,94	0,21	0,57	
D	23	26.09.2019	9,6	2,8	12	<0,2	<1	<1	16,2	0,79	0,91	0,38	23	11,5	4	16,1	0,2	<1	<1	28,9	1,2	0,53	0,61	
E	27	30.09.2019	10,5	2,8	12,8	<0,2	<1	<1	17,3	0,86	0,24	0,41	24	13	4	18	0,14	<1	<1	30	1,5	0,19	0,64	
F	35	08.10.2019	11,5	2,8	15,2	<0,2	<1	<1	18	0,92	0,36	0,44	24	13,9	4	21,1	0,17	<1	<1	31,1	1,9	0,25	0,67	
G	43	16.10.2019	13,2	2,9	16,2	<0,2	<1	<1	18,8	1	0,35	0,45	24	15,6	4,1	23,2	0,17	<1	<1	32,1	2,4	0,28	0,7	
H	58	31.10.2019	14	2,9	16,9	<0,2	<1	<1	19,8	1,2	0,31	0,47	24	15,8	4,1	24,1	0,19	<1	<1	33,2	3,3	0,43	0,75	
I	73	15.11.2019	14,7	2,9	16,9	<0,2	<1	<1	20,9	1,4	0,2	0,49	23	15,9	4,1	24,3	<0,1	<1	<1	34,4	3,7	0,17	0,78	
K	87	29.11.2019	15,3	2,9	16,9	<0,2	<1	<1	21,5	1,8	0,29	0,49	23	16,3	4,1	25,3	0,16	<1	<1	35,9	4,4	0,18	0,78	
L	104	16.12.2019	15,8	2,9	17	<0,2	<1	<1	22,1	2,2	0,29	0,49	22	17,4	4,1	26,4	0,33	<1	<1	36,7	5,1	0,42	0,78	
M	134	15.01.2020	17,1	2,9	17,8	<0,2	<1	<1	22,1	2,6	0,36	0,49	22	18,6	4,1	27,4	0,42	<1	<1	36,7	6,3	0,2	0,78	
N	163	13.02.2020	17,9	2,9	18,2	<0,2	<1	1,7	22,1	3,1	0,32	0,49		19	4,1	27,5	0,32	<1	1,2	36,7	7,3	0,31	0,78	
Final	182	03.03.2020	18,2	2,9	18,5	<0,2	0,28	1,7	22,1	3,7	0,3	0,49	22	19,1	4,1	27,7	0,3	0,44	1,2	36,7	7,8	0,29	0,78	
Sample			IG_BH03_PW015																					
Sub-samples	Time	Date	Na	K	Ca	Mg	Sr	F	Cl	SO4	NO3	Br	Br/Cl											
	days		mg/l	mg/l	mg/l	mg/l	mg/l	mg/l	mg/l	mg/l	mg/l	mg/l												
Preparation		16.09.2019																						
A	1	17.09.2019	5,5	2,7	7,8	<0,2	<1	<1	9,5	0,91	0,21	0,34	36											
B	16	19.09.2019	7,7	3,1	9,4	<0,2	<1	<1	14,3	1,3	<0,2	0,45	31											
C	20	23.09.2019	11	3,5	13,2	<0,2	<1	<1	21,2	2,1	<0,2	0,69	33											
D	23	26.09.2019	12,4	3,6	13,8	<0,2	<1	<1	22,9	2,7	0,2	0,73	32											
E	27	30.09.2019	13,7	3,6	14,9	<0,2	<1	<1	24	3,1	<0,2	0,77	32											
F	35	08.10.2019	15	3,6	16,3	<0,2	<1	<1	24,9	3,7	0,2	0,8	32											
G	43	16.10.2019	17,6	3,6	18,2	<0,2	<1	<1	25,9	4,2	<0,2	0,825	32											
H	58	31.10.2019	18,9	3,6	19,5	0,21	<1	<1	27,2	5,2	<0,2	0,86	32											
I	73	15.11.2019	19,9	3,6	19,7	<0,2	<1	<1	28	5,8	<0,2	0,89	32											
K	87	29.11.2019	20,5	3,6	19,7	<0,2	<1	<1	28,9	6,2	<0,2	0,91	31											
L	104	16.12.2019	21,6	3,6	19,8	<0,2	<1	<1	29,5	6,6	<0,2	0,91	31											
M	134	15.01.2020	23,9	3,6	19,9	0,28	<1	<1	29,5	7,4	<0,2	0,91	31											
N	163	13.02.2020	25,1	3,6	20	0,2	<1	1,7	29,5	8,1	<0,2	0,91	31											
Final	182	03.03.2020	25,4	3,6	20	<0,2	0,37	1,7	29,5	9,7	<0,2	0,91	31											
Sample			IG_BH03_PW017											IG_BH03_PW019										
Sub-samples	Time	Date	Na	K	Ca	Mg	Sr	F	Cl	SO4	NO3	Br	Br/Cl	Na	K	Ca	Mg	Sr	F	Cl	SO4	NO3	Br	Br/Cl
	days		mg/l	mg/l	mg/l	mg/l	mg/l	mg/l	mg/l	mg/l	mg/l	mg/l		mg/l	mg/l	mg/l	mg/l	mg/l	mg/l	mg/l	mg/l	mg/l	mg/l	
Preparation		10.10.2019																						
A	1	11.10.2019	7,1	4,9	29,3	<0,2	<2	<1	49,1	0,46	<0,2	0,94	19	8,1	4,6	43	<0,2	<2	<1	80,3	0,48	<0,2	1,9	24
B	40	13.10.2019	10,5	6,3	42,8	<0,2	<2	<1	72,3	0,79	<0,2	1,3	18	11,7	6	60,5	<0,2	<2	<1	115	0,61	<0,2	2,6	23
C	44	17.10.2019	13,5	6,9	56,2	0,23	<2	<1	97,2	1,03	<0,2	1,7	17	14	6,5	73,1	0,22	<2	<1	145	0,72	<0,2	3,2	22
D	48	21.10.2019	14,5	7,1	62,2	0,28	<2	<1	120	1,4	<0,2	2,2	18	15,6	6,7	82,7	0,25	<2	<1	186	0,83	<0,2	4,1	22
E	51	24.10.2019	15,5	7,3	66,3	0,29	<2	<1	125	1,5	<0,2	2,3	18	16,8	6,7	88,2	<0,2	<2	<1	192	0,99	<0,2	4,3	22
F	58	31.10.2019	17,1	7,4	68,3	0,3	<2	<1	130	1,9	<0,2	2,35	18	17,9	6,7	90,8	0,22	<2	<1	196	1,1	<0,2	4,5	23
G	66	08.11.2019	17,6	7,4	70,2	0,33	<2	<1	136	2,1	<0,2	2,4	18	18,7	6,7	93,2	<0,2	<2	<1	199	1,3	<0,2	4,7	24
H	85	27.11.2019	18	7,4	71,2	0,35	<2	<1	139	2,5	<0,2	2,4	17	19	6,7	94,2	0,24	<2	<1	202	1,5	<0,2	4,8	24
I	97	09.12.2019	18,8	7,4	73,7	0,24	<2	<1	139	2,9	<0,2	2,4	17	19,2	6,7	95,5	0,23	<2	<1	204	1,7	<0,2	4,8	24
K	111	23.12.2019	20,7	7,4	74,3	0,5	<2	<1	139	3,4	<0,2	2,4	17	20,7	6,7	96,9	0,28	<2	<1	204	2,1	<0,2	4,8	24
L	127	08.01.2020	21,9	7,4	76,3	0,49	<2	<1	139	3,8	<0,2	2,4	17	22,5	6,7	98,7	0,28	<2	<1	204	2,4	<0,2	4,8	24
M	157	07.02.2020	22,3	7,4	81,9	3,4	<2	1	139	4,3	<0,2	2,4	17	22,8	6,7	104	0,59	<2	<1	204	2,7	<0,2	4,8	24
N	171	21.02.2020	22,6	7,4	82,1	0,67	<2	1,1	139	5	<0,2	2,4	17	23,2	6,7	109	0,39	<2	<1	204	2,9	<0,2	4,8	24
Final	182	03.03.2020	22,8	7,4	82,2	0,52	1,51	1,2	139	5,4	<0,2	2,4	17	23,3	6,7	110	0,35	1,92	0,92	204	3,4	<0,2	4,8	24

APPENDIX III

Error Calculations

APPENDIX III-1

Gravimetric Water Content

The water content is calculated according to $WC_{grav} = \frac{m_{pw}}{m_{core,wet}}$

Where WC_{grav} = gravimetric water content, m_{pw} = mass of pore water, $m_{core,wet}$ = mass of the wet core sample

Error calculation after Gaussian error propagation

$$\sigma(WC_{grav}) = \sqrt{\left(dWC_{grav}dm_{PW} \times \sigma(m_{PW})\right)^2 + \left(dWC_{grav}dm_{core,wet} \times \sigma(m_{core,wet})\right)^2}$$

Analytical errors (error of measurement)

$s(m_{pw})$ = difference between $m_{core,dry\ surface}$ before and after drying + 0.05 g (=variations at end of drying); The constant of 0.05 g is the empirically derived uncertainty associated to the drying process of the surface, i.e. loss of water from the core surface.

$s(m_{core,wet})$ = difference between $m_{core,dry\ surface}$ before and after experiment

Both uncertainties include the mass difference of the individual cores before and after the experiments (cf. Appendix II).

Derivations

$$dWC_{grav}dm_{pw} = \frac{100}{m_{core,wet}}$$

$$dWC_{grav}dm_{core,wet} = \frac{-100 \times m_{pw}}{(m_{core,wet})^2}$$

APPENDIX III-2

Water Loss Porosity

The water-loss (connected porosity), ϕ_{WL}, is calculated according to

$$\phi_{WL} = WC_{wet} \times \frac{\rho_{bulk,wet}}{\rho_{water}}$$

where WC_{wet} is the water content based on the wet weight of the rock sample and $\rho_{bulk,wet}$ the bulk wet density of the rock. The density of water, ρ_{water}, is assumed to be 1 g/cm^3.

The conversion of the formula leads to

$$\phi_{WL} = \frac{m_{pw} \times 100}{r^2 \times h \times \pi \times \rho_{water}}$$

where r = radius of the core pieces, h = height of the core.

Error calculation after Gaussian error propagation

$$\sigma(\phi_{WL}) = \sqrt{\left(d\phi_{WL}dm_{PW} \times \sigma(m_{PW})\right)^2 + \left(d\phi_{WL}dr \times \sigma(r)\right)^2 + \left(d\phi_{WL}dh \times \sigma(h)\right)^2 + \left(d\phi_{WL}d\rho_{water} \times \sigma(\rho_{water})\right)^2}$$

Analytical errors (error of measurement)

s(m_{pw}) = difference between $m_{core,dry\ surface}$ before and after drying + 0.05 g (=variations at end of drying)

s(r) = 0.02 cm

s(h) = 0.2 cm

s(r_{water}) = 0.03 g/cm^3

Derivations

$$d\phi dm_{pw} = \frac{100}{r^2 \times h \times \pi \times \rho_{water}}$$

$$d\phi dr = \frac{-m_{pw} \times 100 \times 2r \times h \times \pi \times \rho_{water}}{(r^2 \times h \times \pi \times \rho_{water})^2}$$

$$d\phi dh = \frac{-m_{pw} \times 100 \times r^2 \times \pi \times \rho_{water}}{(r^2 \times h \times \pi \times \rho_{water})^2}$$

$$d\phi dh = \frac{-m_{pw} \times 100 \times r^2 \times \pi \times h}{(r^2 \times h \times \pi \times \rho_{water})^2}$$

APPENDIX III-3

Porewater Cl- and Br Concentration

Calculations

$$C_{PW} = \frac{(m_{PW} + m_{TWi} - \sum^{n} m_s) \times C_{TW\infty} - (m_{TWi} \times C_{TWi}) + \sum^{n} m_s \times C_s}{m_{PW}}$$

where C_{pw} = porewater concentration; m_{pw} = mass of porewater; m_{TWi} = initial mass of test water; C_{TWi} = initial Cl-concentration of test water; m_s = mass of sub sample used for time series; C_s = Cl concentration of sub sample used for time series.

Error calculation after Gaussian error propagation

$$\sigma(C_{PW}) = \sqrt{\begin{aligned}&\left(dC_{PW}dm_{PW} \times \sigma(m_{PW})\right)^2 + \left(dC_{PW}dm_{TWi} \times \sigma(m_{TWi})\right)^2 + \\ &+\left(dC_{PW}dC_{TW\infty} \times \sigma(C_{TW\infty})\right)^2 + \left(dC_{PW}dC_{TWi} \times \sigma(C_{TWi})\right)^2 + \\ &(\sigma(\sum m_S))^2 + (\sigma(\sum m_S \times c_S))^2\end{aligned}}$$

Analytical errors (error of measurement)

$\sigma(m_{PW})$ = difference between $m_{core,dry\ surface}$ before and after drying + 0.05 g (=variations at end of drying

$\sigma(m_{TWi})$ = difference between $m_{TWi} – m_S$-$m_{TW\infty}$-2ml (2 ml = remaining water in the cylinder

$\sigma(C_{TWi})$ = 5% (Cl) and 10 % (Br) of the analysed concentration

$\sigma(C_{TW\infty})$ = 5% (Cl) and 10 % (Br) of the analysed concentration

$\sigma(m_S)$ = 0.05 ml

$\sigma(C_S)$ = 5% (Cl) and 10 % (Br) of the analysed concentration

Derivations

$$dC_{PW}dm_{PW} = \frac{C_{TW\infty} * m_{PW} - \left[C_{TW\infty} * (m_{PW} + m_{TWi}) - C_{TW} * m_{TWi}\right]}{m_{PW}^{\ 2}}$$

$$dC_{PW}dm_{TWi} = \frac{(C_{TW\infty} - C_{TWi}) * m_{PW}}{m_{PW}^{\ 2}}$$

$$dC_{PW}dC_{TW\infty} = \frac{(m_{PW} - m_{TWi}) * m_{PW}}{m_{PW}^{\ 2}}$$

$$dC_{PW}dC_{TWi} = \frac{-m_{TWi} * m_{PW}}{m_{PW}^{\ 2}}$$

$$\sigma\left(\sum(m_s)\right) = \left(Nr_S \times \sigma(m_S)\right)$$

$$\sigma\left(\sum(m_S \times C_S)\right) = \left(Nr_S \times C_{S,ave} \times \sigma(m_S)\right) + \left(Nr_S \times m_S \times \sigma(C_S)\right)$$

APPENDIX III-4

Br*1000/Cl Mass Ratio of Porewater

Br*1000/Cl porewater mass ratio = R

Error calculation after Gaussian error propagation

$$\sigma(R) = \sqrt{\left(dRdC_{Br} \times \sigma(C_{Br})\right)^2 + \left(dRdC_{Cl} \times \sigma(C_{Cl})\right)^2}$$

Analytical errors (error of measurement)

$\sigma(C_{Cl})$ = Error of porewater Cl concentration calculated according to AIII-3

$\sigma(C_{Br})$ = Error of porewater Br concentration calculated according to AIII-3

Derivations

$$dRdC_{Br} = \frac{1000}{C_{Cl}}$$

$$dRdC_{Cl} = \frac{-1000 \times C_{Br}}{C_{Cl}^2}$$

APPENDIX III-5

Calculation of Isotopic Signatures of Matrix Porewater

Calculation

$$C_{PW} = \frac{C_{TW\infty(Std1)} \times m_{TW(Std2)} \times m_{Rock(Std1)} \times (C_{TW\infty(Std2)} - C_{TW^0(Std2)}) - C_{TW\infty(Std2)} \times m_{TW(Std1)} \times m_{Rock(Std2)} \times (C_{TW\infty(Std1)} - C_{TW^0(Std1)})}{m_{TW(Std2)} \times m_{Rock(Std1)} \times (C_{TW\infty(Std2)} - C_{TW^0(Std2)}) - m_{TW(Std1)} \times m_{Rock(Std2)} \times (C_{TW\infty(Std1)} - C_{TW^0(Std1)})}$$

m_{PW} = mass of porewater (g)

m_{TW} = mass of test water (g)

C_{TW} = isotopic signature of test water at the beginning of the experiment (‰)

$C_{TW\infty}$ = isotopic signature of test water after equilibration (‰)

Std 1 = Experiment 1 applying standard 1

Std 2 = Experiment 2 applying standard 2

Error calculation after Gaussian error propagation

$$\sigma(C_{PW}) = \sqrt{\begin{aligned}&\left(dC_{PW}\,dm_{TW(Std1)} \times \sigma(m_{TW(Std1)})\right)^2 + \left(dC_{PW}\,dm_{TW(Std2)} \times \sigma(m_{TW(Std2)})\right)^2 + \\ &+\left(dC_{PW}\,dC_{TW(Std1)} \times \sigma(C_{TW(Std1)})\right)^2 + \left(dC_{PW}\,dC_{TW(Std2)} \times \sigma(C_{TW(Std2)})\right)^2 + \\ &+\left(dC_{PW}\,dC_{TW\infty(Std1)} \times \sigma(C_{TW\infty(Std1)})\right)^2 + \left(dC_{PW}\,dC_{TW\infty(Std2)} \times \sigma(C_{TW\infty(Std2)})\right)^2\end{aligned}}$$

Analytical errors (error of measurement)

$\sigma(m_{TW(Std1)})$ = 0.002 g

$\sigma(m_{TW(Std2)})$ = 0.002 g

$\sigma(C_{TW(Std1)})$ = 0.1 ‰ for ^{18}O and 1.0‰ for ^{2}H

$\sigma(C_{TW(Std2)})$ = 0.1 ‰ for ^{18}O and 1.0‰ for ^{2}H

$\sigma(C_{TW\infty(Std1)})$ = 0.1 ‰ for ^{18}O and 1.0‰ for ^{2}H

$\sigma(C_{TW\infty(Std2)})$ = 0.1 ‰ for ^{18}O and 1.0‰ for ^{2}H

Derivations

$$dC_{PW}\,dm_{TW(Std1)} = \frac{\left(C_{TW(Std1)} - C_{TW\infty(Std1)}\right) \times C_{TW\infty(Std2)}}{\left(m_{TW(Std1)} \times \left(C_{TW(Std1)} - C_{TW\infty(Std1)}\right) - \left(C_{TW(Std2)} - C_{TW\infty(Std2)}\right) \times m_{TW(Std2)}\right)} -$$

$$- \frac{\left(\left(C_{TW(Std1)} - C_{TW\infty(Std1)}\right) \times C_{TW\infty(Std2)} \times m_{TW(Std1)} - \left(C_{TW(Std2)} - C_{TW\infty(Std2)}\right) \times C_{TW\infty(Std1)} \times m_{TW(Std2)}\right) \times \left(C_{TW(Std1)} - C_{TW\infty(Std1)}\right)}{\left(m_{TW(Std1)} \times \left(C_{TW(Std1)} - C_{TW\infty(Std1)}\right) - \left(C_{TW(Std2)} - C_{TW\infty(Std2)}\right) \times m_{TW(Std2)}\right)^2}$$

$$dC_{PW}\,dm_{TW(Std2)} = \frac{-\left(C_{TW(Std2)} - C_{TW\infty(Std2)}\right) \times C_{TW\infty(Std1)}}{\left(m_{TW(Std1)} \times \left(C_{TW(Std1)} - C_{TW\infty(Std1)}\right) - \left(C_{TW(Std2)} - C_{TW\infty(Std2)}\right) \times m_{TW(Std2)}\right)} +$$

$$+ \frac{\left(\left(C_{TW(Std1)} - C_{TW\infty(Std1)}\right) \times C_{TW\infty(Std2)} \times m_{TW(Std1)} - \left(C_{TW(Std2)} - C_{TW\infty(Std2)}\right) \times C_{TW\infty(Std1)} \times m_{TW(Std2)}\right) \times \left(C_{TW(Std2)} - C_{TW\infty(Std2)}\right)}{\left(m_{TW(Std1)} \times \left(C_{TW(Std1)} - C_{TW\infty(Std1)}\right) - \left(C_{TW(Std2)} - C_{TW\infty(Std2)}\right) \times m_{TW(Std2)}\right)^2}$$

$$dC_{PW}\,dC_{TW(Std1)} = \frac{C_{TW\infty(Std2)} \times m_{TW(Std1)}}{\left(m_{TW(Std1)} \times \left(C_{TW(Std1)} - C_{TW\infty(Std1)}\right) - \left(C_{TW(Std2)} - C_{TW\infty(Std2)}\right) \times m_{TW(Std2)}\right)} -$$

$$- \frac{\left(\left(C_{TW(Std1)} - C_{TW\infty(Std1)}\right) \times C_{TW\infty(Std2)} \times m_{TW(Std1)} - \left(C_{TW(Std2)} - C_{TW\infty(Std2)}\right) \times C_{TW\infty(Std1)} \times m_{TW(Std2)}\right) \times m_{TW(Std1)}}{\left(m_{TW(Std1)} \times \left(C_{TW(Std1)} - C_{TW\infty(Std1)}\right) - \left(C_{TW(Std2)} - C_{TW\infty(Std2)}\right) \times m_{TW(Std2)}\right)^2}$$

$$dC_{PW}\,dC_{TW(Std2)} = \frac{-C_{TW\infty(Std1)} \times m_{TW(Std2)}}{\left(m_{TW(Std1)} \times \left(C_{TW(Std1)} - C_{TW\infty(Std1)}\right) - \left(C_{TW(Std2)} - C_{TW\infty(Std2)}\right) \times m_{TW(Std2)}\right)} +$$

$$+ \frac{\left(\left(C_{TW(Std1)} - C_{TW\infty(Std1)}\right) \times C_{TW\infty(Std2)} \times m_{TW(Std1)} - \left(C_{TW(Std2)} - C_{TW\infty(Std2)}\right) \times C_{TW\infty(Std1)} \times m_{TW(Std2)}\right) \times m_{TW(Std2)}}{\left(m_{TW(Std1)} \times \left(C_{TW(Std1)} - C_{TW\infty(Std1)}\right) - \left(C_{TW(Std2)} - C_{TW\infty(Std2)}\right) \times m_{TW(Std2)}\right)^2}$$

$$dC_{PW}\,dC_{TW\infty(Std1)} = \frac{-\left(C_{TW\infty(Std2)} \times m_{TW(Std1)} + \left(C_{TW(Std2)} - C_{TW\infty(Std2)}\right) \times m_{TW(Std2)}\right)}{\left(m_{TW(Std1)} \times \left(C_{TW(Std1)} - C_{TW\infty(Std1)}\right) - \left(C_{TW(Std2)} - C_{TW\infty(Std2)}\right) \times m_{TW(Std2)}\right)} +$$

$$+ \frac{\left(\left(C_{TW(Std1)} - C_{TW\infty(Std1)}\right) \times C_{TW\infty(Std2)} \times m_{TW(Std1)} - \left(C_{TW(Std2)} - C_{TW\infty(Std2)}\right) \times C_{TW\infty(Std1)} \times m_{TW(Std2)}\right) \times m_{TW(Std1)}}{\left(m_{TW(Std1)} \times \left(C_{TW(Std1)} - C_{TW\infty(Std1)}\right) - \left(C_{TW(Std2)} - C_{TW\infty(Std2)}\right) \times m_{TW(Std2)}\right)^2}$$

$$dC_{PW}\,dC_{TW\infty(Std1)} = \frac{-\left(C_{TW\infty(Std2)} \times m_{TW(Std1)} + \left(C_{TW(Std2)} - C_{TW\infty(Std2)}\right) \times m_{TW(Std2)}\right)}{\left(m_{TW(Std1)} \times \left(C_{TW(Std1)} - C_{TW\infty(Std1)}\right) - \left(C_{TW(Std2)} - C_{TW\infty(Std2)}\right) \times m_{TW(Std2)}\right)} +$$

$$+ \frac{\left(\left(C_{TW(Std1)} - C_{TW\infty(Std1)}\right) \times C_{TW\infty(Std2)} \times m_{TW(Std1)} - \left(C_{TW(Std2)} - C_{TW\infty(Std2)}\right) \times C_{TW\infty(Std1)} \times m_{TW(Std2)}\right) \times m_{TW(Std1)}}{\left(m_{TW(Std1)} \times \left(C_{TW(Std1)} - C_{TW\infty(Std1)}\right) - \left(C_{TW(Std2)} - C_{TW\infty(Std2)}\right) \times m_{TW(Std2)}\right)^2}$$

$$dC_{PW}\,dC_{TW\infty(Std2)} = \frac{\left(m_{TW(Std1)} \times \left(C_{TW(Std1)} - C_{TW\infty(Std1)}\right) + C_{TW\infty(Std1)} \times m_{TW(Std2)}\right)}{\left(m_{TW(Std1)} \times \left(C_{TW(Std1)} - C_{TW\infty(Std1)}\right) - \left(C_{TW(Std2)} - C_{TW\infty(Std2)}\right) \times m_{TW(Std2)}\right)} -$$

$$- \frac{\left(\left(C_{TW(Std1)} - C_{TW\infty(Std1)}\right) \times C_{TW\infty(Std2)} \times m_{TW(Std1)} - \left(C_{TW(Std2)} - C_{TW\infty(Std2)}\right) \times C_{TW\infty(Std1)} \times m_{TW(Std2)}\right) \times m_{TW(Std2)}}{\left(m_{TW(Std1)} \times \left(C_{TW(Std1)} - C_{TW\infty(Std1)}\right) - \left(C_{TW(Std2)} - C_{TW\infty(Std2)}\right) \times m_{TW(Std2)}\right)^2}$$

APPENDIX III-6

Calculation of Mass of Porewater by Isotope Diffusive Exchange Technique

Calculation

$$WC_{IsoEx} = \left[\frac{m_{TW(Std\,2)} \times m_{Rock(Std1)} \times (C_{TW^0(Std\,2)} - C_{TW\infty(Std\,2)}) + m_{TW(Std1)} \times m_{Rock(Std\,2)} \times (C_{TW\infty(Std1)} - C_{TW^0(Std1)})}{m_{Rock(Std1)} \times m_{Rock(Std\,2)} \times (C_{TW\infty(Std\,2)} - C_{TW\infty(Std1)})} \right] \times 100$$

m_{PW} = mass of porewater (g)

m_{TW} = mass of test water (g)

C_{TW} = isotopic signature of test water at the beginning of the experiment (‰)

$C_{TW\infty}$ = isotopic signature of test water after equilibration (‰)

Std 1 = Experiment 1 applying standard 1

Std 2 = Experiment 2 applying standard 2

Error calculation after Gaussian error propagation

$$\sigma(m_{PW}) = \sqrt{\begin{aligned} &\left(dm_{PW}\,dm_{TW(Std1)} \times \sigma(m_{TW(Std1)})\right)^2 + \left(dm_{PW}\,dm_{TW(Std\,2)} \times \sigma(m_{TW(Std\,2)})\right)^2 + \\ &+\left(dm_{PW}\,dC_{TW(Std1)} \times \sigma(C_{TW(Std1)})\right)^2 + \left(dm_{PW}\,dC_{TW(Std\,2)} \times \sigma(C_{TW(Std\,2)})\right)^2 + \\ &+\left(dm_{PW}\,dC_{TW\infty(Std1)} \times \sigma(C_{TW\infty(Std1)})\right)^2 + \left(dm_{PW}\,dC_{TW\infty(Std\,2)} \times \sigma(C_{TW\infty(Std\,2)})\right)^2 \end{aligned}}$$

Analytical errors (error of measurement)

$\sigma(m_{TW(Std1)})$ = 0.002 g

$\sigma(m_{TW(Std2)})$ = 0.002 g

$\sigma(C_{TW(Std1)})$ = 0.1 ‰ for ^{18}O and 1.0‰ for ^{2}H

$\sigma(C_{TW(Std2)})$ = 0.1 ‰ for ^{18}O and 1.0‰ for ^{2}H

$\sigma(C_{TW\infty(Std1)})$ = 0.1 ‰ for ^{18}O and 1.0‰ for ^{2}H

$\sigma(C_{TW\infty(Std2)})$ = 0.1 ‰ for ^{18}O and 1.0‰ for ^{2}H

Derivations

$$dm_{PW}\,dm_{TW(Std1)} = \frac{\left(C_{TW(Std1)} - C_{TW\infty(Std1)}\right)}{\left(C_{TW\infty(Std1)} - C_{TW\infty(Std\,2)}\right)}$$

$$dm_{PW}\,dm_{TW(Std\,2)} = \frac{-\left(C_{TW(Std\,2)} - C_{TW\infty(Std\,2)}\right)}{\left(C_{TW\infty(Std1)} - C_{TW\infty(Std\,2)}\right)}$$

$$dm_{PW}\,dC_{TW(Std1)} = \frac{m_{TW(Std1)}}{\left(C_{TW\infty(Std1)} - C_{TW\infty(Std\,2)}\right)}$$

$$dm_{PW}\,dC_{TW(Std\,2)} = \frac{-m_{TW(Std\,2)}}{\left(C_{TW\infty(Std1)} - C_{TW\infty(Std\,2)}\right)}$$

$$dm_{PW}\,dC_{TW\infty(Std1)} = \left(\frac{-1}{\left(C_{TW\infty(Std1)} - C_{TW\infty(Std\,2)}\right)} - \frac{\left(C_{TW(Std1)} - C_{TW\infty(Std1)}\right)}{\left(C_{TW\infty(Std1)} - C_{TW\infty(Std\,2)}\right)^2}\right) \times m_{TW(Std1)} + \left(C_{TW(Std\,2)} - C_{TW\infty(Std\,2)}\right) \times m_{TW(Std\,2)}$$

$$dm_{PW}\,dC_{TW\infty(Std\,2)} = \left(\frac{\left(C_{TW(Std1)} - C_{TW\infty(Std1)}\right) \times m_{TW(Std1)}}{\left(C_{TW\infty(Std1)} - C_{TW\infty(Std\,2)}\right)^2} + \frac{1}{\left(C_{TW\infty(Std1)} - C_{TW\infty(Std\,2)}\right)^2} - \frac{\left(C_{TW(Std\,2)} - C_{TW\infty(Std\,2)}\right)}{\left(C_{TW\infty(Std1)} - C_{TW\infty(Std\,2)}\right)^2}\right) \times m_{TW(Std\,2)}$$

Hydroisotop

GOLDER

golder.com